Drug Delivery by Enzyme-Responsive Nanoformulation – Exploring Novel Cancer Treatments

Inauguraldissertation

Zur

Erlangung der Würde eines Doktors der Philosophie

vorgelegt der

Philosophisch-Naturwissenschaftlichen Fakultät

der Universität Basel

von

Daniel Simon Ehrsam

von Basel

Basel, 2020

Genehmigt von der Philosophisch-Naturwissenschaftlichen Fakultät auf Antrag von

Prof. Dr. Henriette Meyer zu Schwabedissen

Prof. Dr. Oliver Germershaus

Basel, den 15.09.2020

Prof. Dr. Martin Spiess (Dekan)

Introduction

Summary and Aims

Even though tumor treatment has achieved remarkable successes in recent years, cancer is still one of the severest diseases there is. According to statistics published by the WHO, cancer is the second leading cause of death worldwide (*1*). Chemotherapy is one of the most widely applied cancer treatment methods since it emerged in the 1940s. Despite of research and development efforts made meanwhile, many compounds used in chemotherapy present major drawbacks. Nanotechnology, as an addon to the anti-cancer drug development, is a promising strategy to cope with certain shortcomings of otherwise encouraging compounds. In this PhD thesis introduction, the reader will be given the understanding, basics and vocabulary to successfully navigate through the publications. At first, the basics of cancer are discussed and points of attack for treatments are described. Then, a short overview will present the development of chemotherapeutics from the beginnings up to nanomedicine.

In our studies, we explored different approaches to developing enzyme-triggered nanoformulations. Our enzyme-responsive formulations were tested in vitro and, to some extent, in vivo.

The conclusion is focused on putting the nanoformulation in context with current progress and presuming opportunities and risks.

Cancer

In general – what is cancer?

The cells forming the human body are in a constant physiological turnover throughout its lifetime. In developed organs, older differentiated cells are replaced by newly formed cells deriving from stem cells. The balance between cell death and stem cell division allows tissue homeostasis and therefore preserves the proper functioning of our body. Whereas an imbalance of these two processes is connected to diseases like degenerative disorders or cancer (*2*).

Cancer is a collective term for many related diseases emerging from body cells. These diseases are characterized by abnormal cell growth and spreading of affected cells from the site of origin to other sites in the body (metastases). The cause of cancer can be found in an altered genome similar to genetic diseases, with the difference that the alterations are mainly acquired over a lifetime and only to a minor extent inherited (*3*).

Cancer is distinguishable from many other diseases. It is not a lack or reduction of function, but rather an alteration of cellular processes. Mutated genes contributing to the development of cancer can be divided into two categories: **oncogenes and tumor suppressor genes (*4*)**. 'Oncogene' is a general term for genes that encode proteins capable of inducing cancer. Oncogenes are genes that can lead to the development of cancer when expressed at high levels. In physiological conditions, proto-oncogenes, the progenitors of oncogenes, are encoding proteins that regulate cell growth, survival and division of cells. An increased activity of oncogenes results in altered or increased levels of these proteins (oncoproteins), which in turn deregulate signaling pathways and unbalance cellular processes. Proto-oncogenes change into oncogenes by acquiring gain-of-function mutations (*4*). Oncogenes having undergone such gain-of-function mutations act dominantly, meaning that an alternation in only one of two alleles is sufficient to induce cancer.

For tumorgenesis, oncogene activation is of equal importance to tumor suppressor gene inactivation. Tumor suppressor genes are genes encoding proteins, which are able to inhibit cell proliferation. Tumor suppressor genes work in an opposite fashion to oncogenes (*4*). A functional reduction or loss of tumor suppressor genes is essential for tumor progression. Loss-of-function mutations in tumor suppressor genes generally follow

the two-hit hypothesis, meaning that both alleles must be affected to promote tumor development (*5*).

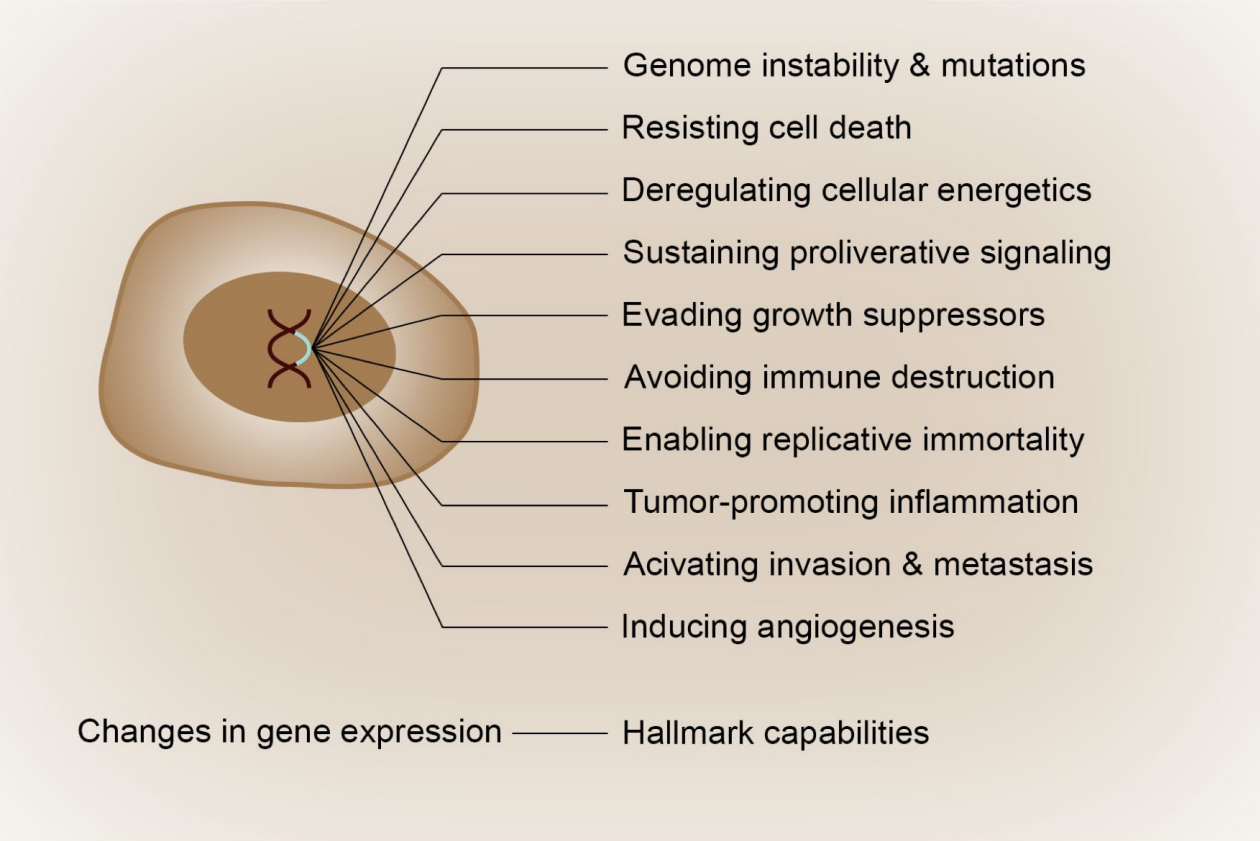

Figure 1: Hallmarks of cancer. Mutations in cancer related genes lead to changes in gene expression and ultimately to the cancer specific hallmarks. The hallmarks of cancer can be considered as observable traits or behavior patterns of tumor tissues. These changes allow the tumor to grow out of control, evade the immune system, and ignore signals leading to cell death. adapted from (6).

The changes in oncogenes and tumor suppressor genes have an impact on the behavior of the affected cells. The behavioral differences deriving from gene mutations were summarized by Hanahan et al. in ten **cancer hallmarks (*6*)**. These hallmarks include immortality, evading cell death, immune response and growth suppressors, deregulating cellular energetics, promoting inflammation, invasion and metastasis, mutation and genome instability, and inducing angiogenesis. In other words, there are ten common properties that are influenced by cancer to evade the immune system, grow out of control,

and ignore signals normally leading to cell death (*6*). The hallmarks of cancer are representing the behavior of tumors (shown in figure 1).

It is worth mentioning that the cancer hallmarks must be seen as properties of a cell population. The individual cells within such a population may display a variety of these traits and to various degrees. Tumor tissues are characterized by a complex interplay of individual specialized cancer cells similar to organs in the body. This is also known as tumor cell heterogeneity (*7*). There are three model theories explaining the origins of the intratumor heterogeneity: the cancer stem cell, the stochastic, and the clonal evolution theory (*7*).

The cancer stem cell theory proposes a hierarchical tumor organization, similar to the organization of normal tissue (*7*). Within the tumor, there are cancer stem cells capable of renewing and being the progenitor of more differentiated cancer cells (*8*).

The stochastic theory hypothesizes that a tumor originates from a single mutated cell. As the tumor progresses, the cells accumulate an increasing number of mutations (*9*).

The clonal evolution theory states that mutated tumor cells with an evolutionary advantage can outcompete others. When subclones evolve side-by-side, genetic diversity of the tumor is achieved (*9*). The clonal evolution theory seems to apply to both, the stochastic and the cancer stem cell model.

Angiogenesis as an example of a hallmark and the influence of matrix metalloproteinase 9 (MMP9) and cathepsin B's (ctsb) influence on cancer

Cells need nutrients and oxygen to fuel their metabolism and respiration to keep up their metabolic rate. The resulting metabolic waste and carbon dioxide must be removed. This is where angiogenesis, the formation of new blood vessels, is of great importance (*10*). In physiological conditions, the process of angiogenesis is highly regulated and plays a crucial role during embryogenic development, wound healing, or the menstruation cycle to name just a few of them (*11*). Since critical nutrients and metabolic waste can only diffuse about 200 μm, fast growing tumors would soon reach their expansion limit. Tumor growth therefore relies on the ability to induce angiogenesis or otherwise the tumor becomes dormant (*12*). The majority of all tumors depend on recruitment of blood vessels to maintain growth and to escape the primary site (metastasize).

Tumor Angiogenesis is influenced by hypoxia in the microenviroment, but only to a certain degree. A greater impact have mutated genes (tumor suppressor genes and oncogenes) (*10*). This leads to altered expression of tumor suppressor genes (p53, PTEN, and VHL) and oncogenes (ras, src, and HER-2) (*13, 14*). For example, a gain-of-function mutation of ras may lead to induction of the transcriptional activator hypoxia-inducible-factor 1 (HIF-1) activity. As a result, HIF-1 increases the VEGF expression, which upregulates the MMP-9 expression (*15, 16*). MMP-9 is a protease known to play a role in the proteolytic network of cancer. In addition to MMP-9, cathepsin B and urokinase-type plasminogen activator act as important parts of this network (*17*).

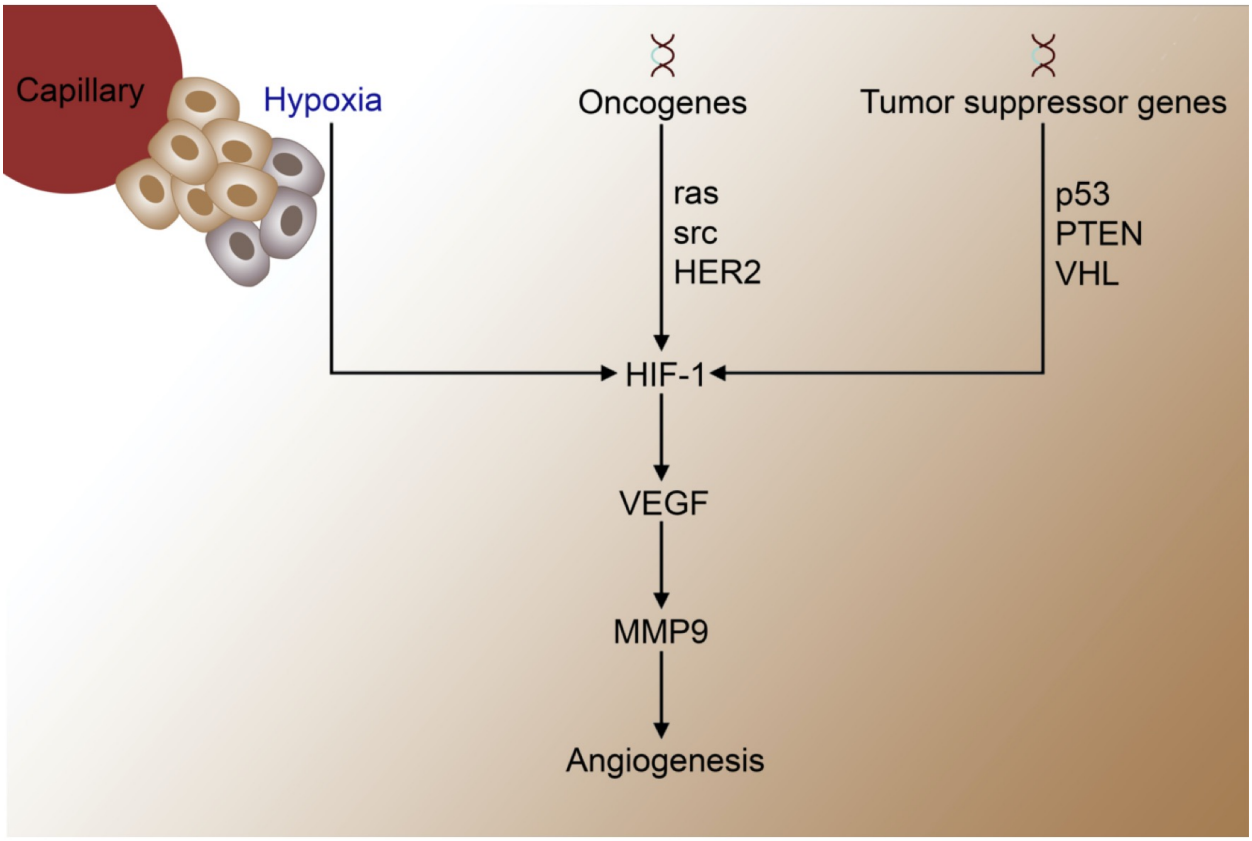

Figure 2; Hypoxia-inducible-factor 1 (HIF-1) expression in tumors and angiogenesis. Dysregulated proliferation of tumor cells leads to hypoxia. Hypoxia induces the expression of HIF-1 and as a result angiogenesis increased. The hypoxia-induced pathways surrounding HIF-1 are highly affected by altered expression of oncogenes (e.g. ras, src, HER2) and tumor suppressor genes (e.g. p53, PTEN, VHL). Adapted from (15, 18, 19).

Both, cysteine protease cathepsin B and gelatinase MMP-9, have been reported to participate in tumor angiogenesis. Furthermore, they intermingle in a complex protease activation cascade. On the one hand, extracellular cathepsin B activity leads to degradation of tissue inhibitor of metalloproteinases 1 (TIMP1) (*20*). TIMP1 is an inhibitor of MMP-9, the dysregulation of which has been observed in cancer (*21*). On the other hand, cathepsin B activates pro-urokinase-type plasminogen activator (pro-uPA) to its active form uPA (*22*). uPA facilitates the conversion of plasminogen to plasmin. Plasmin for its part, activates pro-MMP-3 (*23*) and active MMP-3 is converting pro-MMP-9 to active MMP-9.

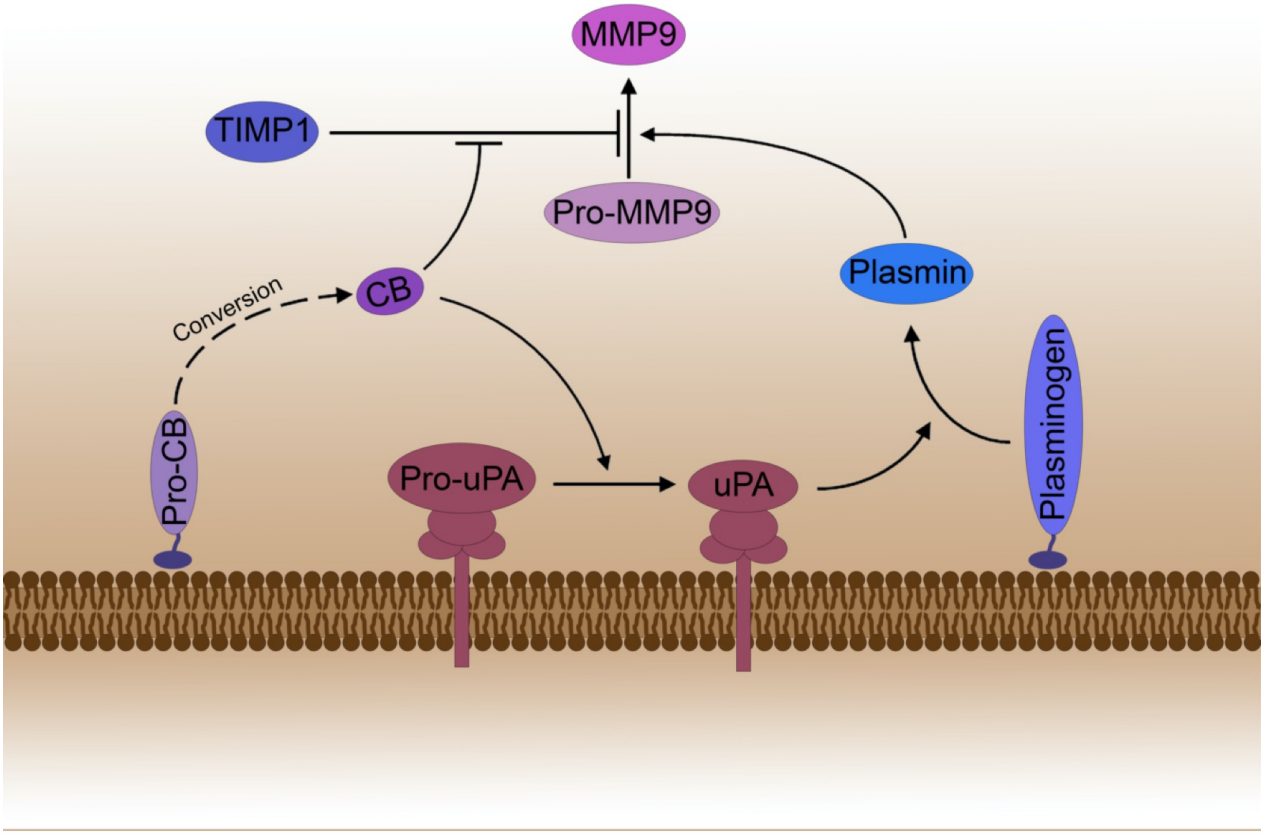

Figure 3: Simplified scheme picturing the relationship between cathepsin B (CB) and MMP9. CB initiates a proteolytic cascade which results in the activation of urokinase-type plasminogen (Pro-uPA → uPA) and inactivation of tissue inhibitor of MMPs like TIMP1. uPA cleaves plasminogen to form the active plasmin. Pro-MMP9 is activated by plasmin to form MMP9. TIMP1 acts as an inhibitor of activated MMP9 and therefore has an impact on MMP9 activity. Adapted from (20, 22, 24).

Cancer Therapy

Development of Chemotherapeutics

Based on the state of knowledge, early anti-cancer drug development focused on delivering compounds capable of inhibiting the cancer-typical uncontrolled cell proliferation. Therefore, early anti-cancer drugs mainly focused on the inhibition of cell division. They include alkylating agents, antifolates, antimetabolites, mitotic and topoisomerase inhibitors (*25*).

Unfortunately, many promising compounds that were discovered in screenings had unfavorable pharmacokinetic characteristics like poor solubility or stability, which led to the development of the prodrug approach. The **prodrug** approach is a successful method to improve solubility and stability of a drug compound by modifying its chemical structure (*26*). Prodrugs are precursors of active drugs that have to undergo a biotransformation step before developing their pharmacological effect. This can be achieved by either prodrug conjugation or prodrug degradation (*27*). During prodrug conjugation, the compound is altered by a conjugation reaction. The conjugate possesses an increased chemical complexity resulting in its pharmacological activity. In contrast, prodrug degradation decreases the chemical complexity of the molecule by cleaving off a masking group, whereby the active compound is released (*27*).

Besides the prodrug approach there is also the possibility to increase the solubility and stability of drugs by using nanoparticulated drug delivery systems (*28*). ‘Nanomedicine’ is a collective term for the medical application of nanotechnology. Nanotherapeutics use a variety of different nano-scaled drug delivery systems consisting of different materials. This is including lipids, polymers, dendrimers, inorganic material, conjugates, viral capsids or cellular membrane (*29, 30*). Usually the drug is either stored within the nanoparticle, covalently bound or electrostatically interacts with the delivery system. In common is the size of the nanoparticles, which typically ranges from 100-500 nm (*31*).

Although problems with physicochemical properties or the pharmacokinetic profile of anti-cancer drugs can be overcome or at least mitigated with the prodrug or drug delivery system approach, other adverse effects often still remain.

Since the selectivity to cancer cells was based on targeting fast dividing cells, early anti-cancer drugs suffered from severe adverse effects.

As a result of extensive research into tumor biology, a broader understanding was achieved of how the disease emerges and develops (*25*). As mentioned in the previous chapter, insight into tumor genetics led to the postulation of the tumor hallmarks. The tumor hallmarks are the result of signaling networks being seized by cancer and thereby enabling tumor formation. The specific pathways responsible for the ten cancer hallmarks were identified as new and promising points of interaction or targets to influence tumor formation and growth (*6*). Due to the high inter- and intra-tumor heterogeneity of cancer, a large variety of anti-cancer drugs were developed to target different pathways. This new therapy form was called targeted therapy (*25*).

Another method to increase selectivity and reduce the exposure of the whole body to the drugs, is **drug targeting**. This approach utilizes drug delivery systems like drug conjugates, prodrugs or nanoformulations, which are activated or accumulated at or close to the site of intended use. The tumor targeting by these drug delivery systems can be divided into stimuli-responsive, passive and active targeting.
Besides their targeting abilities, nanoparticles have some additional advantages. They can carry hardly soluble drugs and therefore overcome solubility issues. Furthermore, nanoparticles can be used for simultaneous administration of several drugs to prevent drug resistance.

Targeting

Passive targeting

The most prominent physiological condition used for passive targeting is the enhanced permeability and retention effect (EPR). The EPR, first described by Matsumura and Maeda, allows nanocarriers and macromolecules to be accumulated in tumors and inflamed tissue. The phenomenon is based on the quickly developed blood vessel network in tumors with greater permeability and a defective lymphatic drainage. The initial observation of Matsumura and Maeda led to development and successful introduction of several passive targeted nanocarriers (*32*). These include liposomal nanocarriers (Doxil, Marqibo, DaunoXome Onivyde, Myocet, Caelyx), polymeric nanocarriers (Genexol-PM, SMANCS), and protein-conjugates (Abraxane).

Unfortunately, as described above, tumors exhibit a high degree of inter- and intra-tumoral heterogeneity influencing how pronounced the EPR effect is. Therefore, passive targeting of tumors using the EPR effect is highly variable and depends on the tumor type, size, stage and its genetic makeup (*33, 34*).

The physiochemical properties like size, surface charge, shape, and elasticity play also an important role when developing nanocarriers or other macromolecules with the intention to passively target tumors (*35*). Initially, passive accumulation in tumors was observed with proteins. The behavior of proteins as a drug carriers is hard to predict due to their unique conformation and charge, but also their tendency to denature and degrade (*36*). Since polymer or lipid-based nanocarriers are less variable, they were chosen to further investigate passive targeting. In extensive research of interaction or behavior prediction, many properties of importance were found. Is the nanocarrier less than 10 nm in diameter, the elimination by kidney will occur fast (*37*). Nanocarriers with a weight of over 40000 Da evade the renal filtration (*38*). Large nanocarriers of more than 200 nm in diameter will be cleared by the reticulo-endothelial system (RES) (*38*). The RES is a system of the human body to get rid of dead and abnormal cells, tissues and xenobiotics. The cells belonging to this system are highly phagocytic and they present antigens to lymphocytes leading to antibody secretion. Concerning the surface properties of nanocarriers, hydrophilic and neutral or negatively charged carrier-surfaces are considered best to avoid uptake of the nanocarriers into the RES (*38*). A vastly used solution for nanocarriers with hydrophobic or cationic surfaces is modification of the surface with a hydrophilic surface-coating (e.g. polyethylene glycol). Nanocarriers come in a variety of shapes, such as spheres, cylinders, cubes, hemispheres, ellipsoids, cones and more. The shape of the nanocarrier has an impact on internalization and therefore phagocytosis. For example, non-spherically shaped carriers are more likely to avoid phagocytosis (*38*).

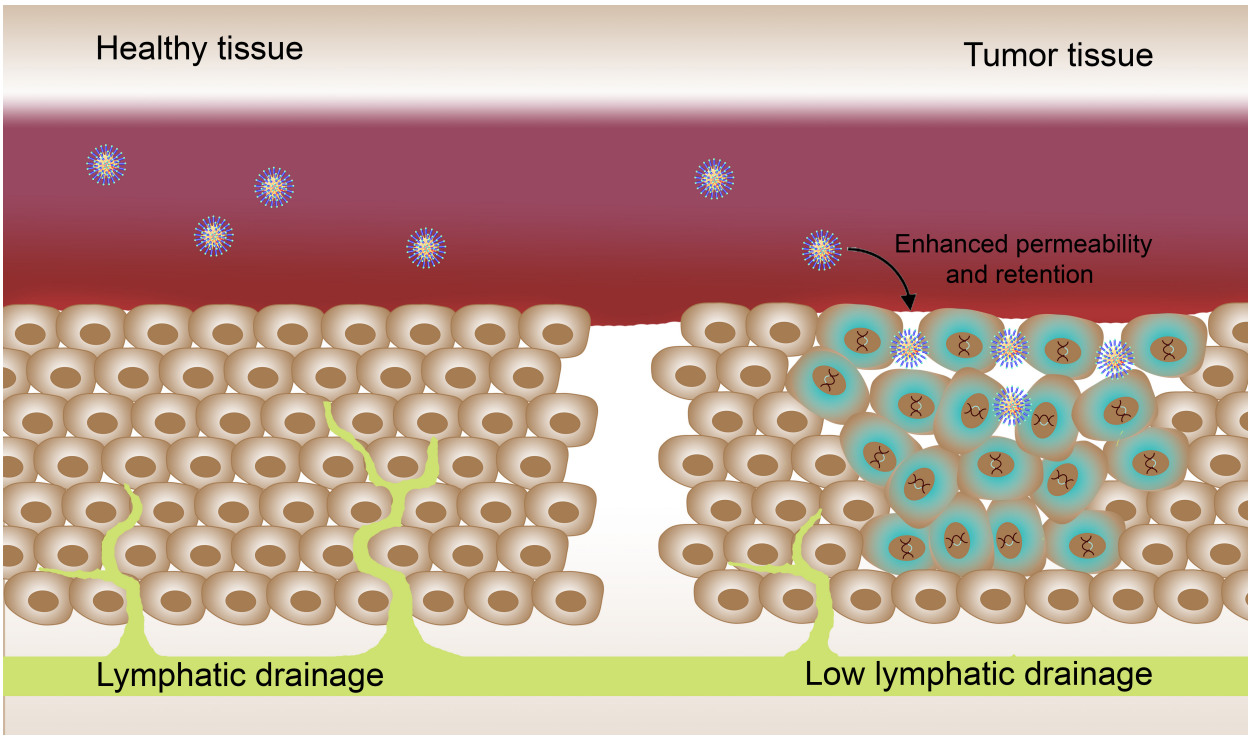

*Figure 4: Passive targeting of tumor by nanoparticles. (**left side**) Representation of blood vessels in healthy tissue. The vessel wall is tight and lymphatic drainage is functional. (**right side**) Representation of passive targeting of nanoparticles in tumor tissue. Extravasation of nanoparticles through the gap junctions of the leaky blood vessels in the tumor tissue (turquoise underlay) occurs. The lymph vessels are underdeveloped, and lymphatic drainage is reduced. This effect is also known as enhanced permeability and retention effect.*

Stimuli-responsive drug targeting or smart drug delivery systems

As the name indicates, stimuli-responsive drug targeting utilizes triggers for releasing the active compound at the intended site of action. These stimuli can be divided into endogenous and exogenous stimuli (*39*). Endogenous stimuli are chemical or biochemical properties of the targeted area which differ from the ones of normal tissue. They include pH, redox-potential, enzyme expression and host-guest recognition. Exogenous stimuli are of physical nature which can be applied externally (from outside of the body). These include light, thermal, ultra-sonic, magnetic or electric stimuli (*38*).

Basically, there are two possible approaches for enzyme-responsive drug formulations. One is to incorporate the enzyme labile component into the design of the drug delivery system. The unmodified drug is stored inside the drug delivery system and as soon as the enzyme labile component is digested by the enzyme in question, the drug is released for uptake or action at the target area (*40*). Alternatively, the enzyme labile component can itself be a part of a drug conjugate. Such drug conjugates are either building blocks for drug delivery systems like nanoparticles which are held together by intermolecular forces, or are interlinked molecule clusters themselves which are covalently bonded. Here, the active drug is released after digestion of the building block, almost like a prodrug (*40*).

Active targeting

In contrast to passive targeting which exploits changes in the physiology of the affected area for accumulation, active targeting utilizes specific targeting moieties. These active targeting moieties bind to expressed or overexpressed targets on the cell surface and therefore allow an accumulation of the nanocarrier at the intended site of action. For active targeting multiple moieties can be employed including antibodies, peptides, and small molecules (*41*). Usually active targeting is used in combination with passive targeting to achieve improved specificity to the tumor (*35*). For example, passive targeting allows the nanocarrier to accumulate in the malignant tissue based on the EPR effect and by active targeting a retention of the nanocarrier is accomplished leading to an improved pharmacodynamic and pharmacokinetic profile of the drug. Finally, controlled or sustained release of the payload can be accomplished (*40*).

Aim of the thesis

As many promising small molecule chemotherapeutics suffer from unfavorable physicochemical characteristics or adverse effects due to their off-target effects, drug targeting and nanotechnology represent promising strategies to cope with the limits of conventional anti-cancer drugs and extend their applicability.
The goal of this thesis was to research and explore drug delivery systems containing a stimuli-responsive release mechanism. Based on previous work in our lab, special attention was given to enzymes participating in tumor angiogenesis as trigger stimuli. The main aim was subdivided into the following sub-goals.

- Selection of an extracellular enzyme as a trigger for stimuli-responsive nanomedicine
    - Search for suitable enzymes
    - Identification of suitable tumor entities using patient sample and database survey

- Development and formulation of enzyme-triggered release systems
    - Exploring different approaches

- Characterization of the enzyme-triggered release formulations
    - Physical appearance
    - Physico-chemical features

- In vitro testing
    - Identification of suitable in vitro model systems
    - Testing enzyme triggered release in vitro

- In vivo testing
    - Using zebrafish for distribution studies
    - Exploration of RT-qPCR for tumor size detection in zebrafish

Results

Results I

"Synthesis and Characterization of PDMS−PMOXA-Based Polymersomes Sensitive to MMP-9 for Application in Breast Cancer"

Fabiola Porta [1§], Daniel Ehrsam [1§], Claudia Lengerke [2], Henriette E Meyer Zu Schwabedissen [1]

§ F.P. and D.E. contributed equally to this work.

Affiliations:

[1] Biopharmacy, Department of Pharmaceutical Sciences, University of Basel, Klingelbergstrasse 50, 4056 Basel, Switzerland.

[2] Department of Biomedicine, University Hospital of Basel, Hebelstrasse 20, 4031 Basel, Switzerland.

Contribution Daniel Ehrsam: Study design, acquisition, analysis and interpretation of data, drafting of manuscript.

PMID: 30274515 DOI: 10.1021/acs.molpharmaceut.8b00521

molecular pharmaceutics

Article

Cite This: *Mol. Pharmaceutics* 2018, 15, 4884−4897

pubs.acs.org/molecularpharmaceutics

Synthesis and Characterization of PDMS−PMOXA-Based Polymersomes Sensitive to MMP-9 for Application in Breast Cancer

Fabiola Porta,[†,§] Daniel Ehrsam,[†,§] Claudia Lengerke,[‡] and Henriette E. Meyer zu Schwabedissen*[,†]

[†]Biopharmacy, Department of Pharmaceutical Sciences, University of Basel, Klingelbergstrasse 50, 4056 Basel, Switzerland

[‡]Department of Biomedicine, University Hospital of Basel, Hebelstrasse 20, 4031 Basel, Switzerland

Supporting Information

ABSTRACT: Cytotoxic compounds used to treat cancer are often associated with adverse events. The development of formulations activated by tumor-specific triggers would allow a reduction of systemic exposure while maintaining therapeutic concentrations in the tumor. One enzyme with proteolytic activity reported to be involved in tumor progression and assumed to be enhanced in the tumor environment is the matrix metalloproteinase 9 (MMP-9). In our study, we aimed to develop surface-modified PDMS−PMOXA polymersomes able to release their cytotoxic payload upon digestion by MMP-9. To test the applicability of such a system in breast cancer, this tumor entity was assessed for MMP-9 expression, supporting breast cancer as a potential target. The surface-modified polymersomes were synthesized and formulated resulting in paclitaxel-loaded particles of about 320 ± 153.15 nm in size with a surface potential of 0.04 ± 0.007 mV. After the expression and activity of MMP-9 in MCF7 cells were verified, this cell line was used for further analysis. Treatment of MCF7 cells with the polymersomes significantly reduced cell viability, this effect was abolished after addition of MMP-inhibitors, suggesting proteolytic activation. In zebrafish embryos, the polymersomes were observed in the circulation with some enrichment in liver and agglomerates in the caudal veins. Importantly, in zebrafish embryos xenografted with mKate2-expressing MCF7 cells, the amount of tumor cells, quantified by detecting the copies of the heterologously expressed fluorescent protein, significantly decreased after treatment with PDMS−PMOXA−SRL−paclitaxel polymersomes. Taken together, our data suggest that polymersomes modified with an MMP-9 labile peptide and loaded with paclitaxel can be formulated, and that these particles exert pharmacological activity upon enzymatic digestion.

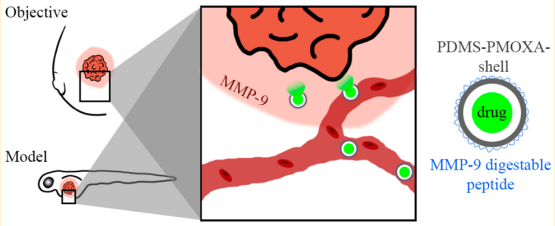

KEYWORDS: *enzyme triggered release, breast cancer, PDMS−PMOXA polymersomes, MMP-9, paclitaxel, zebrafish in vivo testing*

INTRODUCTION

A systemic therapeutic intervention with anticancer drugs is hampered by accumulation of the clinically applied chemotherapeutic in healthy organs where it induces unwanted side effects. The occurrence of these off-target effects significantly limits clinically applied doses. The pharmaceutical formulation of cytotoxic compounds provides the possibility to significantly change its pharmacokinetics and thereby its pharmacological profile.

Nanoformulations can be considered as a pharmaceutical packaging system aiming at delivering the payload directly to the pharmacological target.[1] There are multiple chemical options for the design of a nanoformulation using organic or inorganic compounds to generate nanoparticles. One example is the use of organic self-assembling phospholipids to formulate liposomal drug delivery systems,[2] such as the currently clinically applied formulation of doxorubicin (Caelyx), which is successfully used in the treatment of breast cancer.[3] Another example are silica mesoporous-based nanoparticles, which are forming large porous structures and are able to encapsulate a variety of therapeutics, such as small molecules, peptides, proteins, and genes.[4] Even if silica mesoporous nanoparticles allow surface modification,[5] they still exhibit some degree of toxicity, especially related to their size and shape.[6]

In order to overcome complicated synthetic strategies and undesired effects, chemists designed a wide spectrum of block copolymers with enhanced biocompatibility and self-assembling features to generate nanosized drug delivery systems.[7] Among them, poly(dimethylsiloxane)-poly-*b*-(methyloxazoline) (PDMS−PMOXA) has attracted attention due to its capability to form polymersomes with high biocompatibility and very low toxicity.[8,9] Due to their chemical properties, PDMS−PMOXA polymersomes can even be applied as a model system to test transmembrane transport, as demonstrated by Jaskiewic et al.[10,11] In addition, surface modification of PDMS−PMOXA polymersomes can be performed by applying straightforward approaches, as described previously.[9,12]

Received: May 17, 2018
Revised: September 4, 2018
Accepted: October 1, 2018
Published: October 1, 2018

DOI: 10.1021/acs.molpharmaceut.8b00521
Mol. Pharmaceutics 2018, 15, 4884−4897

However, the rational design of a nanoformulation not only considers encapsulation but also delivery and targeting. Efficient intracellular drug delivery has been shown for lipopeptide modified liposomal formulations where the cargo is placed into the intracellular space by membrane fusion.[13] Moreover, targeting moieties, such as antibodies, have previously been tested as a possibility to navigate nanoparticles in the human organism with enhanced accumulation in cells expressing the targeted epitope.[14,15] However, another approach to efficiently deliver bioactive compounds into targeted areas is inspired by the concept of prodrugs, where small molecules are enzymatically activated in close vicinity of the drug target.[16] Extending the concept would allow for the consideration of enzyme-triggered drug release of the formulated cargo as a process of bioactivation. However, such a concept in oncology would be based on enzymes with high activity in the microenvironment of malignant-transformed cells.

One enzyme family repeatedly reported to be highly active in the surrounding of malignant-transformed cells is the family of matrix metalloproteinases (MMPs). This family of zinc-dependent endopeptidases participates in various physiological functions, including angiogenesis, inflammation, reproduction, growth, and development, due to their proteolytic activity.[17] In the context of malignancies, MMPs are assumed to play a critical role in tumor progression, as they are capable of degrading the basement membrane, and therefore they provide space for tumor mass expansion and tumor cell evasion, leading to metastasis formation. Furthermore, MMPs are involved in neovascularization and angiogenesis in tumors.[18] The gelatinases matrix metalloproteinase 2 (MMP-2) and matrix metalloproteinase 9 (MMP-9) are part of the protein family of MMPs. Both, MMP-2 and, especially, MMP-9 participate in those actions. In detail, MMP-9 has been shown to directly influence tumor progression enhancing tumor cell invasiveness and thereby metastasis formation.[19,20] Furthermore, MMP-9 has been reported to promote angiogenesis[21,22] and inhibit T-lymphocytes.[23] Even if MMP-9 activates inhibitors of angiogenesis, such as tumstatin,[24] the overall effect is considered to be tumorigenic. Importantly, MMP-9 in the cancer microcompartment derives from different cell types, including the malignant-transformed cell itself, but also from surrounding stromal cells and locally invading inflammatory cells trying to battle the rogue cells.[25,26] Despite the versatility of the functions, there are reports associating MMP-9 expression and activity with breast cancer prognosis in humans,[27,28] thereby suggesting that this gelatinase could be used to design a nanoparticle with enzymatic drug release in this tumor entity. Notably, MMP-mediated drug release has previously been tested by others showing MMP-9-triggered release of therapeutics from silica nanoparticles,[29] from polymer−peptide conjugates,[30] from liposomes,[31] and from fiber-forming micelles.[32] Those studies underline the feasibility of using MMPs as a trigger for enzyme-triggered nanoformulations.

It is the aim of this study to synthesize and characterize PDMS−PMOXA polymersomes featuring MMP-9-triggered drug release for the treatment of breast cancer. As it is a prerequisite for the applicability, enhanced expression of MMP-9 mRNA was verified, comparing healthy and malignant-transformed breast tissue. After verification of expression, PDMS−PMOXA diblock copolymers were formulated as nanosized carriers loaded with paclitaxel. The surface was then modified using an MMP-9 sensitive peptide in order to enable the enzyme-triggered drug release. Our approach includes viability assays in cells and an investigation on pharmacological efficacy of our loaded polymersomes in xenografted zebrafish embryos.

EXPERIMENTAL SECTION

In Silico Analysis Using the GEO Database. Data sets including information about breast cancer were extracted from the GEO database (https://www.ncbi.nlm.nih.gov/geo/) using the following search terms: human, data expression profiling, and breast tissue. This search revealed 103 data sets. Studies reporting on 6 or more non-malignant-transformed tissue samples and at least 6 malignant-transformed tissue samples were selected for further analysis. Normalized data on the expression of MMP-9 were extracted and analyzed using GraphPad Prism (version 6, GraphPad Software Inc., La Jolla CA, USA).

Multiplex PCR for Gene Expression Analysis in Breast Cancer Samples. The basis for the determination of transcripts in breast cancer was the commercially obtained collection of cDNA (CSRT103, Origene, Rockville, USA). The number of transcripts was assessed by multiplex real-time PCR using the following TaqMan assays, Hs01032443_m1-VIC, Hs01548727_m1-ABY, Hs00234579_m1-FAM, and Hs00427620-m1-JUN, to quantify proliferation marker Ki-67 (Ki-67), MMP-2, MMP-9, and TATA-box binding protein (TBP), respectively. The reaction was carried out in a volume of 15 μL containing 0.75 μL of each TaqMan assay, 4.5 μL cDNA, 7.5 μL TaqMan multiplex Mastermix, and the ViiA 7 Real-Time PCR System as recommended by the manufacturer (Applied Biosystems, LubioSciences, Lucerne, Switzerland). For determination of copy numbers, a serial dilution of standards consisting of the cloned PCR amplicon was used. The number of transcripts in each sample was calculated by linear regression. The obtained data were analyzed using GraphPad Prism (version 6).

Immunohistochemical Staining of MMP-9 in Human Breast Cancer Tissue. The MMP-9 protein was detected in breast cancer using a commercially obtained array of paraffin-embedded tissue sections summarizing malignant-transformed and non-malignant-transformed samples of various tissues (MTU951, Pantomics, Richmond, USA). The tissue sections were first deparaffinized in two changes of xylol and then rehydrated in a decreasing ethanol series ranging from 96 to 50%, followed by a heat induced epitope retrieval in 0.1 M citrate buffer (pH = 6.0), and quenching of endogenous peroxidase with 3%-H_2O_2-methanol for 20 min. Then, the slides were exposed for 1 h to blocking solution (5%-FCS−1%-BSA−TBS-T). MMP-9 was detected with the primary anti-MMP-9-antibody (ab76003, abcam, Cambridge, UK, diluted 1:1000). After incubation overnight at 4 °C, the tissue slides were washed repeatedly in phosphate-buffered saline (PBS; 13.7 mM NaCl, 2.7 mM KCl, 8.1 mM Na_2HPO_4, 1.8 mM KH_2PO_4, pH adjusted to 7.4), followed by an incubation for 2 h with the secondary antibody (HRP-coupled goat anti-rabbit, 1:100, Bio-Rad, Cressier, Switzerland) at room temperature. After several washing steps in PBS, HRP was visualized with 1 mg/mL of diaminobenzidine (DAB) diluted in 0.05 M phosphate buffer containing 0.02% H_2O_2. Nuclei were stained with hematoxylin solution. Finally, the staining was examined by light microscopy, and images were taken using the Leica

DOI: 10.1021/acs.molpharmaceut.8b00521
Mol. Pharmaceutics 2018, 15, 4884−4897

DMi8 microscope (Leica, Heerbrugg, Switzerland) and the LAS software Version 4.6 (Leica).

Cell Culture. The breast cancer cell lines MDA-MB-468 (ATCC HTB-132) and MCF7 (ATCC HTB-22) were commercially obtained (American Tissue Culture Collection, Wesel, Germany). The cells were cultured in Dulbecco's modified Eagle medium (DMEM) (Sigma-Aldrich, Buchs, Switzerland) with an addition of (v/v) 10% fetal calf serum (FCS) (Sigma-Aldrich) and 1% GlutaMAX (BioConcept, Allschwil, Switzerland) at 37 °C in a humidified atmosphere with 5% CO_2.

Enrichment of Secreted Proteins in the Supernatant of Cultured Cells. To collect extracellular proteins, cells were seeded at a density of 1×10^6 cells/10 cm dish. At 80% confluence, growth medium was replaced by 10 mL of basal medium (DMEM−1% GlutaMAX) in order to avoid contamination with bovine serum proteins. After 24 h in culture, the culture supernatant was collected and supplemented with (w/v) 10% trichloric acid. After 15 min of equilibration on ice, the precipitated protein was collected by centrifugation for 20 min at 17 000*g* and 4 °C. Subsequently, the precipitate was washed twice with ice-cold acetone (5 mL). Then, the protein was air-dried for 30 min at room temperature, and finally solubilized in 6 M urea. Protein content was determined by the Bradford assay (Thermo Fischer, Reinach, Switzerland) following the manufacturer's instructions.

Zymography To Determine Gelatinase Activity in the Cell Culture Supernatant. Gelatinase activity was assessed by zymography. For this purpose, the protein samples were supplemented with nonreducing Laemmli-buffer (8% sodium dodecyl sulfate (SDS), 40% glycerol, bromophenol blue in 1 M Tris-HCl, pH 6.8) and then separated by SDS-10% PAGE, where the gel contained 0.7 mg/mL gelatin. After PAGE, the gels were washed three times for 10 min at room temperature under constant shaking with wash buffer I (2.5% Triton-X-100, 10 mM $CaCl_2$, 1 μM $ZnCl_2$, and 30.5 mM sodium azide in 50 mM Tris-HCl, pH 7.5). To allow the gelatinases to digest the gelatin, the gels were incubated for 24 h at 37 °C in wash buffer II (1% Triton-X-100, 10 mM $CaCl_2$, 1 μM $ZnCl_2$, and 30.5 mM sodium azide in 50 mM Tris-HCl, pH 7.5). Subsequently, the gels were stained with Coomassie Blue (0.5 Vol-% Coomassie Brilliant Blue R-250, 10% acetic acid, and 30% ethanol) for 24 h at room temperature and then destained in 10% acetic acid−30% ethanol. Finally, the staining of the zymogram was imaged and digitized with the ChemiDoc MP (Bio-Rad).

Western Blot Analysis. Prior to separation by SDS-PAGE, protein samples were supplemented with Laemmli-buffer (Sigma-Aldrich) and heated to 95 °C for 5 min. The samples were then separated by SDS-PAGE using the Mini Trans-Blot Cell (Bio-Rad) and blotted onto a nitrocellulose membrane (GE Healthcare, Glattbrug, Switzerland). The blot was first stained with Ponceau S (Sigma-Aldrich) followed by incubation with 5%-FCS−0.1%-BSA−TBS-T for at least 1 h. The respective primary antibody (MMP-9: ab76003 (1:3000), abcam; mKate2: ab233 (1:3000), Evrogen, Moscow, Russia; actin: sc-1616 (1:1000), Santa Cruz Biotechnology, Dallas, TX, USA) was incubated overnight at 4 °C, followed by three washing steps with TBS-T, an hour incubation with the respective secondary horseradish-peroxidase-coupled antibody and additional washings with TBS-T. The secondary HRP-coupled antibody was then visualized by chemiluminescence of the ECL Plus Solutions A and B (Thermo Scientific), and images were taken using the ChemiDoc MP and the Image Lab Software (Bio-Rad).

Synthesis of Carboxyl-Terminated and *N*-Hydroxysuccinimide (NHS)-Activated Poly(dimethylsiloxane)-*b*-poly(methyloxazoline). The synthesis of the *N*-hydroxysuccinimide (NHS)-activated polymer was performed as previously described.[12] Briefly, a solution of 15.6 μmol (101.40 mg) poly(dimethylsiloxane)-*b*-poly(methyloxazoline) (PDMS−PMOXA; M_n = 5000-*b*-1300, PDI = 1.25, Polymer Source Inc., Quebec, Canada) in 5 mL of dichloromethane was prepared in a round-bottom flask. After cooling the mixture to 4 °C in an ice bath, 87.4 μmol (8.75 mg) succinic anhydride, 15.6 μmol (1.91 mg) dimethylamino pyridine (DMAP), and 79.5 μmol (11 μL) of triethylamine (TEA) were slowly added. After removal from the ice bath, the reaction was carried out overnight at room temperature. The final compound was purified by ultrafiltration for 24 h (membrane MWCO of 1 kDa, Spectrapor, Breda, Netherlands). After recovery of the carboxy-modified PDMS−PMOXA in a quantitative yield, the structure was confirmed performing Fourier transform infrared (FT-IR) spectroscopy. Briefly, 1 mg of the compound was placed on the diamond crystal for analysis and measured in the ALPHA FT-IR spectrometer Platinum ATR with a single reflection diamond (Bruker, Fälladen, Switzerland). Data were analyzed using the OPUS software version 6.3 (Bruker). Subsequently, the final product was dissolved in 5 mL of dichloromethane in a round-bottom flask and cooled to 4 °C. Then, 65.4 μmol (10.2 mg) 1-ethyl-3-(3-(dimethylamino)-propyl) carbodiimide (EDAC) and 100 μmol (11.5 mg) NHS were added. The reaction was then carried out overnight at room temperature. The final compound was recovered by performing dialysis for 24 h in dichloromethane. NHS-activated PDMS−PMOXA was obtained in a quantitative yield; the modification was confirmed again by FT-IR analysis.

Formulation of PDMS−PMOXA Polymersomes Loaded with Paclitaxel and Coated with the SRL-Peptide. Paclitaxel-loaded polymersomes were formulated by applying the thin film technique.[33] In detail, 0.55 μmol (3.5 mg) of PDMS−PMOXA−OH and 0.23 μmol (1.5 mg) of PDMS−PMOXA−NHS were dissolved in dichloromethane. Then, 100 μL of paclitaxel (10 mg/mL, Medchemtronica AB, Stockholm, Sweden) in dichloromethane was added, followed by thin film formation using a rotary evaporator at reduced pressure (rotational speed: 120 rpm). Next, the film was dried for 20 min at high vacuum and then hydrated in 1 mL of PBS. Polymersomes were formed after a brief sonication for 30 s in an ultrasound water bath, followed by a series of extrusions (9 times each) using polycarbonate membranes with a pore size of 400, 200, and 100 nm, respectively. To a suspension of 1 mg/mL of polymersomes in PBS, 10 μL of 4.7 mM *p*-maleimidophenyl isocyanate (PMPI) in DMSO was added, and the solution was stirred for 8 h at room temperature to allow for the modification of the polymersome surface. The custom synthesized peptide Fmoc-Ahx-SRLSLPGC (Ahx = aminocaproic acid; Biomatik, Cambridge, Ontario, Canada) was deprotected. In detail, the 10.6 μmol (10 mg) peptide was dissolved in 300 μL of dimethylformamide (DMF), and then 0.77 μmol (76 μL) piperidine was added to the solution, followed by stirring for 1 h at room temperature. The deprotected peptide was recovered by precipitation in cold ether. The white crystalline precipitate was then dissolved in PBS to a final concentration of 10 mg/mL. Ten microliters of

DOI: 10.1021/acs.molpharmaceut.8b00521
Mol. Pharmaceutics 2018, 15, 4884−4897

the deprotected peptide and 10 μL of EDAC (10 mg/mL) in Milli-Q water were added to 1 mL of the polymersome solution (5 mg/mL) and then stirred overnight at room temperature. Finally, the modified and loaded polymersomes were purified for 1 h by ultrafiltration (MWCO 12−14 kDa, Spectrapor) at room temperature against PBS. The amount of peptide cross-linked to the surface of polymersomes was determined by a bicinchoninic acid assay (BCA, Thermo Fisher, Reinach, Switzerland) using 25 μL of polymersomes and the infinite 200 Pro (Tecan, Männedorf, Switzerland) as recommended by the manufacturer.

Assessment of Hydrodynamic Radius and Surface Charge of the Polymersomes. The hydrodynamic radius of the polymersomes was measured by the dynamic light scattering (DLS) technique using the Malvern Zetasizer NanoSeries (Malvern Instruments GmbH, Herrenberg, Germany). Samples were first degassed using the Thermo Vac sample degassing and thermostat system (MicroCal, Malvern Instruments GmbH). Aliquots of 40 μL were loaded in disposable plastic cuvettes and were analyzed at 25 °C after 2 min of equilibration. The Zetasizer software version 7.11 was applied (Malvern Instruments GmbH). A laser light with a backscattering angle of 173° was used. For determination of the surface charge, 5 μL of the polymersome suspension (5 mg/mL) was diluted in 795 μL of Milli-Q water and loaded in capillary-folded disposable cuvettes equipped with gold electrodes. The zeta potential was measured with the Malvern Zetasizer NanoSeries. Data were analyzed using the Zetasizer software (Malvern), the CONTIN algorithm, and bt applying the Smoluchowsky equation.[34]

Determination of the Encapsulation Efficiency. The encapsulation efficiency was determined by HPLC analysis. To disrupt the SRL-modified polymersome membrane, triton-X (Merck, Zug, Switzerland) and acetonitrile (VWR International, Dietikon, Switzerland) were added to the polymersomes. Specifically, 25 μL of 5 mg/mL polymersome (theoretically containing 1 mg/mL paclitaxel), 25 μL of 0.4% triton-X in water, and 50 μL of acetonitrile were combined, vortexed, and centrifuged for 3 min at 8000 rpm. The amount of paclitaxel was determined by HPLC (Agilent 1100 equipped with an diode array and evaporating light scattering detector, Agilent Technologies, Basel, Switzerland) using ddH_2O (buffer A) and acetonitrile (buffer B, VWR International, Dietikon, Switzerland) and a Poroschell C18 column (3.0 mm × 100 mm 2.7-μm, Agilent Technologies, Basel, Switzerland). The starting conditions were 50% A, 50% B, shifting from min 1 to 11 to 0% A, 100% B, with a flow rate of 0.45 mL/min. Paclitaxel was eluting after 5.0 min. The concentration of encapsulated paclitaxel was calculated using a standard curve (AUC versus concentration).

Preparation of Fluorescent Polymersomes. Fluorescently labeled polymersomes were generated by incorporating 3,3′-dioctadecyloxacarbocianine perchlorate (DiO, Sigma-Aldrich) into the polymersome membranes. Briefly, a stock solution of 25 mg/mL DiO in ethanol was prepared, and 5 μL of this solution was added to the dichloromethane solution of PDMS−PMOXA. After the thin film formation under vacuum and rehydration in PBS, polymersomes were prepared as described above.

Generation of mKate2-Expressing MCF7 Cells. The coding sequence of mKate2 (pmKate2-N vector, Evrogen) was transferred into pcDNA3.1-Hygro using the restriction enzymes *Bam*HI and *NotI* (Fast Digest Enzymes, Thermo Scientific). After sequence verification (Microsynth, Balgach, Switzerland), the plasmid was transfected in MCF7 cells using the JETprime transfection reagent (0.5 μL/μg DNA, Polyplus, Illkirch-Graffenstaden, France) according to the manufacturer's instructions. Single-cell clones were cultivated in the presence of 300 ng/mL hygromycin. Expression of mKate2-fluorescence was monitored with the Infinite M200Pro (Tecan; excitation 588 nm/emission 633 nm) or by fluorescence microscopy (Leica).

Determination of Cellular Doubling Time. To determine the doubling time, 50 000 cells/well were seeded on 12-well plates. The number of cells was quantified 24, 48, 72, and 96 h post seeding using the CASYton cell counter (OLS GmbH & Co, Bremen, Germany). Furthermore, the fluorescence signal was measured using the Infinite M200Pro plate reader (Tecan) to correlate the cell number to the fluorescent signal. All measurements were performed in biological and technical triplicates.

Assessment of Cellular Viability of Breast Cancer Cell-Lines. MCF7 cells were seeded at a density of 7500 cells/well in 96-well plates. One day after seeding, the cells were exposed for 48 h to a serial dilution of the polymersomes or paclitaxel in culture medium. The solvent DMSO served as control in all experiments. In order to determine the influence of MMP-activity, paclitaxel-loaded polymersomes were tested for their influence on cell viability in the presence or absence of 40 nM of MMP-2-inhibitor (Calbiochem MMP-2 Inhibitor IV, Sigma-Aldrich) and 40 nM MMP-9-inhibitor (Calbiochem MMP-9 Inhibitor I, Sigma-Aldrich). After 48 h in culture, cell viability was determined using the Resazurin Fluorometric Cell Viability Kit (PromoCell GmbH, Heidelberg, Germany). Here, viable cells mediate the metabolism of resazurin to resafurin, which is fluorescent. Fluorescence was detected using the Infinite M200Pro plate reader (Tecan; excitation = 530 nm, emission = 590 nm). Viability was calculated as the fold of the solvent control after subtracting the fluorescence of the medium control, as follows:

$$\text{fold of control} = \frac{\text{sample} - \text{control medium}}{\text{control} - \text{control medium}}$$

The inhibitory potency was estimated by nonlinear curve fitting of the normalized values using the GraphPad Prism software (version 6).

Hematoxylin−Eosin Staining of Cultured Cells. MCF7 were seeded at a density of 100 000 cells/well on coverslips prepared in 12-well plates. One day after being seeded, paclitaxel (2.5, 10, or 25 μM final concentration) was added. After 48 h of incubation, the cells were fixed for 20 min in 50% methanol in acetone, followed by 15 min of nuclei staining with Hemalum solution acid according to Mayer (Carl Roth GmbH, Arlesheim, Switzerland). Then, the cells were washed once in distilled water and rinsed in tap water for 10 min, followed by 1 min incubation with Eosin Y (Carl Roth GmbH), 0.15% (w/v) in acidified 75% ethanol. Finally, the cells were dehydrated with an increasing ethanol series ranging from 80 to 100% (2 min each), followed by a 2 min incubation in xylene. The coverslips were mounted on slides using Roti-Histokitt II (Carl Roth GmbH). Images were taken with the Leica DMi8 microscope.

***Danio rerio* Husbandry Conditions.** *Danio rerio* (zebrafish) experiments were performed under license number 1024H. Fish were maintained under a cycle of 14 h of light and 10 h of darkness in dedicated water tanks and were fed

DOI: 10.1021/acs.molpharmaceut.8b00521
Mol. Pharmaceutics 2018, 15, 4884−4897

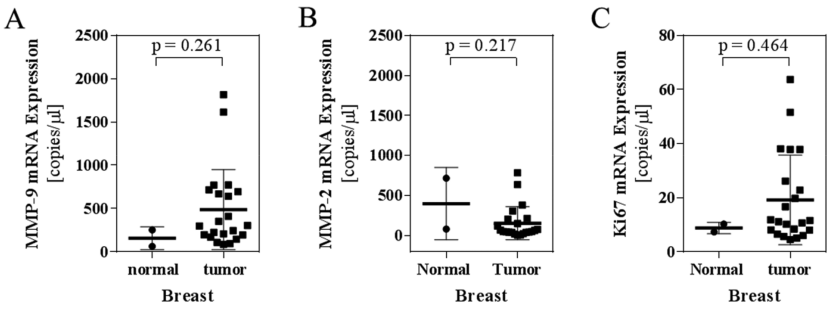

Figure 1. Comparison of MMP-9 mRNA expression in normal and malignant-transformed breast tissue. The amount of mRNA was determined in malignant and non-malignant-transformed human breast tissue. The number of copies of MMP-9 (A), MMP-2 (A), and the proliferation marker Ki-67 (C) was assessed . Data are shown as mean ± SD; each point represents the number of copies detected in 1 µL of commercially obtained cDNA of one individual. Mann−Whitney test.

once a day. Following fertilization, embryos were collected and maintained in E3 medium (5 mM NaCl, 0.17 mM KCl, 0.33 mM $CaCl_2$, and 0.33 mM $MgSO_4$) at 29 °C until injection on day 2 post fertilization (dpf).

Xenografting of Zebrafish Embryos. Tübingen zebrafish embryos at 2 dpf were dechorionated for 8 min at 37 °C in a solution of 1 mg/mL pronase (Roche, Basel, Switzerland) in E3 medium. After exposure, the embryos were extensively washed in E3 medium. After the dechorionated fish were anesthetized with tricaine (0.003%, MS222, Sigma-Aldrich), mKate2-MCF7 cells were injected. All experiments were terminated at 6 dpf with an overdose of tricaine. For xenografting, mKate2-MCF7 breast cancer cells were injected in the posterior region of the yolk of an anesthetized zebrafish embryo. Briefly, cells were trypsinized (Sigma-Aldrich) and washed with culture medium. Thereafter, pelleted cells were resuspended in 500 µL of culture medium and loaded in a microcapillary injection needle connected to the pneumatic picopump PV830 (WPI Europe, Berlin, Germany), and 50 cells per embryo were injected. Following the grafting, zebrafish embryos were recovered in fresh E3 medium for at least 1 h prior to proceeding with further experiments (imaging or injection of polymersomes).

Injection and Visualization of Polymersomes in Zebrafish Embryos. At 2 dpf, zebrafish embryos, *Tg*(kdrl:mKate2-CAAX) for fluorescent polymersomes or Tübingen zebrafish for xenografted embryos, were anesthetized in 0.003% tricaine (Sigma-Aldrich) and bleached in 0.003% phenyl thiourea (PTU, TCI Europe, Zwjindrecht, Belgium), after being suspended in E3 medium. After being embedded in 0.7% low melting agarose (Carl Roth), 1 nL of a suspension of DiO-labeled polymersomes or PDMS−PMOXA−SRL−paclitaxel were injected in the common cardinal vein (CCV) using the pneumatic picopump PV830 (WPI Europe). Zebrafish were then recovered in fresh E3 medium before proceeding with laser confocal scanning microscopy analysis with the Zeiss LSM 880 with Airyscan (Zeiss, Oberkochen, Germany) of anesthetized and then immobilized embryos. Imaging was conducted 1 h after polymersome injection or 1 day after xenografting using a 10× plan APO objective with a numerical aperture of 0.45 and the 488 and 555 nm lasers. Images were generated with ImageJ2.[35]

Real-Time PCR To Determine mKate2 Expression. After injection of mKate2-expressing breast cancer cells, the amount of xenografted cells was quantified by applying real-time PCR. Briefly, mRNA was extracted from the zebrafish 4 days after xenografting using the PeqGold extraction kit (AxonLab, Baden, Switzerland). The resulting mRNA was reverse-transcribed using the Multiscribe reverse transcriptase (Applied Biosystem, Thermo Fischer, Zug, Switzerland). The amount of mKate2 mRNA was determined using the following primers, mKate2-for 5′-TGTACGGCAGCAAAACCTTC-3′ and mKate2-rev 5′-ACTCTCTCCCATGTGAAGCC-3′ (Microsynth), and the SYBR Green PCR Master Mix (Thermo Fisher). The reaction and analysis by applying a serial dilution of the PCR-product was carried out as described above.

Statistical Analysis. Statistical analysis was performed using the data of at least 3 independent experiments, the GraphPad prisms software (version 6, GraphPad Software Inc., La Jolla, CA, USA), and the respective statistical test mentioned in the context of the data report. A *p*-value below 0.05 was considered statistically significant.

RESULTS

Comparison of MMP-9 mRNA Expression in Normal and Malignant-Transformed Breast Tissue. Expression of gelatinases in human breast cancer tissue was assessed determining the amount of mRNA by quantitative real-time PCR in commercially obtained samples. As shown in Figure 1A, we observed a trend for higher expression of MMP-9 in malignant-transformed tissue compared to normal breast tissue (mean copy numbers ± SD; non-malignant-transformed vs malignant-transformed; 157.7 ± 132, n = 2 vs 487.4 ± 462, n = 22; Mann−Whitney test, p = 0.261). Particularly in malignant-transformed tissue, there was high interindividual variability in MMP-9 expression, which was also seen by assessing the amount of Ki-67, a marker of cellular proliferation. Further analysis considering the reported tumor stage and tumor grade suggested that even if not statistically significant, there might be an influence of higher tumor grade on MMP-9 expression (Supporting Information (SI), Figures 1A and S1D). Assessing expression of MMP-9 by immunohistochemical staining of breast cancer samples further supported the finding of MMP-9 being associated with the development of breast cancer (Figure S2). In order to verify the notion, we analyzed publicly available expression data gathered in larger populations. Searching for data sets containing at least six data points in each group revealed five data sets, which were further analyzed. As shown in Figure S3 and Table S1, all GEO data sets (GDS 2250, GDS 4114, GSE 45827, and GSE 28884), despite one (GSE 65194), meeting the search criteria showed significantaly higher MMP-9 expression in malignant-transformed tissue

DOI: 10.1021/acs.molpharmaceut.8b00521
Mol. Pharmaceutics 2018, 15, 4884−4897

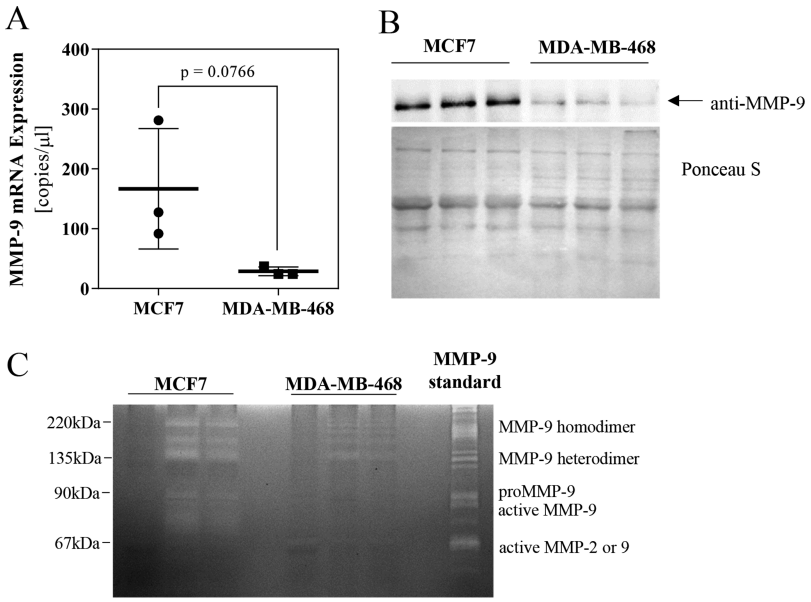

Figure 2. Characterization of MMP-9 expression and activity in commonly applied cellular models of breast cancer. (A) MMP-9 mRNA expression in an ER-negative (MCF7) and in an ER-positive (MDA-MB468) cell line (n = 3 independent samples, Kruskal–Wallis test). (B) Western blot analysis of extracellular MMP-9 in enriched cell culture supernatant. Ponceau S staining of separated and transferred proteins served as the loading control. (C) Gelatin-zymography showing gelatinase activity in cell culture supernatant comparing MCF7 and MDA-MB-468 cells. Recombinant MMP-9 is the MMP-9 standard that served as the control.

compared to normal breast tissue, thereby consolidating our findings. In detail, GDS 2250 (non-malignant-transformed, n = 7; malignant-transformed, n = 8) summarizing data on basal- and nonbasal-like breast cancer showed a significant difference between cancer tissue and normal tissue ($p < 0.0001$; mean ± SD; nonmalignant vs malignant, 5.858 ± 1.298 vs 8.91 ± 1.547). GDS 4114, analyzing the stroma associated with invasive breast tumors (non-malignant-transformed, n = 6; malignant-transformed, n = 6), also revealed this difference in MMP-9-mRNA expression. GSE 45827 compares normal tissue and primary breast cancer samples (non-malignant-transformed, n = 11; malignant-transformed, n = 141), concluding in a significant increase in MMP-9-mRNA-expression in malignant-transformed breast tissue. Furthermore, GDS 28884, which contained data on basal-like carcinoma and invasive ductal carcinoma (normal breast tissues, n = 11; noninvasive, n = 17; and invasive breast carcinomas, n = 151), described for both, invasive and noninvasive breast tissue, had a significantly higher MMP-9-mRNA-expression compared to normal breast tissue. However, GSE 65194 (non-malignant-transformed, n = 11; malignant-transformed, n = 153) showed no significant difference between normal and malignant-transformed breast tissue.

Characterization of Cell Models of Human Breast Cancer. We selected two cell models of human breast cancer, namely, the estrogen receptor (ER) positive MCF7 and the ER negative MDA-MB-468 cells, and characterized them for expression and function of MMP-9. Quantification of MMP-9-mRNA revealed a trend to higher amounts of MMP-9 mRNA in MCF7 compared to MDA-MB-468 (mean copy numbers ± SD; MCF7 vs MDA-MB-468; 166.9 ± 100.6, n = 3, vs 28.7 ± 7.3, n = 3; Mann–Whitney test; p= 0.077; Figure 2A). However, MMP-9 mRNA encodes for a pro-enzyme, which is proteolytically activated prior to cellular excretion,[36] and the concept of the herein synthesized and characterized polymersomes is based on the extracellular activity of the gelatinase. Accordingly, we quantified the amount of MMP-9 in the supernatant of cultured cells (secretome). As shown in Figure 2B and C, we observed significantly higher amounts and activity of MMP-9 detected by Western blot analysis and zymography, respectively.

Synthesis and Characterization of the Paclitaxel-Loaded and SRL-Modified PDMS–PMOXA Polymersomes. PDMS–PMOXA polymersomes were formulated by rehydrating the thin film of PDMS–PMOXA in PBS, followed by a series of extrusions applying polycarbonate membranes. After formulation, the surface was modified by covalently binding the MMP-9 cleavable SRL-peptide to the polymer chains using a standard coupling approach and Michael addition chemistry (Figure 3A,B). For the loading of paclitaxel, the polymersomes were formed in the presence of this active compound. For all polymeric formulations (loaded and nonloaded polymersomes), the hydrodynamic diameter was assessed prior to and after peptide surface modification. Surface modification of PDMS–PMOXA polymersomes did not significantly change the diameter of the polymersomes (mean diameter ± SD; PDMS–PMOXA, 138.78 ± 3.99 nm, vs PDMS–PMOXA–SRL, 138.10 ± 25.91 nm; n = 6 independent experiments; $p > 0.05$; unpaired t-test) (compare Figure S4). Similar results were obtained for paclitaxel-loaded polymersomes (mean diameter ± SD; PDMS–PMOXA–paclitaxel vs PDMS–PMOXA–SRL–paclitaxel, 189.57 ± 32.66 nm vs 459.53 ± 14.66 nm; unpaired t-test; $p > 0.05$ for n = 6 independent experiments; Figure S4). However, statistically significant changes in size distribution were observed upon loading when comparing surface-modified

DOI: 10.1021/acs.molpharmaceut.8b00521
Mol. Pharmaceutics 2018, 15, 4884–4897

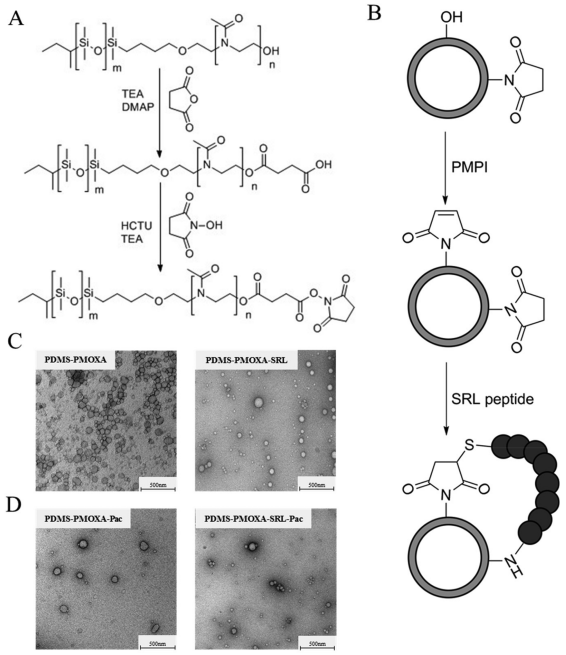

Figure 3. Synthesis and characterization of MMP-9-labile polymersomes loaded with paclitaxel. (A) Schematic depicting the chemical modification of PDMS−PMOXA with succinic anhydride and subsequent activation with NHS. (B) Schematic depicting the design of the polymersome with the SRL-peptide surface modification after thin film formulation. TEM of PDMS−PMOXA polymersomes before (C) and after paclitaxel loading (D). Scale bar: 500 nm.

(PDMS−PMOXA−SRL vs PDMS−PMOXA−SRL−paclitaxel; $n = 6$; $p < 0.05$; unpaired *t*-test) or unmodified polymersomes (PDMS−PMOXA vs PDMS−PMOXA−paclitaxel; $n = 6$; $p < 0.05$; unpaired *t*-test). Figure S4 shows an almost Gaussian distribution of the assessed diameter at day 1 for all but the PDMS−PMOXA−SRL−paclitaxel polymersomes, suggesting a perturbation of the structure for the latter. Testing the stability of all polymersomes revealed the most pronounced changes in size distribution for PDMS−PMOXA−paclitaxel without SRL surface modification (PDMS−PMOXA−paclitaxel day 1 vs day 10; 159.87 ± 1.27 nm vs 200.80 ± 5.43 nm; $n = 3$; $p < 0.05$; unpaired *t*-test). However, for both formulations loaded with paclitaxel, a significant change in diameter was observed after 10 days of storage. While the unmodified polymersomes significantly increased in size (about 25%), the surface-modified particles shrank by about 20% (PDMS−PMOXA−SRL−paclitaxel day 1 vs day 10; 459.53 ± 14.66 nm vs 368.50 ± 16.31 nm; $n = 3$; $p < 0.05$; unpaired *t*-test). The notion of a different size distribution at day 1 was confirmed by transmission electron microscopy (TEM) (Figure 3C,D), where the paclitaxel-loaded polymersomes exhibited more disperse structures, while the other formulations appeared spherical. The PDMS−PMOXA−SRL polymersomes loaded with paclitaxel kept their spherical form but appeared to aggregate. No significant changes in diameter were observed in unloaded polymersomes (PDMS−PMOXA day 1 vs day 10; 141.33 ± 3.40 nm vs 143.80 ± 3.39 nm; PDMS−PMOXA−SRL day 1 vs day 10; 115.23 ± 2.16 nm vs 117.97 ± 3.39 nm; $n = 3$; $p < 0.05$; unpaired *t*-test). Finally, determination of the surface charge revealed an initial zeta-potential of −30.1 ± 0.7 mV for PDMS−PMOXA polymersomes, which significantly changed to −20.7 ± 3.2 mV after SRL-peptide coupling (PDMS−PMOXA vs PDMS−PMOXA−SRL; $n = 3$ independent experiments; $p < 0.05$; unpaired *t*-test). For polymersomes loaded with paclitaxel, a surface charge of −27 ± 0.6 mV was observed, which tended to neutrality after the SRL-peptide coupling of 0.04 ± 0.007 mV (PDMS−PMOXA−paclitaxel vs PDMS−PMOXA−SRL−paclitaxel; $n = 3$; $p < 0.05$; unpaired *t*-test). The encapsulation efficacy of PDMS−PMOXA−SRL polymersomes averaged at 47.97%.

Influence of PDMS−PMOXA−SRL−Paclitaxel Polymersomes on Cellular Viability. The formulation (stock solution: 1 mg/mL) was tested for antiproliferative activity in MCF7 cells. At first, the antiproliferative effect of paclitaxel in MCF7 cells was verified revealing an IC_{50} of 10.74 nM (CI 4.09−28.21 nM, Figure 4A,B). Subsequent comparison of PDMS−PMOXA−SRL−paclitaxel and PDMS−PMOXA−SRL polymersomes as the control demonstrated an antiproliferative activity of the paclitaxel-loaded polymersomes. Assessment of concentration dependency revealed no significant influence on cellular viability in the presence of the PDMS−PMOXA−SRL (Figure 4C) but showed a cytotoxic effect of PDMS−PMOXA−SRL−paclitaxel with an IC_{50} of 50.94 ng/mL (CI 22.1−117.3 ng/mL, Figure 4D). Considering the observed encapsulation efficacy in PDMS−PMOXA−SRL−paclitaxel, the polymersomes exhibited an inhibitory potency comparable to paclitaxel alone. The estimated IC_{50} of encapsulated paclitaxel was 11.93 nM (CI 5.18−27.47 nM). The influence of gelatinase activity on the cytotoxic effect of the formulation was verified exposing MCF7 cells to the SRL−paclitaxel polymersomes pretreated with synthetic MMP-9 in the presence and absence of the Calbiochem MMP-9 inhibitor I (40 nM) and/or the Calbiochem MMP-2 inhibitor IV (40 nM). As shown in Figure 5, the cell viability was significantly higher in the presence of the MMP-inhibitors, supporting the idea of a release mechanism that is triggered by MMPs. The obtained data suggest that the mechanism allowing release of paclitaxel is enhanced in the presence of MMPs, leading to a stagnation of cell growth. By using MMP-2 and -9 inhibitors during the cell viability assays, MMPs were identified as contributor to the enzyme-modulated release of paclitaxel from our polymersomes. However, comparing the viability of cells treated with polymersomes (mean viability fold of control ± SD; 0.86 ± 0.08), polymersomes with the MMP-2 inhibitor (1.16 ± 0.10), polymersomes with the MMP-9 inhibitor (1.24 ± 0.15), and polymersomes with the MMP-2 and MMP-9 inhibitors (1.01 ± 0.14) suggested that both MMP-2 and MMP-9 contribute to the release of paclitaxel from the polymersomes.

Generation and Characterization of mKate2-MCF7 Cells. In the next step, we aimed to apply a cancer model of xenografted *Danio rerio* to test the antiproliferative activity of the herein synthesized polymersomes. Prior to xenotransplantation, mKate2-MCF7 cells were generated and characterized. As shown in Figures 6A and Figure S5, the cells expressed high amounts of the fluorescent protein. Stably transfected cells are commonly cultured under constant selection. In order to determine whether the lack of selection pressure, as it will occur after xenotransplantation, influences the expression of mKate2, we investigated the influence of hygromycin on the fluorescence of cultured cells. This analysis revealed no

DOI: 10.1021/acs.molpharmaceut.8b00521
Mol. Pharmaceutics 2018, 15, 4884−4897

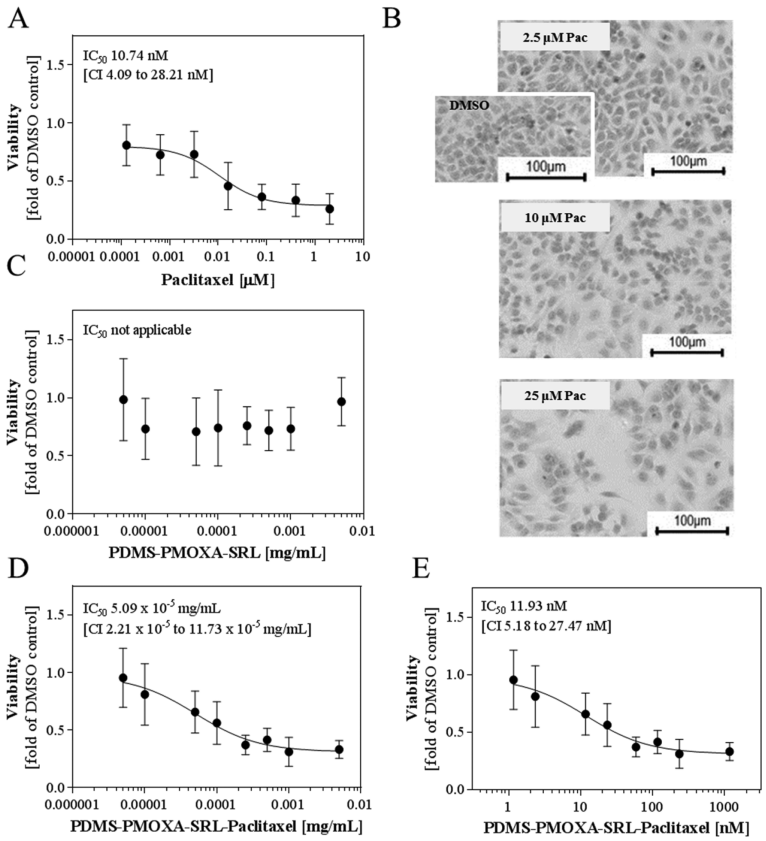

Figure 4. Influence of paclitaxel and paclitaxel polymersomes on cellular viability of MCF7 cells. The influence of increasing concentrations of paclitaxel on cellular viability was determined (A). The loss of cells was verified by hematoxylin−eosin staining of MCF7 cells exposed to the cytotoxic compound (B). MCF7 cells were exposed to increasing amounts of the surface-modified polymersomes (C) and PDMS−PMOXA−SRL−paclitaxel polymersomes (D). Considering the encapsulation efficacy, the PDMS−PMOXA−SRL−paclitaxel polymersomes exhibited a similar inhibitor potency (E) as paclitaxel (A). Data are shown as mean ± SD of $n = 3$ independent experiments. The IC_{50}-values were estimated by nonlinear regression.

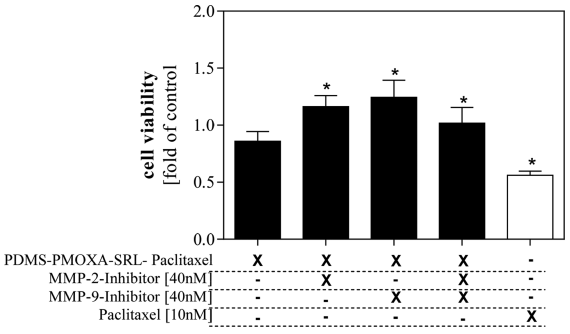

Figure 5. Effect of MMP-inhibitors on the cytotoxic effect of the PDMS−PMOXA−SRL−paclitaxel. The cellular viability of MCF7 cells was determined in the presence and absence of the MMP-2 and/or MMP-9 inhibitor. Data are shown as mean ± SD of $n = 3$ independent experiments. *$p < 0.05$. One-way ANOVA with Dunnett's multiple comparisons test.

significant difference by comparing cells with and without hygromycin selection (Figure 6B). The same result was obtained by assessing the amount of mKate2 by Western blot analysis (SI Figure 6). Furthermore, and more importantly, the expression of mKate2 did not significantly influence the doubling time of the transfected cells (Figure 6C).

Distribution of Polymersomes in Zebrafish Embryos. The distribution of fluorescently labeled (DiO) PDMS−PMOXA−SRL and unmodified PDMS−PMOXA polymersomes was assessed in a transgenic zebrafish line expressing the fluorescent protein mKate2 in the vasculature (*Tg*(kdrl:mkate2-CAAX)). Following injection of the DiO-labeled polymersomes, the distribution was inspected microscopically (Figure 7A,B).

For both formulations, a similar behavior was observed after injection. Both SRL-modified and unmodified PDMS−PMOXA polymersomes were circulating and exhibited enrichment in the region of the embryo's liver and agglomerates of fluorescent polymersomes in the caudal vein plexus, suggesting uptake of these polymersomes by immune cells. The aggregates did not influence the movement of the fluorescently labeled polymersomes in the zebrafish's vasculature.

Influence of PDMS−PMOXA−SRL−Paclitaxel Polymersomes on MCF7-Xenografted Zebrafish. MCF7-mKate 2 cells were used to xenograft wild-type zebrafish

DOI: 10.1021/acs.molpharmaceut.8b00521
Mol. Pharmaceutics 2018, 15, 4884−4897

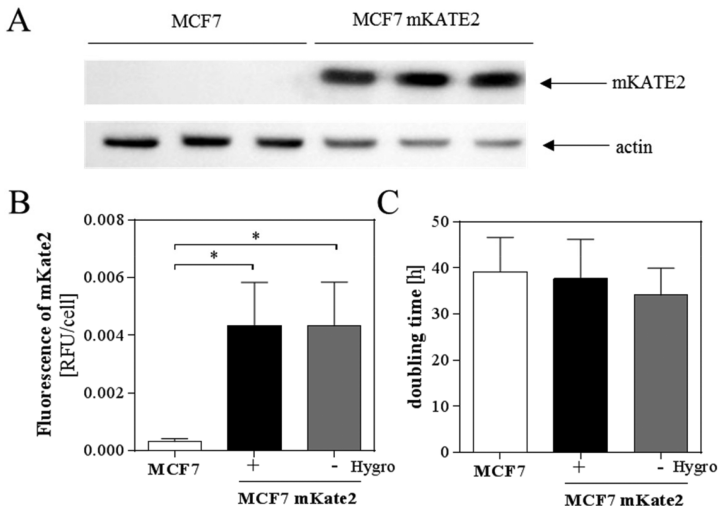

Figure 6. Establishment and characterization of stably transfected fluorescent MCF7-cells. Expression of the fluorescent protein was verified by Western blot analysis (A) comparing stably transfected and nontransfected MCF7 cells. The influence of hygromycin on mKate2 fluorescence/cell (B) and doubling time (C) was assessed in cultured cells. Data are shown as mean ± SD of $n = 3$ independent experiments. *$p < 0.05$. One-way ANOVA with Tukey's multiple comparisons test.

embryos at 2 dpf. After recovery overnight, the xenografted zebrafish were imaged by fluorescent microscopy. As shown in Figure 7C, the fluorescent MCF7 cells were enriched in the posterior region of the yolk. Moreover, cell clusters were observed in the tail (Figure 7C2). In order to assess the antitumor activity of the PDMS−PMOXA−SRL−paclitaxel polymersomes, the amount of mKate2-mRNA was determined by quantitative real-time PCR (Figure 7D). Quantification of mKate2 copies revealed that embryos treated with the active compound paclitaxel showed a significantly decreased amount of fluorescent cells compared to untreated embryos. Similar results were obtained for the formulated paclitaxel (mean copies/fish ± SD; untreated vs paclitaxel vs PDMS−PMOXA−SRL−paclitaxel; 2512 ± 468 vs 34.67 ± 19.14 vs 105.3 ± 46.29; $n = 3$ independent experiments; $p < 0.05$; one-way ANOVA with Tukey's multiple comparisons test).

■ DISCUSSION

Taken together, we are reporting the increased expression of MMP-9 in human breast cancer. Indeed, comparing mRNA expression in patient-derived breast cancer tissues with non-malignant-transformed breast tissue revealed a trend toward higher expression of the gelatinase. This observation was verified using publicly available expression data reporting on larger populations. Our finding on increased MMP-9 mRNA expression in breast cancer tissue is in accordance with a report by Zhang et al., showing a link between MMP-9 mRNA amount and tumor size (T staging) or the formation of lymph node metastasis (N staging). Notably, no difference between histological type (ductal vs lobular) and MMP-9 expression was observed in their study.[37] Furthermore, Tang et al. report an association of the MMP-9 protein amount detected by immunohistochemistry with clinicopathological parameters.[38] Notably, increased expression of MMP-9 in breast cancer has been linked to patient outcome (overall survival rate).[38−40] Even though breast malignancies summarize multiple cancer phenotypes, the enhanced expression of MMP-9 in the tumor microenvironment makes it a potential target tissue for the herein investigated PDMS−PMOXA−SRL−paclitaxel polymersomes. In order to test the functionality of the investigated formulation in vitro, we searched for a suitable cell-based test system. Assessing two commonly used cell lines, namely, the ER-positive MCF7 and the ER-negative MDA-MB-468, for MMP-9 expression and activity showed significantly higher amounts of the enzyme in MCF7 cells (Figure 2). Our findings are in accordance with those published by Yousef et al. reporting the expression of MMP-9 in multiple breast cancer cell lines.[39] However, there are reports suggesting that gelatinases are not present in breast cancer cell lines,[41] while others show expression and activity.[42] Bachmeier et al. even reported much higher expression of the gelatinases in MDA-MB-468 compared to MCF7 cells.[43] Taken into account that the expression of MMPs is modulated by multiple transcriptional and post-transcriptional mechanisms,[44−46] and even culture conditions,[43] we decided to use the cell line where we verified expression and activity of the gelatinase MMP-9.

For the synthesis of metalloproteinase-sensitive polymersomes, the diblock copolymer PDMS−PMOXA was used, as the FDA already approved synthetic polymers containing PDMS or PMOXA for the use in contact-lens material.[47] The previously reported ease of modification of the diblock copolymer using Michael addition or standard coupling techniques[12,48] allowed for the modification of the surface with the metalloproteinase sensitive SRL-peptide. This particular peptide has previously been reported by Steinhagen et al., who provided evidence for its use as a linker for proteinase driven release of a functional protein from polymer surfaces.[49] However, Samuelson et al. used another MMP-9 cleavable peptide sequence, the AVR-peptide, and tested it as an enzyme-sensitive linker for doxorubicin or paclitaxel to NanoDendrons and its application in breast cancer.[50] They observed a prompt and effective response in breast cancer cells for both compounds linked by the peptide to NanoDendrons. However, comparing the applicability of the above-mentioned peptides (AVR and SRL) in primary human coronary artery muscle cells, we observed that in this cellular system, where

DOI: 10.1021/acs.molpharmaceut.8b00521
Mol. Pharmaceutics 2018, 15, 4884−4897

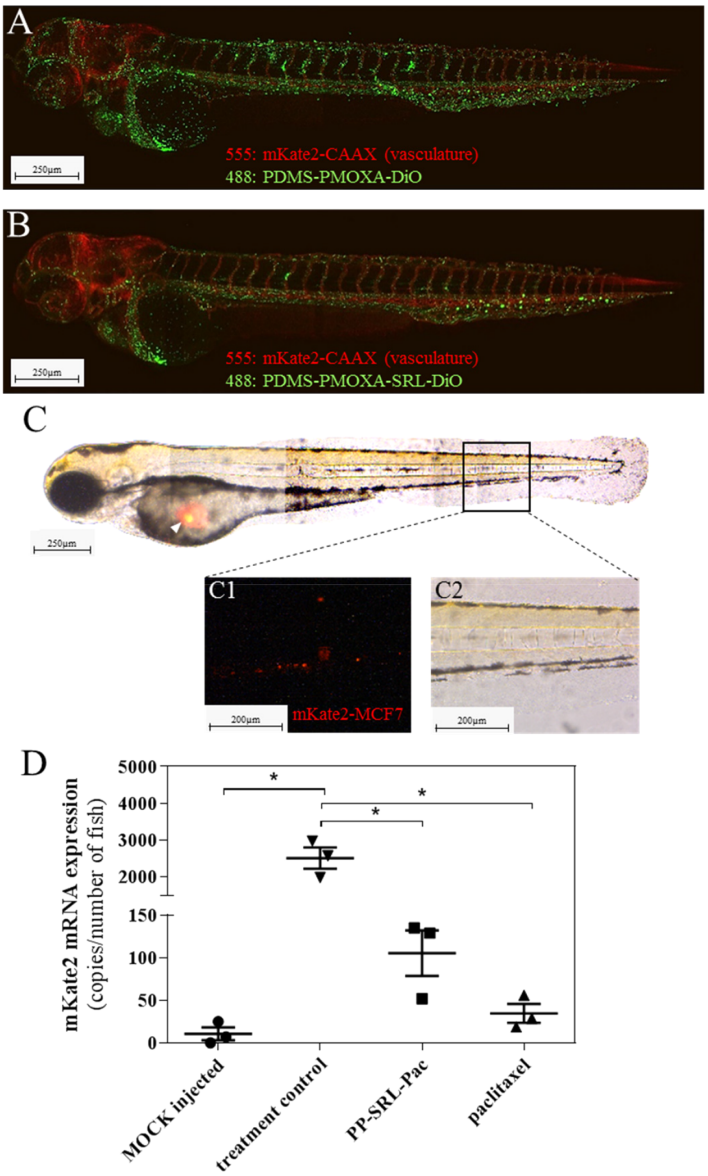

Figure 7. Distribution and pharmacological efficacy of PDMS−PMOXA polymersomes in zebrafish embryos. Unmodified (A) and SRL-peptide surface-modified (B) DiO-labeled polymersomes were injected in the transgenic zebrafish line *Tg*(CAAX:mKate2) expressing mKate2 in the vasculature. Distribution of the fluorescently labeled polymersomes was determined by confocal laser scanning microscopy. Representative images of $n = 3$ independent experiments are shown. The pharmacological activity of PDMS−PMOXA−SRL−paclitaxel (PP−SRL−Pac) polymersomes was assessed in xenografted zebrafish. First, wild-type zebrafish were xenografted with MCF7-mKate2 cells injected in the posterior region of the yolk. Fluorescently labeled cells formed a tumor mass in the injection region (arrow), as detected by confocal laser scanning microscopy. Fluorescent cells were also observed in the caudal region of the embryo after one night of recovery at 29 °C (C1, C2). The amount of cancer cells was quantified determining the number of mKate2 copies by qPCR in MOCK-injected and xenografted zebrafish embryos treated with either paclitaxel or the formulated polymersomes PDMS−PMOXA−SRL−paclitaxel (PP−SRL−Pac; D). Data are expressed as the mean ± SD of three independent experiments; * $p < 0.05$. One way ANOVA with Tukey's multiple comparisons test. Scale bar: 250 μm.

only MMP-9 activity was detected, the SRL-peptide was much more likely cleaved, releasing paclitaxel from a modified surface, than if the AVR peptide was used as the linker. Our finding suggested that there is a higher affinity of MMP-9 toward the SRL-peptide.[51]

In general, the diameter of rigid spherical polymersomes should be between 120 and 200 nm to prevent clearance in capillary beds or lymph nodes, splenic filtration, and entrapment in the space of Disse and hepatic parenchyma.[52] Assessing the hydrodynamic diameter of the unloaded polymersomes suggested no significant change in the average

DOI: 10.1021/acs.molpharmaceut.8b00521
Mol. Pharmaceutics 2018, 15, 4884−4897

diameter after the membrane cross-link. The observed mean diameter of about 150 nm is comparable to that previously reported by Kiene et al. for PDMS−PMOXA-based polymersomes.[48] However, the size distribution was significantly changed after loading with paclitaxel, and the surface cross-linking of loaded polymersomes even resulted in a loss of the Gaussian distribution, as determined by DLS. The determination of size distribution was supplemented by electron microscopic imaging, where homogeneous vesicles were observed prior to cargo loading, while more disperse particles were observed after the loading. Increased hydrodynamic diameter and a loss of Gaussian distribution has previously been reported for pH-sensitive PEG−Fu−DiTT polymersomes, where the observed changes have been explained by swelling.[53] Accordingly, one may speculate that loading of the herein investigated polymersomes with the large lipophilic molecule induced swelling of the polymersomes. Assuming that this is not due to water movement, one may speculate that paclitaxel was inserted in the membrane of the polymersomes. This notion is supported considering that peptide cross-linking did not significantly alter the size of polymersomes as observed by us and others.[48] We assume that the formation of the polymersomes occurs via self-assembly of the diblock copolymer chains, and surface modification with the SRL-peptide forms a stabilizing capsule. The MMP-9 cleaves the peptide, resulting in a destabilization of the capsule shell and allowing the cargo to permeate.

Prior to the testing of the herein synthesized PDMS−PMOXA−SRL polymersomes in breast cancer cells, paclitaxel sensitivity of MCF7 cells was verified, revealing that this compound significantly influenced the viability of these cells. Our findings are in accordance with those by Pavlikova et al.[54] Subsequently, PDMS−PMOXA−SRL polymersomes were assessed for their impact on cell viability, revealing no influence of the unloaded, while paclitaxel-loaded polymersomes significantly reduced cellular viability determined by metabolic activity. However, De Vocht et al.[47] tested the biocompatibility of the triblock copolymer PDMS−PMOXA−PDMS in primary rat hepatocytes. They observed LDH leakage and a change in hepatocyte morphology at higher doses (>500 μg/mL) and an exposure of more than 3 days in this cell system, suggesting some cytotoxicity, while Kiene et al. did not observe cytotoxic effects testing the diblock copolymer in HepG2 cells, a model of human hepatocytes.[48] Our findings in MCF7 also suggest no influence on cellular viability, testing a maximum concentration of 100 μg/mL and 48 h of exposure.

When testing the influence of MMP inhibitors on the cytotoxic effect of paclitaxel−SRL polymersomes, we observed a significantly reduced toxicity, suggesting that the bioactive compound is released from the polymersomes upon digestion of the cross-linked peptide. However, the effect was most pronounced in the presence of inhibitors for both gelatinases, namely, MMP-9 and MMP-2, suggesting that the latter is present in cultured breast cancer cells and also contributes to the cleavage of the peptide, even if we were not able to detect MMP-2 by zymography. Inhibition of MMP-9 may have resulted in elevated MMP-2 activity, which may be explained by their overlapping role in ECM modulation or the accumulation of substrates like fibronectin.[55] Even though our data show that the pharmacological effect of paclitaxel is triggered by MMP-9 digest, whereby suggesting that paclitaxel is indeed released most likely by permeation,[10,11] the molecule still has to find its way into cells. Combing the herein described MMP-9 triggered activation with direct delivery to the cytosol by transmembrane fusion, as shown by Yang et al., would be an even more sophisticated approach combining delivery and targeting.[13] Compounds with poor cellular uptake would benefit from such an approach.

Chakraborty et al. recently summarized the applicability of the zebrafish model to enumerate toxicity of nanoparticles.[56] In accordance to van Pomeren et al., who tested polystyrene nanoparticles,[57] we applied this vertebrate model to determine the distribution of the herein characterized polymersomes. However, in our case, the administration route was a direct injection of the polymersomes in the circulation and not a passive absorption of the particles by the embryo skin. In a similar manner, Sieber et al. established zebrafish as a novel in vivo model for investigating systemic circulation of nanoparticles after injection into circulation.[58] Using a transgenic zebrafish line with fluorescently labeled vasculature, we observed the PDMS−PMOXA−SRL polymersomes in the circulation with some enrichment in the liver and visible agglomerates in the vasculature of the caudal region, suggesting a possible uptake of the polymersomes by macrophages, similar to the observations by Campbell et al.[59] The observed hepatic accumulation is a common phenomenon, nanoparticles often tend to accumulate in the fish liver,[60,61] presumably due to its central detoxifying function. However, whether a potential hepatic accumulation is associated with enhanced hepatotoxicity warrants further studies on the herein designed polymersomes in higher animal models.

Xenografting of zebrafish embryos with human cancer cell lines has previously been applied for multiple tumor entities.[62] We have used MCF7 cells stably transfected with mKate2 and injected them in the yolk of zebrafish embryos at 2 dpf. Applying this approach, we observed the formation of tumor masses in injected fish, while cell clusters in the caudal region suggested metastasis formation in this model. However, Mercatali et al. observed no engrafting of MCF7 cells after application in the Duct of Couvier, even if the triple negative breast cancer cell line MDA-MB-231 formed a relevant tumor mass in their experimental set up.[63] Furthermore, data by Ren et al. show that the MDA-MB-231 cells exhibit a high metastatic phenotype, while this property was less pronounced using MCF-10 cells (an additional breast cancer cell line).[64] In our study, we verified the engrafting of the injected tumor cells determining the amount of mKate2 by PCR, the same approach was applied to determine the antitumor activity of the herein established polymersomes. The application of PCR to detect cells in zebrafish embryos has previously been reported by Pruvot et al.[65] In addition to verified engrafting, we were able to show that treatment with paclitaxel or formulated paclitaxel significantly reduced the amount of tumor cells, suggesting that the herein designed PDMS−PMOXA−SRL−paclitaxel exerts antitumor activity.

Taken together, we have designed matrix metalloproteinase-sensitive polymersomes for paclitaxel. The polymersomes exhibited a diameter commonly assumed to be usable as an in vivo drug delivery system. However, loading with the lipophilic cargo significantly increased the observed diameter, which we assume to reflect the swelling of the polymersomes. Importantly, testing of the formulation in breast cancer cells, which were selected due to the observed enhanced expression of MMP-9 in malignant-transformed tissue, revealed pharmacological activity, which was significantly influenced by the addition of MMP-9 inhibitors. By applying a xenograft model

DOI: 10.1021/acs.molpharmaceut.8b00521
Mol. Pharmaceutics 2018, 15, 4884−4897

in zebrafish based on fluorescently labeled MCF7 cells, which were engrafting in the host, we were able to show antitumor activity of the herein designed polymersome.

■ ASSOCIATED CONTENT

Supporting Information

The Supporting Information is available free of charge on the ACS Publications website at DOI: 10.1021/acs.molpharmaceut.8b00521.

Data on the expression of gelatinases depending on tumor stages, images of MMP-9 detected by immunohistochemistry in normal and malignant-transformed breast tissue, details on the analysis of MMP-9 expression in data sets of the GEO, data on the characterization of MCF7-mKate2 cells, and data on the size distribution and stability of polymersomes (PDF)

■ AUTHOR INFORMATION

Corresponding Author

*E-mail: h.meyerzuschwabedissen@unibas.ch; Phone: 0041-61 207 1495.

ORCID

Henriette E. Meyer zu Schwabedissen: 0000-0003-0458-4579

Author Contributions

§F.P. and D.E. contributed equally to this work.

Notes

The authors declare no competing financial interest.

■ ACKNOWLEDGMENTS

This work was supported by funds of the Biopharmacy and the Novartis University Basel Excellence Scholarships for Life Science obtained by F.P. We want to thank Andrea Buerer for proofreading the manuscript. Furthermore, the authors want to thank Prof. Markus Affolter (Biocenter, University of Basel) for kindly providing the pmKate2-N vector and Dr. Sandro Sieber (Pharmaceutical Technology, Department of Pharmaceutical Sciences, University of Basel) for his support with the zebrafish experiments.

■ ABBREVIATIONS

BSA, bovine serum albumin; DMEM, Dulbecco's modified Eagle medium; EDAC, 1-ethyl-3-(3-(dimethylamino)propyl) carbodiimide; FCS, fetal calf serum; FT-IR, Fourier transform infrared; GEO, gene expression omnibus; GDS, GEO data set; GSE, GEO series on expression; MMP-9, matrix metalloproteinase 9; MMP-2, matrix metalloproteinase 2; NHS, *N*-hydroxisuccinimide; PAGE, polyacrylamide gel electrophoresis; PCR, polymerase chain reaction; PDMS−PMOXA, poly(dimethylsiloxane)−poly b-(methyloxazoline); PTU, phenyl thiourea; TBS-T, tris buffered saline with Tween-X-100; TEA, trimethylamine; SDS, sodium dodecyl sulfate;

■ REFERENCES

(1) Kamaly, N.; Yameen, B.; Wu, J.; Farokhzad, O. C. Degradable Controlled-Release Polymers and Polymeric Nanoparticles: Mechanisms of Controlling Drug Release. *Chem. Rev.* **2016**, *116* (4), 2602−63.

(2) Torchilin, V. P. Liposomes as targetable drug carriers. *Crit. Rev. Ther. Drug Carrier Syst.* **1985**, *2* (1), 65−115.

(3) O'Brien, M. E.; Wigler, N.; Inbar, M.; Rosso, R.; Grischke, E.; Santoro, A.; Catane, R.; Kieback, D. G.; Tomczak, P.; Ackland, S. P.; Orlandi, F.; Mellars, L.; Alland, L.; Tendler, C.; Group, C. B. C. S. Reduced cardiotoxicity and comparable efficacy in a phase III trial of pegylated liposomal doxorubicin HCl (CAELYX/Doxil) versus conventional doxorubicin for first-line treatment of metastatic breast cancer. *Ann. Oncol* **2004**, *15* (3), 440−449.

(4) Wang, Y.; Zhao, Q.; Han, N.; Bai, L.; Li, J.; Liu, J.; Che, E.; Hu, L.; Zhang, Q.; Jiang, T.; Wang, S. Mesoporous silica nanoparticles in drug delivery and biomedical applications. *Nanomedicine* **2015**, *11* (2), 313−27.

(5) Porta, F.; Lamers, G. E.; Zink, J. I.; Kros, A. Peptide modified mesoporous silica nanocontainers. *Phys. Chem. Chem. Phys.* **2011**, *13* (21), 9982−5.

(6) Li, L.; Liu, T.; Fu, C.; Tan, L.; Meng, X.; Liu, H. Biodistribution, excretion, and toxicity of mesoporous silica nanoparticles after oral administration depend on their shape. *Nanomedicine* **2015**, *11* (8), 1915−24.

(7) Kaditi, E.; Mountrichas, G.; Pispas, S.; Demetzos, C. Block copolymers for drug delivery nano systems (DDnSs). *Curr. Med. Chem.* **2012**, *19* (29), 5088−100.

(8) Broz, P.; Benito, S. M.; Saw, C.; Burger, P.; Heider, H.; Pfisterer, M.; Marsch, S.; Meier, W.; Hunziker, P. Cell targeting by a generic receptor-targeted polymer nanocontainer platform. *J. Controlled Release* **2005**, *102* (2), 475−88.

(9) Egli, S.; Nussbaumer, M. G.; Balasubramanian, V.; Chami, M.; Bruns, N.; Palivan, C.; Meier, W. Biocompatible functionalization of polymersome surfaces: a new approach to surface immobilization and cell targeting using polymersomes. *J. Am. Chem. Soc.* **2011**, *133* (12), 4476−83.

(10) Jaskiewicz, K.; Larsen, A.; Lieberwirth, I.; Koynov, K.; Meier, W.; Fytas, G.; Kroeger, A.; Landfester, K. Probing bioinspired transport of nanoparticles into polymersomes. *Angew. Chem., Int. Ed.* **2012**, *51* (19), 4613−7.

(11) Jaskiewicz, K.; Larsen, A.; Schaeffel, D.; Koynov, K.; Lieberwirth, I.; Fytas, G.; Landfester, K.; Kroeger, A. Incorporation of nanoparticles into polymersomes: size and concentration effects. *ACS Nano* **2012**, *6* (8), 7254−62.

(12) Dieu, L. H.; Wu, D.; Palivan, C. G.; Balasubramanian, V.; Huwyler, J. Polymersomes conjugated to 83−14 monoclonal antibodies: in vitro targeting of brain capillary endothelial cells. *Eur. J. Pharm. Biopharm.* **2014**, *88* (2), 316−24.

(13) Yang, J.; Bahreman, A.; Daudey, G.; Bussmann, J.; Olsthoorn, R. C.; Kros, A. Drug Delivery via Cell Membrane Fusion Using Lipopeptide Modified Liposomes. *ACS Cent. Sci.* **2016**, *2* (9), 621−630.

(14) Torchilin, V. P. Multifunctional nanocarriers. *Adv. Drug Delivery Rev.* **2006**, *58* (14), 1532−55.

(15) Perche, F.; Torchilin, V. P. Recent trends in multifunctional liposomal nanocarriers for enhanced tumor targeting. *J. Drug Delivery* **2013**, *2013*, 705265.

(16) Lesniewska-Kowiel, M. A.; Muszalska, I. Strategies in the designing of prodrugs, taking into account the antiviral and anticancer compounds. *Eur. J. Med. Chem.* **2017**, *129*, 53−71.

(17) Van den Steen, P. E.; Dubois, B.; Nelissen, I.; Rudd, P. M.; Dwek, R. A.; Opdenakker, G. Biochemistry and molecular biology of gelatinase B or matrix metalloproteinase-9 (MMP-9). *Crit. Rev. Biochem. Mol. Biol.* **2002**, *37* (6), 375−536.

(18) Deryugina, E. I.; Quigley, J. P. Matrix metalloproteinases and tumor metastasis. *Cancer Metastasis Rev.* **2006**, *25* (1), 9−34.

(19) Hanahan, D.; Weinberg, R. A. The hallmarks of cancer. *Cell* **2000**, *100* (1), 57−70.

(20) Hanahan, D.; Weinberg, R. A. Hallmarks of cancer: the next generation. *Cell* **2011**, *144* (5), 646−74.

(21) Mira, E.; Lacalle, R. A.; Buesa, J. M.; de Buitrago, G. G.; Jimenez-Baranda, S.; Gomez-Mouton, C.; Martinez, A. C.; Manes, S. Secreted MMP9 promotes angiogenesis more efficiently than constitutive active MMP9 bound to the tumor cell surface. *J. Cell Sci.* **2004**, *117*, 1847−57.

(22) Deryugina, E. I.; Quigley, J. P. Tumor angiogenesis: MMP-mediated induction of intravasation- and metastasis-sustaining neovasculature. *Matrix Biol.* **2015**, *44*−*46*, 94−112.

DOI: 10.1021/acs.molpharmaceut.8b00521
Mol. Pharmaceutics 2018, 15, 4884−4897

(23) Gorelik, L.; Flavell, R. A. Immune-mediated eradication of tumors through the blockade of transforming growth factor-beta signaling in T cells. *Nat. Med.* **2001**, *7* (10), 1118−22.
(24) Maeshima, Y.; Sudhakar, A.; Lively, J. C.; Ueki, K.; Kharbanda, S.; Kahn, C. R.; Sonenberg, N.; Hynes, R. O.; Kalluri, R. Tumstatin, an endothelial cell-specific inhibitor of protein synthesis. *Science* **2002**, *295* (5552), 140−143.
(25) Egeblad, M.; Werb, Z. New functions for the matrix metalloproteinases in cancer progression. *Nat. Rev. Cancer* **2002**, *2* (3), 161−74.
(26) Bekes, E. M.; Schweighofer, B.; Kupriyanova, T. A.; Zajac, E.; Ardi, V. C.; Quigley, J. P.; Deryugina, E. I. Tumor-recruited neutrophils and neutrophil TIMP-free MMP-9 regulate coordinately the levels of tumor angiogenesis and efficiency of malignant cell intravasation. *Am. J. Pathol.* **2011**, *179* (3), 1455−70.
(27) Min, K. W.; Kim, D. H.; Do, S. I.; Kim, K.; Lee, H. J.; Chae, S. W.; Sohn, J. H.; Pyo, J. S.; Oh, Y. H.; Kim, W. S.; Lee, S. Y.; Oh, S.; Choi, S. H.; Park, Y. L.; Park, C. H. Expression patterns of stromal MMP-2 and tumoural MMP-2 and −9 are significant prognostic factors in invasive ductal carcinoma of the breast. *APMIS* **2014**, *122* (12), 1196−206.
(28) Li, H.; Qiu, Z.; Li, F.; Wang, C. The relationship between MMP-2 and MMP-9 expression levels with breast cancer incidence and prognosis. *Oncol. Lett.* **2017**, *14* (5), 5865−5870.
(29) van Rijt, S. H.; Bolukbas, D. A.; Argyo, C.; Datz, S.; Lindner, M.; Eickelberg, O.; Konigshoff, M.; Bein, T.; Meiners, S. Protease-mediated release of chemotherapeutics from mesoporous silica nanoparticles to ex vivo human and mouse lung tumors. *ACS Nano* **2015**, *9* (3), 2377−89.
(30) Chu, D. S.; Sellers, D. L.; Bocek, M. J.; Fischedick, A. E.; Horner, P. J.; Pun, S. H. MMP9-sensitive polymers mediate environmentally-responsive bivalirudin release and thrombin inhibition. *Biomater. Sci.* **2015**, *3* (1), 41−5.
(31) Elegbede, A. I.; Banerjee, J.; Hanson, A. J.; Tobwala, S.; Ganguli, B.; Wang, R.; Lu, X.; Srivastava, D. K.; Mallik, S. Mechanistic studies of the triggered release of liposomal contents by matrix metalloproteinase-9. *J. Am. Chem. Soc.* **2008**, *130* (32), 10633−42.
(32) Kalafatovic, D.; Nobis, M.; Javid, N.; Frederix, P. W.; Anderson, K. I.; Saunders, B. R.; Ulijn, R. V. MMP-9 triggered micelle-to-fibre transitions for slow release of doxorubicin. *Biomater. Sci.* **2015**, *3* (2), 246−9.
(33) Grafe, D.; Gaitzsch, J.; Appelhans, D.; Voit, B. Cross-linked polymersomes as nanoreactors for controlled and stabilized single and cascade enzymatic reactions. *Nanoscale* **2014**, *6* (18), 10752−61.
(34) Sze, A.; Erickson, D.; Ren, L.; Li, D. Zeta-potential measurement using the Smoluchowski equation and the slope of the current-time relationship in electroosmotic flow. *J. Colloid Interface Sci.* **2003**, *261* (2), 402−10.
(35) Rueden, C. T.; Schindelin, J.; Hiner, M. C.; DeZonia, B. E.; Walter, A. E.; Arena, E. T.; Eliceiri, K. W. ImageJ2: ImageJ for the next generation of scientific image data. *BMC Bioinf.* **2017**, *18* (1), 529.
(36) Gialeli, C.; Theocharis, A. D.; Karamanos, N. K. Roles of matrix metalloproteinases in cancer progression and their pharmacological targeting. *FEBS J.* **2011**, *278* (1), 16−27.
(37) Zhang, M.; Teng, X. D.; Guo, X. X.; Li, Z. G.; Han, J. G.; Yao, L. Expression of tissue levels of matrix metalloproteinases and their inhibitors in breast cancer. *Breast* **2013**, *22* (3), 330−4.
(38) Tang, D.; Piao, Y.; Zhao, S.; Mu, X.; Li, S.; Ma, W.; Song, Y.; Wang, J.; Zhao, W.; Zhang, Q. Expression and correlation of matrix metalloproteinase-9 and heparanase in patients with breast cancer. *Med. Oncol.* **2014**, *31* (7), 26.
(39) Yousef, E. M.; Tahir, M. R.; St-Pierre, Y.; Gaboury, L. A. MMP-9 expression varies according to molecular subtypes of breast cancer. *BMC Cancer* **2014**, *14*, 609.
(40) Liu, Y.; Xin, T.; Jiang, Q. Y.; Huang, D. Y.; Shen, W. X.; Li, L.; Lv, Y. J.; Jin, Y. H.; Song, X. W.; Teng, C. CD147, MMP9 expression and clinical significance of basal-like breast cancer. *Med. Oncol.* **2013**, *30* (1), 366.
(41) Singer, C. F.; Kronsteiner, N.; Marton, E.; Kubista, M.; Cullen, K. J.; Hirtenlehner, K.; Seifert, M.; Kubista, E. MMP-2 and MMP-9 expression in breast cancer-derived human fibroblasts is differentially regulated by stromal-epithelial interactions. *Breast Cancer Res. Treat.* **2002**, *72* (1), 69−77.
(42) Klassen, L. M. B.; Chequin, A.; Manica, G. C. M.; Biembengut, I. V.; Toledo, M. B.; Baura, V. A.; de O Pedrosa, F.; Ramos, E. A. S.; Costa, F. F.; de Souza, E. M.; Klassen, G. MMP9 gene expression regulation by intragenic epigenetic modifications in breast cancer. *Gene* **2018**, *642*, 461−466.
(43) Bachmeier, B. E.; Albini, A.; Vene, R.; Benelli, R.; Noonan, D.; Weigert, C.; Weiler, C.; Lichtinghagen, R.; Jochum, M.; Nerlich, A. G. Cell density-dependent regulation of matrix metalloproteinase and TIMP expression in differently tumorigenic breast cancer cell lines. *Exp. Cell Res.* **2005**, *305* (1), 83−98.
(44) Johnson, J. L.; Pillai, S.; Pernazza, D.; Sebti, S. M.; Lawrence, N. J.; Chellappan, S. P. Regulation of matrix metalloproteinase genes by E2F transcription factors: Rb-Raf-1 interaction as a novel target for metastatic disease. *Cancer Res.* **2012**, *72* (2), 516−26.
(45) Frank, A.; David, V.; Aurelie, T. R.; Florent, G.; William, H.; Philippe, B. Regulation of MMPs during melanoma progression: from genetic to epigenetic. *Anti-Cancer Agents Med. Chem.* **2012**, *12* (7), 773−82.
(46) Shan, Y. Q.; Ying, R. C.; Zhou, C. H.; Zhu, A. K.; Ye, J.; Zhu, W.; Ju, T. F.; Jin, H. C. MMP-9 is increased in the pathogenesis of gastric cancer by the mediation of HER2. *Cancer Gene Ther.* **2015**, *22* (3), 101−7.
(47) De Vocht, C.; Ranquin, A.; Willaert, R.; Van Ginderachter, J. A.; Vanhaecke, T.; Rogiers, V.; Versees, W.; Van Gelder, P.; Steyaert, J. Assessment of stability, toxicity and immunogenicity of new polymeric nanoreactors for use in enzyme replacement therapy of MNGIE. *J. Controlled Release* **2009**, *137* (3), 246−54.
(48) Kiene, K.; Schenk, S. H.; Porta, F.; Ernst, A.; Witzigmann, D.; Grossen, P.; Huwyler, J. PDMS-b-PMOXA polymersomes for hepatocyte targeting and assessment of toxicity. *Eur. J. Pharm. Biopharm.* **2017**, *119*, 322−332.
(49) Steinhagen, M.; Hoffmeister, P. G.; Nordsieck, K.; Hotzel, R.; Baumann, L.; Hacker, M. C.; Schulz-Siegmund, M.; Beck-Sickinger, A. G. Matrix metalloproteinase 9 (MMP-9) mediated release of MMP-9 resistant stromal cell-derived factor 1alpha (SDF-1alpha) from surface modified polymer films. *ACS Appl. Mater. Interfaces* **2014**, *6* (8), 5891−9.
(50) Samuelson, L. E.; Scherer, R. L.; Matrisian, L. M.; McIntyre, J. O.; Bornhop, D. J. Synthesis and in vitro efficacy of MMP9-activated NanoDendrons. *Mol. Pharmaceutics* **2013**, *10* (8), 3164−74.
(51) Gliesche, D. G.; Hussner, J.; Witzigmann, D.; Porta, F.; Glatter, T.; Schmidt, A.; Huwyler, J.; Meyer Zu Schwabedissen, H. E. Secreted Matrix Metalloproteinase-9 of Proliferating Smooth Muscle Cells as a Trigger for Drug Release from Stent Surface Polymers in Coronary Arteries. *Mol. Pharmaceutics* **2016**, *13* (7), 2290−300.
(52) Moghimi, S. M.; Hunter, A. C.; Murray, J. C. Long-circulating and target-specific nanoparticles: theory to practice. *Pharmacol. Rev.* **2001**, *53* (2), 283−318.
(53) Scarpa, E.; Bailey, J. L.; Janeczek, A. A.; Stumpf, P. S.; Johnston, A. H.; Oreffo, R. O.; Woo, Y. L.; Cheong, Y. C.; Evans, N. D.; Newman, T. A. Quantification of intracellular payload release from polymersome nanoparticles. *Sci. Rep.* **2016**, *6*, 29460.
(54) Pavlikova, N.; Bartonova, I.; Balusikova, K.; Kopperova, D.; Halada, P.; Kovar, J. Differentially expressed proteins in human MCF-7 breast cancer cells sensitive and resistant to paclitaxel. *Exp. Cell Res.* **2015**, *333* (1), 1−10.
(55) Das, S.; Banerji, A.; Frei, E.; Chatterjee, A. Rapid expression and activation of MMP-2 and MMP-9 upon exposure of human breast cancer cells (MCF-7) to fibronectin in serum free medium. *Life Sci.* **2008**, *82* (9−10), 467−76.
(56) Chakraborty, C.; Sharma, A. R.; Sharma, G.; Lee, S. S. Zebrafish: A complete animal model to enumerate the nanoparticle toxicity. *J. Nanobiotechnol.* **2016**, *14* (1), 65.

DOI: 10.1021/acs.molpharmaceut.8b00521
Mol. Pharmaceutics 2018, 15, 4884−4897

(57) van Pomeren, M.; Brun, N. R.; Peijnenburg, W.; Vijver, M. G. Exploring uptake and biodistribution of polystyrene (nano)particles in zebrafish embryos at different developmental stages. *Aquat. Toxicol.* **2017**, *190*, 40−45.
(58) Sieber, S.; Grossen, P.; Detampel, P.; Siegfried, S.; Witzigmann, D.; Huwyler, J. Zebrafish as an early stage screening tool to study the systemic circulation of nanoparticulate drug delivery systems in vivo. *J. Controlled Release* **2017**, *264*, 180−191.
(59) Campbell, F.; Bos, F. L.; Sieber, S.; Arias-Alpizar, G.; Koch, B. E.; Huwyler, J.; Kros, A.; Bussmann, J. Directing Nanoparticle Biodistribution through Evasion and Exploitation of Stab2-Dependent Nanoparticle Uptake. *ACS Nano* **2018**, *12* (3), 2138−2150.
(60) Jang, M. H.; Kim, W. K.; Lee, S. K.; Henry, T. B.; Park, J. W. Uptake, tissue distribution, and depuration of total silver in common carp (Cyprinus carpio) after aqueous exposure to silver nanoparticles. *Environ. Sci. Technol.* **2014**, *48* (19), 11568−74.
(61) Kashiwada, S. Distribution of nanoparticles in the see-through medaka (Oryzias latipes). *Environ. Health Perspect.* **2006**, *114* (11), 1697−702.
(62) Konantz, M.; Balci, T. B.; Hartwig, U. F.; Dellaire, G.; Andre, M. C.; Berman, J. N.; Lengerke, C. Zebrafish xenografts as a tool for in vivo studies on human cancer. *Ann. N. Y. Acad. Sci.* **2012**, *1266*, 124−37.
(63) Mercatali, L.; La Manna, F.; Groenewoud, A.; Casadei, R.; Recine, F.; Miserocchi, G.; Pieri, F.; Liverani, C.; Bongiovanni, A.; Spadazzi, C.; de Vita, A.; van der Pluijm, G.; Giorgini, A.; Biagini, R.; Amadori, D.; Ibrahim, T.; Snaar-Jagalska, E. Development of a Patient-Derived Xenograft (PDX) of Breast Cancer Bone Metastasis in a Zebrafish Model. *Int. J. Mol. Sci.* **2016**, *17* (8), e1375.
(64) Ren, J.; Liu, S.; Cui, C.; Ten Dijke, P. Invasive Behavior of Human Breast Cancer Cells in Embryonic Zebrafish. *J. Visualized Exp.* **2017**, No. 122, 122.
(65) Pruvot, B.; Jacquel, A.; Droin, N.; Auberger, P.; Bouscary, D.; Tamburini, J.; Muller, M.; Fontenay, M.; Chluba, J.; Solary, E. Leukemic cell xenograft in zebrafish embryo for investigating drug efficacy. *Haematologica* **2011**, *96* (4), 612−6.

DOI: 10.1021/acs.molpharmaceut.8b00521
Mol. Pharmaceutics 2018, 15, 4884−4897

Results II

"PDMS-PMOXA-Nanoparticles Featuring a Cathepsin B-Triggered Release Mechanism"

Daniel Ehrsam [1], Fabiola Porta [1], Janine Hussner [1], Isabell Seibert [1], Henriette E Meyer Zu Schwabedissen [1]

Affiliations:

[1] Department Pharmaceutical Sciences, University of Basel, Klingelbergstrasse 50, 4056 Basel, Switzerland.

Contribution Daniel Ehrsam: Study design, acquisition, analysis and interpretation of data, drafting of manuscript.

PMID: 31484396 PMCID: PMC6747961 DOI: 10.3390/ma12172836

materials

MDPI

Article

PDMS-PMOXA-Nanoparticles Featuring a Cathepsin B-Triggered Release Mechanism

Daniel Ehrsam, Fabiola Porta, Janine Hussner, Isabell Seibert and Henriette E Meyer zu Schwabedissen *

Department Pharmaceutical Sciences, University of Basel, Klingelbergstrasse 50, 4056 Basel, Switzerland
* Correspondence: h.meyerzuschwabedissen@unibas.ch; Tel.: +41-61-207-14-95

Received: 2 July 2019; Accepted: 30 August 2019; Published: 3 September 2019

Abstract: Background: It was our intention to develop cathepsin B-sensitive nanoparticles for tumor-site-directed release. These nanoparticles should be able to release their payload as close to the tumor site with a decrease of off-target effects in mind. Cathepsin B, a lysosomal cysteine protease, is associated with premalignant lesions and invasive stages of cancer. Previous studies have shown cathepsin B in lysosomes and in the extracellular matrix. Therefore, this enzyme qualifies as a trigger for such an approach. Methods: Poly(dimethylsiloxane)-b-poly(methyloxazoline) (PDMS-PMOXA) nanoparticles loaded with paclitaxel were formed by a thin-film technique and standard coupling reactions were used for surface modifications. Despite the controlled release mechanism, the physical properties of the herein created nanoparticles were described. To characterize potential in vitro model systems, quantitative polymerase chain reaction and common bioanalytical methods were employed. Conclusions: Stable paclitaxel-loaded nanoparticles with cathepsin B digestible peptide were formed and tested on the ovarian cancer cell line OVCAR-3. These nanoparticles exerted a pharmacological effect on the tumor cells suggesting a release of the payload.

Keywords: enzyme-triggered-release; cathepsin B; paclitaxel; nanoparticles; PDMS-PMOXA; cancer; ovarian cancer

1. Introduction

According to the World Health Organization, cancer is one of the leading causes of morbidity and mortality worldwide, and therefore, cancer therapy is an important objective for today's medicinal research [1]. Different therapeutic approaches have been taken so far, from surgical removal to radio- and chemotherapy. The use of anti-proliferative drugs in cancer therapy means that every part of the human body can be reached and, thus, not only the primary cancer can be fought, but also metastasized cells [2]. For most compounds used in chemotherapy though, the mode of action is not exclusive to cancer cells but affects cell proliferation throughout the entire organism. This leads to adverse side effects and limits the doses that can be applied to patients [3,4]. Current efforts in chemotherapeutic drug development aim at increasing the selectivity for cancer cells while reducing the systemic exposure.

Many strategies have been applied to direct small molecules to the target cells. These include drug delivery systems like nanoparticles. Nanoparticles are 3-dimensional supramolecular entities, which are assumed to passively accumulate in the tumor tissue due to the enhanced permeability and retention effect [5]. In detail, macromolecules including nanoparticles are passively enriched in neovascularized tumor tissue as the newly formed blood vessels exhibit not only enhanced perfusion, but also increased permeability. In addition, the lymphatic system in tumors is assumed to be less effective, which is leading to decreased lymphatic drainage from the tumor site. Although the enhanced

permeability and retention effect (EPR) is a very interesting phenomenon, it is also assumed to be heterogeneous in humans [6].

Hitherto, a variety of nanoparticles using many different materials has been developed, investigated and some have been approved for the use in humans [7,8]. Since 1995, the United States Food and Drug Administration (FDA) approved over 50 nanopharmaceuticals; the majority being liposomal, nanocrystal, or polymeric formulations. The latter are comprised of amphiphilic polymers consisting of subunits also known as block copolymers. In detail, linear block copolymers can be divided into the categories of diblock copolymers or of triblock copolymers. Diblock copolymers possess a polar and a non-polar homopolymeric subunit (A-B). Triblock copolymers consist of three homopolymeric subunits (A-B-A or A-B-C), where two subunits can be similar [9]. Nanoparticles formed by block copolymers are known as polymersomes or polymeric nanoparticles depending on the membrane.

An entity of polymersomes, investigated for their application as a drug delivery system, are PDMS-PMOXA polymersomes where the diblock copolymer used for the formulation is poly(dimethyl siloxane)-poly-*b*-(methyloxazoline). So far, these polymersomes were investigated for their toxicological and biocompatibility profile, showing no significant toxicity in in vitro models [10,11] and the subunits have been reported to be biocompatible [12]. A previous study has described that the hydrophilic PMOXA-block is cleared by the kidney from the circulation [13]. Although the PDMS-block is hydrophobic, as long as the molecular weight does not surpass 5 kDa, it undergoes renal elimination [14]. Importantly, polymersomes have the ability to encapsulate bioactive molecules like chemotherapeutics [7], and are therefore, suitable for drug delivery.

Most of the current approved nanoformulations are aiming at improving the pharmacokinetics and pharmacodynamics by packaging/conjugating drugs in/to nanoparticles [15]. However, incorporating an active or triggered release strategy could lead to a dose reduction and therefore, decrease side effects [16,17]. A mechanism that could be utilized for such an approach is triggered release of the payload using tumor-specific elicitors [18]. Here, the tumor-associated expression of enzymes in or close to the targeted tissue offers potential candidates. Especially, enzymes exerting proteolytic activity could be employed to cleave drug–peptide conjugates or to trigger changes in the drug carrier's outer layer [16]. An enzyme qualifying as an elicitor is cathepsin B.

In physiological conditions, cathepsin B is located in the lysosomes [19], where it is involved in the degradation and, therefore, regulation of proteins. Besides proteolysis within the lysosome, cathepsin B is involved in cell death mediation [20], and it contributes to the degradation of the extracellular matrix [21]. Indeed, in cancer, cathepsin B is secreted by tumor cells where it contributes to the degradation and remodeling of the extracellular matrix and whereby facilitating tumor cell invasion into the surrounding tissue [22]. In tumor tissue, cathepsin B seems to be expressed predominantly in areas bordering the extracellular matrix [23]. By analyzing patient samples, increased protein content or activity of cathepsin B have been detected in ovarian [19] and colorectal [24] cancer. A similar enhancement has been observed in a B16 mouse melanoma in vivo model [25]. Jedeszko et al. summarized the core-statements of many publications in a review showing increased expression and activity of cathepsin B in breast, colon, lung, prostate cancer, glioblastoma, and melanoma [26].

In this study, we aimed at using cathepsin B as an elicitor for enzyme-triggered drug release from PDMS-PMOXA-based nanoparticles. The PDMS-PMOXA nanoparticles were used as a platform for surface-modifications. The separate surface-modification steps were surveyed by Fourier-transform infrared (FT-IR) spectroscopy. Because cathepsin B (CTBS) plays a pivotal role in the release mechanism, its mRNA expression was determined in patient derived tumor samples. Accordingly, a suitable in vitro cell model system was identified and subsequently used for in vitro studies on the pharmacological activity of the CTSB-degradable nanoparticles (Supplemental Tables S1 and S2).

2. Materials and Methods

2.1. Materials

Poly(dimethylsiloxane)-b-poly(methyloxazoline) PDMS-PMOXA was purchased from Polymer Source Inc., Ottawa, Canada. Organic solvents were obtained from J.T. Baker, (Deventer, Netherlands), Carl Roth GmbH + Co. KG (Arlesheim, Switzerland), or from Sigma Aldrich (Buchs, Switzerland). p-Maleidoimino phenylisocyanate was purchased from Invitrogen (distributed by Thermo Fisher, Reinach, Switzerland). Double distilled water (ddH_2O) with a resistivity of 18.2 mΩ was generated with a Barnstead Nanopure DiamondTM System (Thermo Fischer).

2.2. Quantitative PCR for Gene Expression Analysis in Cancer Tissue Samples and Representative Cell Lines

To determine CTSB mRNA expression in cancer tissue a cDNA array (CSRT103, Origene, Rockville, MD, USA) was commercially obtained. Furthermore, mRNA of cancer cell lines was isolated using peqGOLD RNA pure (Axon Lab, Baden, Switzerland) and reverse transcribed using the High-Capacity cDNA Reverse Transcription kit (Thermo Fisher). The amount of CTSB was assessed by quantitative real-time PCR (qPCR) using the pre-developed TaqMan^{TM} assays (Thermo Fischer) Hs00947439_m1, the TaqMan® gene expression mastermix, and the ViiA^{TM} 7 Real-Time PCR System. The reaction was carried out in a volume of 15 µL composed of 0.75 µL of the Hs00947439_m1-FAM TaqMan assay, 6.75 µL H_2O, and 7.5 µL TaqMan® Gene Expression Mastermix (Applied Biosystems, LubioSciences, Lucerne, Switzerland). For quantification of copy numbers, a standard curve using cloned PCR amplicon was recorded.

2.3. Immunohistochemical Staining of CTSB in Human Ovary Cancer Tissue

For the detection of CTSB by immunohistochemical staining a commercially obtained array of paraffin embedded tissue sections was used. This array included malignant transformed and non-malignant transformed samples of various tissues (MTU951, BioCat GmbH, Heidelberg, Germany). To deparaffinize the tissue sections, two changes of xylol and rehydration in a decreasing ethanol series ranging from 96% to 0% was executed, followed by a heat induced epitope retrieval in 0.1 M citrate buffer (pH = 6.0, 20 min). The endogenous peroxidase was quenched in a 3%-H_2O_2-methanol-bath for 20 min. To reduce unspecific binding of the antibody, the slides were exposed for 1 h to blocking solution (5% FCS and 1% BSA in PBS). CTSB was detected with the primary anti-CTSB-antibody (sc-13985, Santa Cruz Biotechnology, Inc., Texas, TX, USA) at a dilution of 1:1000 in blocking solution. After incubation with primary antibody overnight at 4 °C, the tissue slides were washed repeatedly in PBS. The tissue slides were then exposed to the secondary HRP-coupled goat-anti-rabbit antibody (Bio-Rad Laboratories Laboratories, Cressier, Switzerland; 1:100) for two hours at room temperature (RT). After several washing steps in PBS, 1 mg/mL of diaminobenzidine (DAB) diluted in 0.05 M phosphate buffer containing 0.02% H_2O_2 was added for visualization of epitope-bound antibody. Nuclei were stained with hematoxylin solution (Carl Roth GmbH + Co. KG) and slides were mounted with Roti®-Histokitt II (Carl Roth GmbH + Co. KG). Finally, the stained tissue slides were imaged with a Leica DMi8 microscope equipped with a DFC 365 FX camera (Leica, Heerbrugg, Switzerland) and the LAS software Version 4.6 (Leica).

2.4. Western Blot Analysis

Protein samples were collected from cultured cells seeded at a density of 1×10^6 cells/ 10 cm dish. After reaching 80% confluence, the culture medium was replaced by the respective medium containing no FCS to avoid contamination with serum proteins. After 24 h, the culture supernatant was collected to enrich the secreted protein. In detail, the supernatant was supplemented with ice-cold 10% trichloroacetic acid, kept on ice for 15 min, and was then centrifuged for 20 min at 17,000 × *g* and 4 °C. The precipitate was washed twice with ice-cold acetone (5 mL), and was then air-dried for 30 min at room temperature. The enriched secreted proteins were finally solubilized in 6 M

system (MicroCal^{TM}, Malvern Instruments GmbH). The samples were measured using a backscattering angle of 173° was used. Data were analyzed using the Zetasizer software 7.11. (Malvern).

2.9. Critical Aggregation Concentration of PDMS-PMOXA

Critical aggregation concentration (CAC) was determined by utilizing the different fluorescence characteristics of pyrene (Sigma-Aldrich) in a hydrophobic or hydrophilic environment [28,29]. Briefly, 500 µL 2.4 µM pyrene in aceton and corresponding amount of PDMS-PMOXA (2500, 250, 25, 2.5, 0.25, 0.025 µg) in acetone were added to a glass vial. The solvent was evaporated for 1.5 h at 40°C and under constant flow of nitrogen. After completely drying the pyrene and PDMS-PMOXA, 1 mL of ultrapure water was added, and particles were formed by ultrasonification. The fluorescence of pyrene was measured with the microplate reader Tecan Infinite M200 Pro (Tecan; excitation 332 nm, emission I_1 = 373 nm and I_3 = 384 nm). To determine the CAC, the pyrene's intensity ratio of I_1/I_3 was plotted against the logarithm of the PDMS-PMOXA concentration.

2.10. Synthesis of Carboxyl Terminated Poly(Dimethylsiloxane)-b-Poly(Methyloxazoline)

Carboxyl terminated poly(dimethylsiloxane)-b-poly(methyloxazoline) (PDMS-PMOXA) was synthesized as described before [30]. Briefly, 15.6 µmol (101.40 mg) of PDMS-PMOXA ($PDMS_{67}$-*b*-$PMOXA_{15}$, Mn = 5000-b-1300, polydispersity index PDI = 1.25) was solved in 5 mL of dichloromethane (DCM). 87.4 µmol (8.75 mg) of succinic anhydride, 15.6 µmol (1.91 mg) of dimethyl aminopyridine (DMAP, Sigma Aldrich), and 79.5 µmol (11 µL) of triethylamine (TEA, Sigma Aldrich) were added to the reaction. The reaction was carried out overnight slowly reaching room temperature. An ultrafiltration using a dialysis membrane (MWCO = 1000, Spectrapor, Spectrum labs, Breda, Netherlands) for 24 h was carried out to purify the reaction. Fourier transformed infrared (FT-IR) spectroscopy was performed to confirm the final compound structure.

2.11. Synthesis of N-Hydroxisuccinimide Activated Poly(Dimethylsiloxane)-b-Poly(Methyloxazoline)

After dissolving the carbonyl terminated poly(dimethylsiloxane)-b-poly(methyloxazoline) in 5 mL of dichloromethane in a round bottom flask, the reaction mixture was cooled to 4 °C. Then, 65.4 µmol (10.2 mg) of N-(3-dimethylaminopropyl)-N'-ethylcarbodiimide hydrochloride (EDAC, Sigma Aldrich) and 100 µmol (11.5 mg) of N-hydroxylsuccinimide (NHS, Sigma Aldrich) were added to the mixture. The final compound was recovered after performing dialysis for 24 h in DCM. The N-hydroxisuccinimide activated poly(dimethylsiloxane)-b-poly(methyloxazoline) was obtained in quantitative yield and FT-IR analysis was performed to confirm the final structure.

2.12. Surface Modification of Polymer Vesicles with the NH2-Ahx-GSGFLGSC Peptide and Paclitaxel Loading

Nanoparticles holding a paclitaxel payload were formulated as described before [30]. The nanoparticles were diluted five times (200 µL nanoparticle suspension in 800 µL PBS) leading to a 1 mg/mL of nanoparticle suspension. To 1 mL of 1 mg/mL of nanoparticle suspension, 10 µL of 4.7 mM p-maleimidophenyl isocyanate (PMPI) in dimethyl sulfoxide (DMSO) were added and stirred overnight at room temperature to allow modification of the nanoparticle surface. The peptide Fmoc-Ahx-GSGFLGSC (GSG; Ahx = aminocaproic acid; Biomatik, Cambridge, Ontario, Canada) was deprotected as described before [30]. In brief, 76 µL of piperidine were added to 10 mg of Fmoc-protected GSG-peptide in 300 µL dimethylformamide and stirred for 1 h at room temperature. A cold ether precipitation was conducted to recover the deprotected GSG-peptide. Ten µL of a 10 mg/mL GSG-peptide solution in PBS and 10 µL EDAC (10 mg/mL in MilliQ water) were added to the 1mg/mL solution of nanoparticles to react overnight at room temperature. After coupling the peptide to the nanoparticle's surface, an additional extrusion similar to the previously described was performed. The nanoparticles were then purified by ultrafiltration (MWCO 12-14 kDa, Spectrapor) overnight at room temperature against PBS.

urea. To determine the protein content, the Bradford assay (Thermo Fischer) was used. Cell lysate was collected harvesting the cells in 5 mM Tris-HCL supplemented with protease inhibitor cocktail (Sigma Aldrich, Buchs, Switzerland), followed by three cycles of freezing thawing in liquid nitrogen. For Western blot analysis protein samples were supplemented with Laemmli and then separated by a 10% SDS-PAGE. Afterwards, the proteins were electrotransferred to a nitrocellulose membrane (Bio-Rad Laboratories). After blocking with 5% FCS/1% albumin in TBS-T, the membranes were exposed overnight and at 4 °C to the primary antibody sc-365558 (Santa Cruz Biotechnology, diluted 1:500) for cathepsin B or sc-47778 (Santa Cruz Biotechnology, diluted 1:1000) for actin. Thereafter, the blot was exposed to the respective HRP-conjugated secondary antibodies (Bio-Rad Laboratories) for 1 h at RT. Pierce™ ECL Western Blotting Substrate (Thermo Fisher) and the ChemiDoc™ MP Imaging System equipped with the image lab software (version 4.1) both from Bio-Rad Laboratories were used for image acquisition.

2.5. Detection of CTSB Activity by Enzymatic Assay

CTSB's activity in OVCAR-3 and OVCAR-5 cells was detected by the liberation of the fluorescent 7-amino-4-methylcoumarin from Z-Arg-Arg 7-amido-4-methylcoumarin (Sigma-Aldrich). The assay was performed according to the instruction manual and as previously described by Barrett et al. [27]. In short, 60 µL of 8 mM L-cysteine-HCl in 352 mM potassium phosphate buffer (including 48 mM sodium phosphate, and 4.0 mM ethylenediaminetetraacetic acid), 70 µL 0.1% Brij 35 solution in purified water, 10 µL of cell lysate or supernatant and 60 µL 0.02 mM of Nα-CBZ-Arg-Arg-7-amido-4-methylcoumarin in 0.1% Brij 35 solution. The release of 7-amino-4-methylcoumarin was measured with the microplate reader Tecan Infinite M200 Pro (Tecan, Männedorf, Switzerland; excitation = 348 nm, emission = 440 nm).

2.6. Cell Culture

The cell lines OVAR-5 (RRID:CVCL_1628), and OVCAR-3 (ATCC HTB-161) were commercially obtained from the American Tissue Culture collection, (Manassas, MA, USA). OVCAR-3 were cultured in RPMI-1640 (BioConcept) supplemented with 20% FCS, 1% non-essential amino acids (MEM-NEAA, BioConcept), and 1% GlutaMAX. OVCAR-5 were cultured in DMEM supplemented with (v/v) 10% FCS, 1% MEM-NEAA, and 1% GlutaMAX. In viability assays, 1% Penicillin/Streptomycin (BioConept) was added to the media. All cell lines were kept at 37 °C in a humidified atmosphere with 5% CO_2.

2.7. Immunofluorescence of Cathepsin B in Ovarian Cancer Cells

OVCAR-5 and OVCAR-3 cells were seeded at a density of 2×10^5 cells/well on cover slips placed in 12 well plates. One day after seeding, cells were fixed with ice-cold methanol-acetone (1:1, v/v) for 5 min at −20 °C. After several washing steps with PBS, unspecific antibody binding was prevented by incubation with 5% normal goat-serum/ 0.3% Triton X-100 in PBS for 1 h at room temperature. Cells were incubated with the primary antibody anti-Cathepsin B (sc-366558, Santa Cruz Biotechnology Inc., Dallas, Texas, TX, USA) diluted in antibody dilution buffer (1% BSA/0.3% Triton X-100 in PBS, 1:10) overnight at 4 °C. After washing with PBS, cells were incubated with the secondary Alexa Fluor™ goat-anti-mouse 568 antibody (Thermo Fisher) diluted in antibody dilution buffer (1:200). After incubation for 1 h at room temperature, cells were washed with PBS and mounted using Roti®-Mount FluorCare containing DAPI for nuclei stain (Carl Roth GmbH + Co. KG). For antibody control, the primary antibody was omitted. Images were taken with the Leica DMi8 Microscope with the MC 170HD camera and LASV4.8 software (Leica Microsystems, Heerbrugg, Switzerland).

2.8. Assessment of Hydrodynamic Radius and Surface Charge of the Nanoparticles

To measure the hydrodynamic radius of the nanoparticles, the dynamic light scattering (DLS) technique was used (Malvern Zetasizer NanoSeries, Malvern Instruments GmbH, Herrenberg, Germany). Briefly, the samples were degassed utilizing a Thermo Vac sample degassing and thermostat

2.13. Determination of the Encapsulation Efficiency.

To determine the encapsulation efficiency, high-performance liquid chromatography (HPLC) analysis was used. The GSG-modified polymer membrane was disrupted by the use of Triton-X (Merck, Zug, Switzerland) in water and acetonitrile (VWR International, Dietikon, Switzerland). In detail, 25 µL of 1 mg/mL nanoparticle (theoretically containing 0.2 mg/mL paclitaxel), 25 µL of 0.4% triton-X in water and 50 µL acetonitrile were combined, vortexed and centrifuged for 3 min at 4000 × *g*. The amount of paclitaxel encapsulated in the nanoparticles was detected with an Agilent 1100-series equipped with diode array and evaporating light scattering detector (Agilent Technologies, Basel, Switzerland). The mobile phase consisted of ddH_2O (buffer A) and acetonitrile (buffer B, VWR International, Dietikon, Switzerland). Separation was achieved with a Poroshell C18 column (3.0 × 100 mm 2.7-micron, Agilent Technologies). Starting at 50% A, 50% B changing from minute 1 to minute 11 to 0% A, 100% B, with a flow rate of 0.45 mL/min. The paclitaxel peak had a retention time of 4.8/4.9 min. To calculate the concentration of encapsulated paclitaxel a paclitaxel standard curve (Cathepsin B Table S3A,B; AUC versus concentration) was recorded.

2.14. Fluorescent Labeling of the Polymeric Nanoparticles

Fluorescent labeling of the polymeric nanoparticles was achieved by incorporating 3,3′-dioctadecyloxacarbocianine perchlorate (DiO, Sigma-Aldrich). In brief, 5 µL of a 25 mg/mL DiO stock solution in ethanol was added to the DCM during preparation of the thin-film layer. The dried thin-film layer was then rehydrated with PBS as described above.

2.15. Release and Uptake of Fluorescently Labeled Nanoparticles

The fluorescently labeled nanoparticles were bound to a Pierce™ maleimide activated black 96-well-plate (Thermo Fisher) according to the manufacturer's manual. In brief, after several washes with washing buffer, 100 µL of a fluorescently-labeled polymeric nanoparticle-solution (200 µg/mL in binding buffer) were added to each well and incubated over night at 4 °C to achieve nanoparticle binding to the plate's surface. The surface binding was followed by additional washes with washing buffer. Not reacted maleimide-groups were deactivated by incubation with 100 µL 10 mg/mL L-cysteine-solution for 1 h at RT. After several washes, 100 µL of 100 µg/mL cathepsin B, 100 µg/mL cathepsin B supplemented with 100 µM CA-074, or PBS solvent control were added, respectively. After incubation for 24 h at 37 °C, the difference in fluorescent signal on the 96-well without supernatant was measures using the microplate reader Tecan Infinite M200 Pro (excitation = 490 nm, emission = 530 nm). The reduction in fluorescent signal measured on the plate's surface was interpreted as evidence of release caused by cathepsin B.

2.16. Cell Viability Assay

OVCAR-3 cells were seeded in 96-well plates at a density of 15,000 cells/well to assess cell viability. To determine the impact of PDMS-PMOXA-GSG-Paclitaxel particles on cell viability, cells were treated one day after seeding with increasing concentrations of paclitaxel (0.01 nM to 1 µM). The content of paclitaxel in the nanoparticles was quantified by HPLC. In order to analyze whether the release of paclitaxel is mediated by cellular cathepsin B, cells were pre-treated with 0.1 µM of the cathepsin B inhibitor CA-074 (Sigma-Aldrich) or DMSO control three hours after seeding. After 24 h, cells were exposed to PDMS-PMOXA-GSG-Paclitaxel with or without 2 µM CA-074. As positive control, cells were incubated with 25 µg/mL cathepsin B from human placenta (Sigma-Aldrich). After 48 h, cell viability was measured using the Fluorometric Cell Viability Kit I (Resazurin) from PromoKine (Vitaris AG, Baar, Switzerland). The microplate reader Tecan Infinite M200 Pro (Tecan) was used for quantification of cell viability (fluorescence, excitation = 530 nm, emission = 590 nm). Data are presented as mean ± SD as percent of control. IC_{50} values were estimated using a three-parameter logistic function assuming a standard slope.

2.17. Statistical Analysis

Statistical analysis was performed with the GraphPad prims software (version 6, GraphPad Software Inc. La Jolla, CA, USA). For statistical analysis of real time PCR a student's t-test or one way ANOVA with multi-comparison was applied. Statistical analyses of cell viability studies were performed by column statistics with one-sample student's t-test. In vitro data points mentioned in this publication consist of at least three independent experiments each performed with two biological replicates. A p-value ≤ 0.05 was considered statistically significant.

3. Results

3.1. Comparison of Cathepsin B in Tumor Entities of Female Organs.

With the intention to confirm presence of the peptidase in malignant transformed cells, the number of cathepsin B mRNA copies was determined in tumor entities originating from cervix, breast, endometrium, and ovary. Comparison of the number of transcripts in healthy and malignant transformed tissue revealed a statistically significant reduction of the amount of transcripts in tumors originating from breast compared to healthy tissue (mean number of CTSB copies ± SD; healthy vs. tumor 13,276 ± 3527 n = 2 vs. 2583 ± 3674 n = 23, Mann–Whitney test; $p = 0.002$). A similar trend was observed for the cervix (mean number of CTSB copies ± SD; healthy vs. tumor 15,502.80 ± 20,072 n = 4 vs. 5207.09 ± 3475 n = 9, Mann–Whitney test; $p = 0.144$), and the endometrium, whereas in tumors originating from ovary, the amount of transcripts did not exhibit this trend (healthy vs. tumor; 3685 ± 1318, n = 3 vs. 6922 ± 6782 n = 21; Mann–Whitney test; $p = 0.172$). Subsequently, we analyzed the data set on the cathepsin B mRNA expression for the impact of the tumor stage (Supplemental Figure S1). There was a statistically significant reduction in breast cancer stage I, II, and III compared to healthy breast tissue (Supplemental Figure S1A; mean copy numbers ± SD normal vs. stage I, II, and III; 13,276 ± 3527; 3593 ± 881.2; 3378 ± 2954; 3831 ± 5088), suggesting that reduction is independent of the tumor stage. No statistically significant differences in cathepsin B mRNA expression was detected comparing different tumor stages in samples deriving from cervix (Supplemental Figure S1B) or endometrium (Supplemental Figure S1C). Interestingly, stage I ovarian carcinoma showed a trend to increased expression of cathepsin B mRNA compared to normal tissue (Supplemental Figure S1D).

To further validate the presence of cathepsin B in ovarian tumor tissue, immunohistochemistry of a healthy ovarian tissue, and an ovarian adenocarcinoma sample was performed. As shown in Figure 1, there was staining of only a limited number of cells in ovarian tissue. In the adenocarcinoma tissue a disperse coloring in the surrounding of the cells was observed, with strong staining in some cells. In cells, CTSB appeared to be localized in intracellular granules. To validate our results assessed on a limited sample size, a literature search was conducted. Six previous publications were found describing increased CTSB expression, content or activity in ovarian cancer compared to healthy tissue (Supplemental Table S2).

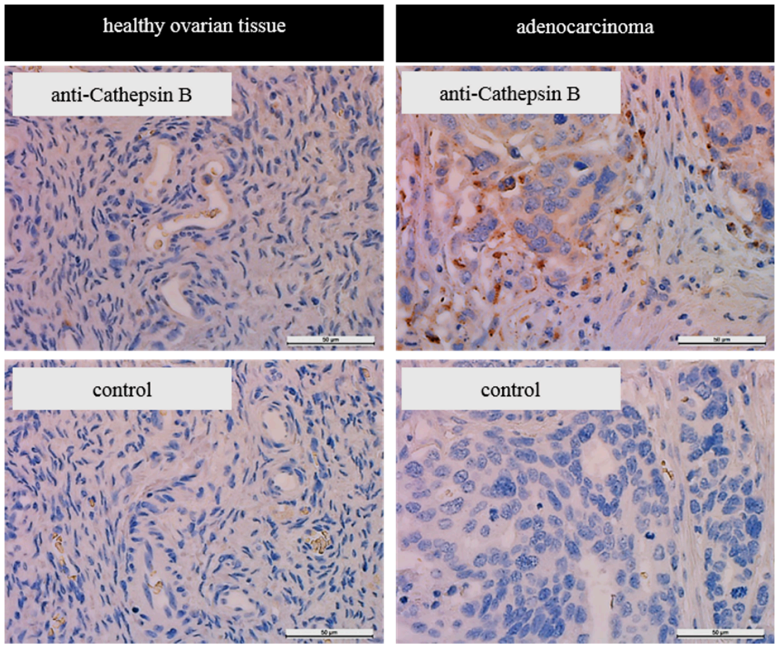

Figure 1. Cathepsin B expression in ovarian carcinoma and healthy tissue. Protein expression was detected by immunohistochemistry in healthy ovarian tissue or ovarian adenocarcinoma. In control sections, the primary antibody was omitted. Scale bar 50 µm.

3.2. Characterization of CTSB Expression in Human Ovarian Cancer Cell Lines.

In order to test the herein described cathepsin B degradable nanoparticles in vitro, we characterized two different ovarian cancer cell lines for the expression of this enzyme in comparison to human ovary. In these two ovarian carcinoma cell lines, namely OVCAR-3 and OVCAR-5, the mRNA expression of cathepsin B was comparable (Figure 2A), even if lower than in the human tissue samples. However, Western blot analysis of the intra- and extracellular protein fraction suggested a much higher amount of cathepsin B in OVCAR-3 compared to OVCAR-5 (Figure 2B). This was even more evident after normalization of the cathepsin B band to that of actin (Figure 2C; mean normalized protein amount ± SD; OVCAR-3 vs. OVCAR-5; intracellular: 1.568 ± 0.0580 vs. 0.4325 ± 0.1415; unpaired t-test; $p = 0.0002$; n = 3; extracellular: OVCAR-3 vs OVCAR-5; 1.587 ± 0.6411 vs. 0.4069 ± 0.2154). Assessing CTSB activity by liberation of 7-amino-4-methylcoumarin from Z-Arg-Arg-7-amido-4-methylcoumarin showed increased turnover in presence of the cell lysate of OVCAR-3 compared to OVCAR-5 (Figure 2D; mean nM of CTSB in 75µg intracellular protein ± SD; OVCAR-3 vs. OVCAR-5; 6.507 ± 0.3852 vs. 4.539 ± 0.2410; unpaired t-test; $p < 0.0001$; n = 3). Similar results were obtained for the extracellular protein fraction (mean nM of CTSB in 100 µg extracellular protein ± SD; OVCAR-3 vs. OVCAR-5; 0.2457 ± 0.4563 vs. not detectable; n = 3), where no CTSB activity was detected in the supernatant of OVCAR-5 cells. Our finding was further confirmed by immunofluorescent staining detecting cathepsin B in the cells. As shown in Figure 2E the staining of cathepsin B was observed in intracellular vesicles and was more intense in the OVCAR-3 cell line. Accordingly, we selected this cell model for further investigations of the herein described nanoparticles.

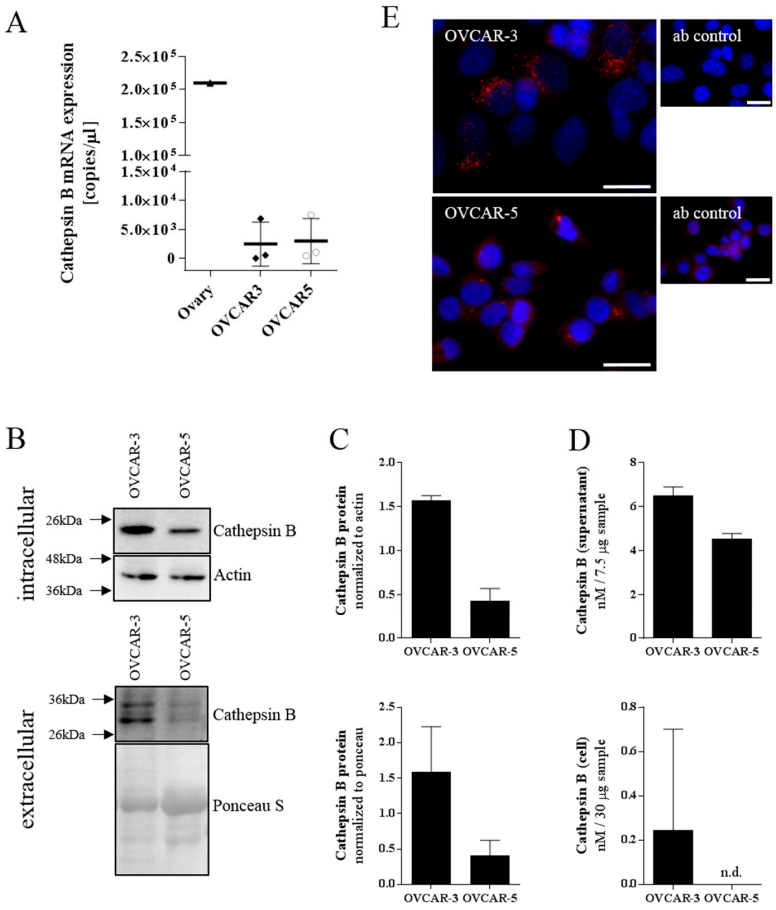

Figure 2. Cathepsin B expression in ovarian cancer cell lines. (**A**) mRNA expression of cathepsin B assessed by qPCR. (**B**) Western blot analysis of cathepsin B, protein loading and actin in cell supernatant and in the cytoplasm of different cell lines. (**C**) Cathepsin B signal from cell supernatant normalized to ponceau S and intracellular cathepsin B signal normalized to actin signal. (**D**) Activity of cathepsin B inside the cells and in the cell supernatant. (**E**) Immunofluorometric microscopy of cathepsin B (red) and nuclei (blue) in ovarian cancer cell lines. Scale bar 25 µm.

3.3. FT-IR Analysis of PDMS-PMOXA Modification Steps

The polymer was modified by standard coupling reactions and the Michael addition. Each synthetic step was characterized by FT-IR to assure the modification. The unmodified PDMS-PMOXA (Figure 3A) showed a distinct peak at 1690 cm^{-1} reflecting the carbonyl stretching. After modification of PDMS-PMOXA with succinic anhydride, an additional peak at 1732 cm^{-1} appeared (Figure 3B). After activation with NHS, additional peaks at 1738 cm^{-1} and 1789 cm^{-1} were visible representing the carbonyl stretching of the COO-NHS ester (Figure 3C). Finally, modification of the nanoparticle surface with the GSG-peptide caused peaks for N-H vibrations (amide-A) at 3368 cm^{-1} and C=O stretching (amide I) at 1635 cm^{-1} (Figure 3D).

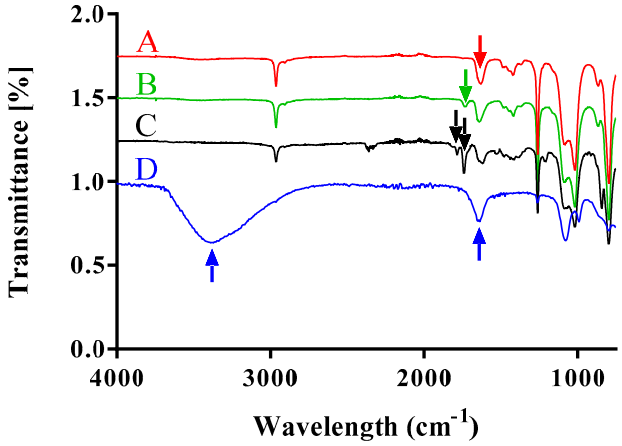

Figure 3. Fourier transform infrared spectra of modified poly(dimethylsiloxane)-poly(methyloxazoline). (**A**) FTIR spectrum of the diblock copolymer before modification. The arrow indicates a peak at 1690 cm^{-1}, which corresponds to the carbonyl stretching of the PMOXA moieties. (**B**) FTIR spectrum of the carboxylic acid modified diblock copolymer. The arrow shows a stretching peak at 1732 cm^{-1} indicating the presence of the carbonyl group. (**C**) FTIR spectrum of the N-hydroxylsuccinimide (NHS) activated polymer. Here, the arrows indicate the peaks at 1738 and 1789 cm^{-1} which show the NHS modification of the polymer (carbonyl stretching in the COO-NHS ester moiety). (**D**) FTIR spectrum of GSG-modified nanoparticles. N–H stretching vibrations at 3368 cm^{-1} (Amide-A) are visible. C=O stretching vibrations (Amide I) peaks at 1635 cm^{-1}.

3.4. Characterization of PDMS-PMOXA-GSG Nanoparticles

Diblock-copolymer PDMS-PMOXA nanoparticles loaded with paclitaxel were formulated using the thin-film technique followed by rehydration in PBS buffer. A series of extrusion was performed to homogenize the size distribution. Finally, the surface of the nanoparticles was cross-linked using the GSG-peptide. The different nanoparticles are schematically depicted in Figure 4A. Subsequently, the hydrodynamic diameter was assessed by dynamic light scattering comparing loaded and unloaded nanoparticles before and after peptide surface-modification. For the unloaded nanoparticles the surface-modification of the nanoparticles did influence the observed hydrodynamic diameter slightly but statistically significant (mean diameter ± SD, PDMS-PMOXA vs. PDMS-PMOXA-GSG; 123.2 ± 0.68 nm vs. 120.43 ± 0.56 nm; n = 3; one-way ANOVA, $p < 0.05$; Figure 4B,C). Loading the surface-modified nanoparticles with paclitaxel did further increase the mean diameter (PDMS-PMOXA-GSG-Paclitaxel; 129.6 ± 1.05 nm; n = 3; one-way ANOVA, $p < 0.05$) as shown in Figure 4D. The size stability of the surface-modified nanoparticles with paclitaxel was determined over a period of 5 days. During that period, the nanoparticles swelled from 129.6 ± 1.05 nm to 143.4 ± 3.58 nm (n = 3; unpaired t-test, $p < 0.05$; Supplemental Figure S2).

A Gaussian distribution of the diameter was observed for all formulations (Figure 4B–D). These results were confirmed by electron microscopy imaging (Figure 4E), where a homogenous vesicular formulation was observable for all nanoparticles. Finally, the PDMS-PMOXA-GSG nanoparticle's drug-loading was assessed by HPLC (Figure S3A,B, Table S3A). The loading averaged at 9.58 ± 0.67% of the deployed concentration resulting in a concentration of 19.17 ± 1.34 µg paclitaxel/mL (Table S3B).

The CAC (Supplemental Figure S4) determined for unloaded PDMS-PMOXA nanoparticles was 4.8 µg/mL (0.744.8 µM). A similar critical micelle concentration (1 µg/mL) was measured for $PDMS_{65}$-*b*-$PMOXA_{14}$ [31].

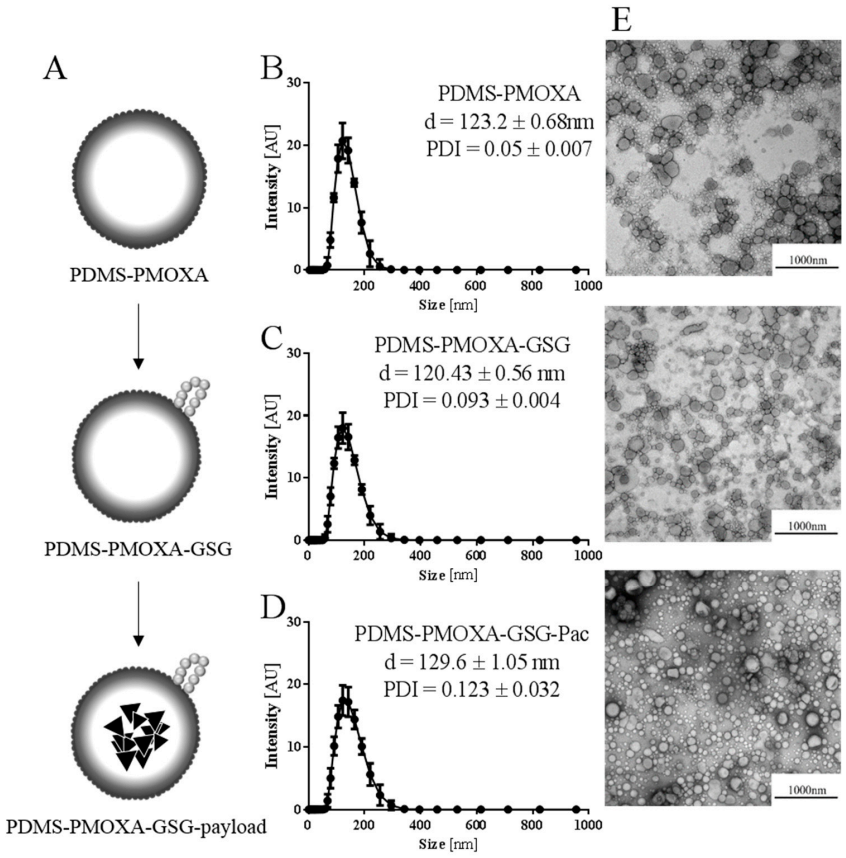

Figure 4. Characterization of nanoparticles by dynamic light scatting and electron microscopy. (**A**) The schematic representation shows the different stages at which diameter and shape was recorded. The impact of the surface-modification on hydrodynamic diameter and shape are illustrated for PDMS-PMOXA particles without surface-modification (**B**) surface-modified PDMS-PMOXA particles without payload (**C**) and surface-modified PDMS-PMOXA particles with paclitaxel payload (**D**) Data are represented as mean ± SD. (**E**) Transmission electron microscopy images reflected the size measured by DLS.

3.5. Influence of Cathepsin B on Fluorescently Labeled GSG-Surface-Modified Nanoparticles

DiO-labeled GSG-surface-modified nanoparticles were covalently bound to a plate surface and then exposed to cathepsin B in order to determine the influence of this enzyme on the nanoparticles. The obtained results showed a significant reduction in residual fluorescent signal after exposure to cathepsin B compared to simultaneous exposure to cathepsin B and the cathepsin B inhibitor CA-074 (Figure 5; mean % of buffer control ± SD; cathepsin B without inhibitor vs. cathepsin B with CTSB inhibitor; 54.07 ± 2.230 vs. 92.29 ± 3.723, $p < 0.05$; paired t-test), suggesting that CTSB treatment influenced the surface of the nanoparticle and thereby the DiO-loading.

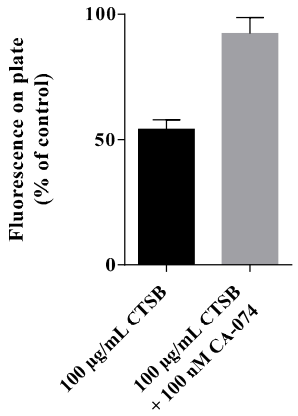

Figure 5. Cathepsin B triggered reduction of DiO-labeled GSG-surface-modified nanoparticles. The influence of cathepsin B was determined after covalently binding DiO-labeled GSG-surface-modified nanoparticles to the surface of a maleimide-plate. The bound nanoparticles were exposed to the enzyme in presence or absence of the CTSB-inhibitor CA-074. Data are reported as mean percent of buffer control + SD of n = 3 experiments.

3.6. Impact of PDMS-PMOXA-GSG-Paclitaxel Particles on Cell Viability

In order to analyze the influence of the paclitaxel-loaded PDMS-PMOXA-GSG-particles on cell viability, OVCAR-3 cells were treated for 48 h and cell viability was determined. The quantity of paclitaxel in these particles was determined before each experiment using HPLC. As demonstrated in Figure 6A, we observed an effect of the nanoparticles on cell viability. This effect was concentration-dependent with an IC_{50} value of 29.93 nM (CI-95% 14.74–60.81 nM). As the activity of cathepsin B is suggested to modulate the release of paclitaxel from these nanoparticles, cells were treated with 50 nM paclitaxel loaded PDMS-PMOX-GSG in presence of 2 µM of the cathepsin B inhibitor CA-074 (compare Figure 6B). Even though we did not observe an increase in cell viability using 2 µM CA-074 (Mean ± SD 50 nM vs. 50 nM with CA-074; 70.94 ± 8.2% vs. 73.79 ± 4.97%) there was a decrease in viability when cells were exposed to the nanoparticles in combination with cathepsin B (62.92 ± 5.81%; one way ANOVA, $p = 0.09$;). Moreover, this effect was slightly reduced by simultaneous treatment with CA-074 (71.36 ± 8.60%; $p = 0.07$). In Figure 6C, the cell viability of unloaded peptide-modified nanoparticles showed no toxic effect on OVCAR-3 cells. Sensitivity of OVCAR-3 cells to paclitaxel was confirmed as shown in Supplemental Figure S5 (IC_{50} = 1.158 nM, CI-95% 0.39 to 3.47 nM). Finally, the CTSB inhibitor CA-074 was tested for its influence on cell viability as shown in Figure 6E (IC_{50} = 70.32µM; CI-95% 30.47–162.3 µM).

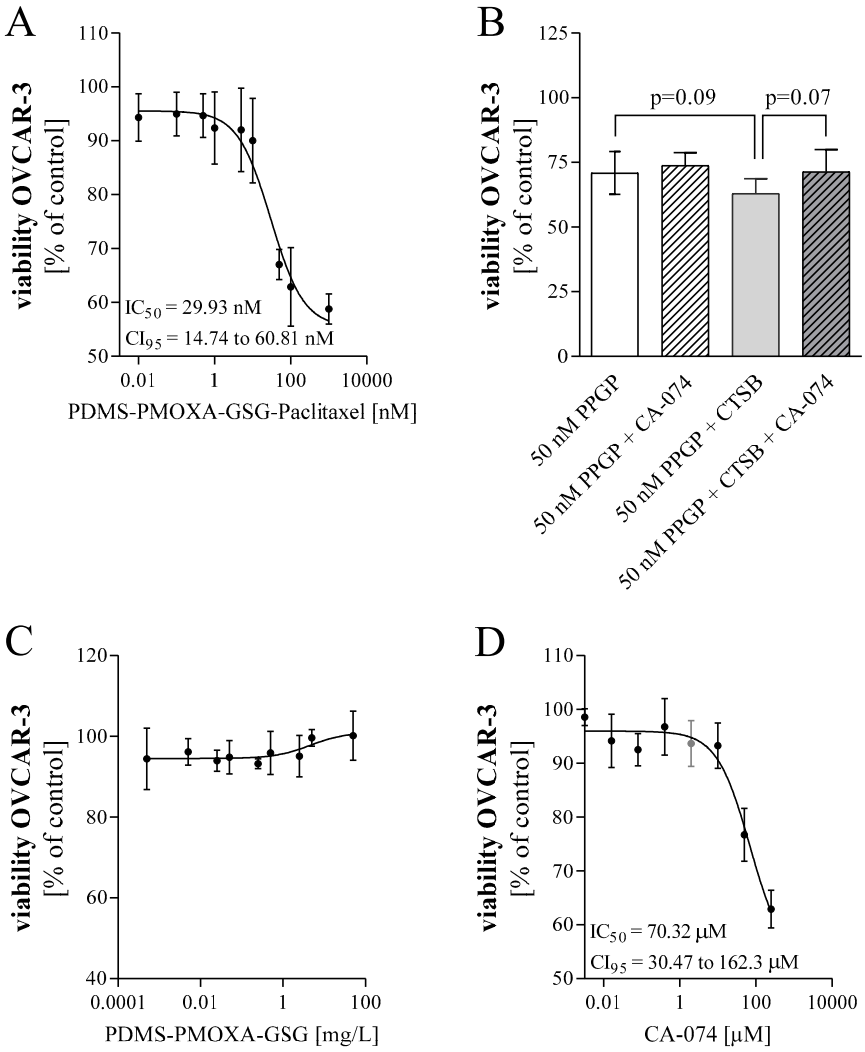

Figure 6. Impact of paclitaxel and paclitaxel-loaded peptide-modified particles (PPGP) on cell viability. (**A**) Cell viability of OVCAR-3 after 48 h exposure to increasing concentrations of paclitaxel-loaded cathepsin B sensitive particles. Viability was assessed using resazurin. IC50 values were calculated fitting the obtained experimental data. (**B**) Cell viability of OVCAR-3 after 48 h exposure to paclitaxel-loaded GSG-modified particles with or without inhibitor CA-074 and/or cathepsin B (CTSB). (**C**) Cell viability of unloaded peptide-modified particles was determined as control. (**D**) Cell viability of OVCAR-3 was determined after 48 h exposure to increasing concentrations of the CTSB-inhibitor CA-074. The grey data point indicates the concentration used in the previous experiment. Data are presented as mean ± SD, of n = 3 experiments each performed in technical triplicates.

4. Discussion

In this study, we investigated cathepsin B digestible particles for delivery of chemotherapeutics to ovarian cancer cells. We loaded PDMS-PMOXA nanoparticles with paclitaxel and modified the particle surface with a cathepsin B cleavable peptide. A suitable in vitro model was selected and characterized before assessing the impact of the formulated nanoparticles on cellular viability.

The herein studied formulation is based on the idea to use cathepsin B as a trigger for release of a chemotherapeutic. The mode of action of this release mechanism requires increased activity of

cathepsin B to ensure the triggering release close to the tumor. Comparison of expression levels of this proteolytic enzyme in healthy and malignant transformed tissue originating from various organs revealed that there is no significant difference in mRNA levels for most of the herein tested tumor entities. In this context it seems noteworthy, that the mRNA expression was assessed in a small collection of samples. Even though the sample number was low, out of the researched tumor-entities, breast cancer showed a significant reduction in cathepsin B mRNA expression compared to healthy tissue. We are not providing data on activity or protein amount. However, Berquin et al. observed decreased mRNA in RAS-transformed MCF-10A epithelial cells, while the amount and activity of the enzyme was increased compared to parenteral cells [32]. Importantly, Krepela et al. also observed increased cathepsin B activity in malignant breast carcinoma tissue [33].

The impact of tumor progression on cathepsin B mRNA expression levels was assessed considering the reported tumor stage. In cervical and endometrial cancer tissue, mRNA expression was not significantly different from healthy tissue. For ovarian carcinoma a trend towards increased mRNA expression levels was observed, especially in stage I tumors. Therefore, ovarian carcinoma was used as a model system for further investigation, supported by findings of a larger scale study on cathepsin B mRNA expression in malignant ovarian carcinoma compared to healthy tissue [34]. Interestingly, their data have shown a higher distribution of mRNA expression in malignant ovarian cancer stage I/II than in stage III/IV, which is similar to our data. Benign tumors on the other hand showed no difference in cathepsin B expression compared to healthy tissue [35]. Although mRNA expression is very interesting to discuss, it is difficult to correlate the expression level to the amount or the activity of cathepsin B due to alternative splicing variants. Concerning the cathepsin B expression, there are many regulatory steps during transcription, post-transcriptional processing, translation, post-translational processing, and trafficking [36]. The transcriptional efficiency can be influenced by different transcriptional starting points [37,38], by alternative promoters [36] and variable pre-mRNA splicing [37,39–41]. In tumor tissue, the mRNA splice-variant lacking exon 2 is assumed to be predominant. This splice-variant has a lower stability due to a shorter untranslated region (UTR) and it is twice as active as the mRNA including exon 2 [37]. The mRNA lacking exon 2 seems to be prone to extracellular release, especially when the expression is increased [42]. In short, the differences in the mRNA sequences are suggested to affect the stability of the mRNA, which influences translation, sorting, and activity of this enzyme [37,42].

Tumors are known for their heterogeneity in many phenotypic features including gene expression [43]. Unsurprisingly, cathepsin B appears to be non-uniformly expressed throughout the tumor but increased expressed at the border to the extracellular matrix [23]. Immunohistochemical staining of tissue sections supported the notion that there is an increased amount of cathepsin B in ovarian tumor tissue compared to healthy ovarian tissue. However, the herein reported immunohistochemistry data are only of limited validity as we are only reporting on one sample. However, they support findings of Scorilas et al. who reported similar results researching tumor tissue deriving ovarian cancer patients by immunohistochemistry [44] and of Warwas et al. describing increased cathepsin B activity in the blood serum of patients with ovarian carcinoma [35].

We characterized the ovarian cancer cell lines OVCAR-3 and OVCAR-5 for their cathepsin B expression. Both cell lines showed similar cathepsin B mRNA expression levels which is in accordance with the GEO dataset GDS4296/227961_at [45]. However, Western blot analysis of intra- and extracellular proteins showed a higher amount of cathepsin B in OVCAR-3 compared to OVCAR-5 cells. This finding was confirmed by immunofluorescent staining leading to OVCAR-3 being selected as the in vitro model system of choice for our study on CTSB-peptide-modified polymersomes.

Following our previous research on an MMP9-sensitive drug delivery system [30], a cathepsin B-sensitive drug delivery system was to be developed and investigated. For cathepsin B, there have been lesser approaches described, making it an interesting topic. Most of the researched formulations were polymer–drug conjugates with cathepsin B triggered release mechanisms [46–48]. These formulations

use either a cathepsin B degradable polymer [46] or peptides like the herein used amino acid sequence Gly-Phe-Leu-Gly [47–51] for the enzyme-triggered release of the payload.

Our nanoparticles appear to be colloidally stable. However, testing the stability of the formulation over a period of 5 days revealed a significant swelling of the nanoparticles. The stability was accomplished by additional extrusion step after loading and modification. After this additional extrusion step the loading efficacy was fairly low at 9.22%, which could also depend on the used peptide.

In the herein used in vitro model system PDMS-PMOXA-GSG nanoparticles loaded with paclitaxel showed an approximately 25-fold decrease in IC_{50} compared to pure paclitaxel. This indicated a gradual release of paclitaxel during exposure with cells. A trend towards increasing cytotoxicity was observed when adding purified cathepsin B to the nanoparticles. This suggests that the added enzyme increases the digestion of the peptide surface layer and, therefore, accelerates release of payload. The cathepsin B inhibitor (CA-074) affects cell viability as it exhibits a cytotoxic effect itself with an IC_{50} of 70.32 µM. Accordingly, it is difficult to differentiate between the effect of the inhibitor and the effect of the drug paclitaxel, especially in a co-treatment. An increase in cell viability was observed after testing the nanoparticles with additional cathepsin B and inhibitor, which is in line with our expectations at a concentration of 2 µM. Treatment of cells with unloaded PDMS-PMOXA-GSG nanoparticles showed no change in cell viability.

Taken together, we report on the formulation of nanoparticles loaded with paclitaxel containing a cathepsin B digestible surface. These nanoparticles were stable with a slight tendency to swell. Furthermore, the surface-modified nanoparticles were tested in a suitable ovarian cell line for their payload release.

Supplementary Materials: The following are available online at http://www.mdpi.com/1996-1944/12/17/2836/s1, Table S1: Cathepsin B gene expression in normal and malignant-transformed tissue. The mRNA copy-numbers were assessed by multiplex real-time PCR in different malignant-transformed tissue. Breast tissue is the only sample with statistically significant difference in cathepsin B mRNA expression, Table S2: Previous publications on cathepsin B in ovarian cancer. Literature research of publications on cathepsin B expression, protein and/or enzyme activity in ovarian cancer tissue samples, Table S3: Calculation of the encapsulation efficiency using the area under the curve. Table A contains AUC and corresponding concentration to calculate the standard curve. In Table B, the paclitaxel contained in the nanoparticles was calculated using the standard curve determined in Table A. Figure S1: Cathepsin B gene expression in normal and malignant-transformed tissue. The mRNA copy-numbers were assessed by multiplex real-time PCR in different malignant-transformed tissue. Depicted is the expression of cathepsin B mRNA in healthy and malignant tissue originating from breast (A), cervix (B), endometrium (C), and ovary (D) tissue, Figure S2: Stability of the paclitaxel-loaded surface modified polymeric nanoparticle. The hydrodynamic diameter was measured after formulation on day 1 (A) and on day 5 (B), Figure S3: Determination of the encapsulation efficiency by HPLC. Examples of HPLC UV-chromatogram recorded at wavelength 225,4 nm for the paclitaxel standard curve (A) and paclitaxel loaded PP-GSG nanoparticles (B). The retention time of paclitaxel lays between 4.8 and 4.9 mintutes, Figure S4: Critical aggregation concentration of PDMS-PMOXA. The critical aggregation concentration of PDMS-PMOXA determined by using pyrene incorporation, a hydrophobic fluorescent probe, Figure S5: Impact of paclitaxel on cell viability. Cell viability of OVCAR-3 after 48 h exposure to paclitaxel with increasing concentrations of paclitaxel. Viability was assessed using resazurin. IC_{50} values were calculated. Mean ± SD, n = 3 in technical triplicates.

Author Contributions: Conceptualization, D.E., F.P., J.H and H.E.M.z.S.; methodology, D.E., F.P., J.H. and H.E.M.z.S.; formal analysis, D.E.; investigation, DE., J.H., I.S., H.E.M.z.S.; resources, H.E.M.z.S; writing—original draft preparation, D.E. and J.H.; writing—review and editing, D.E., J.H. & H.E.M.z.S.; visualization, D.E.; supervision, H.E.M.z.S.; project administration, D.E. and H.E.M.z.S.; funding acquisition, H.E.M.z.S.

Funding: This research received no external funding.

Conflicts of Interest: The authors declare no conflict of interest.

References

1. Bray, F.; Ferlay, J.; Soerjomataram, I.; Siegel, R.L.; Torre, L.A.; Jemal, A. Global cancer statistics 2018: GLOBOCAN estimates of incidence and mortality worldwide for 36 cancers in 185 countries. *CA: A Cancer J. Clinicians* **2018**, *68*, 394–424. [CrossRef] [PubMed]
2. Chabner, B.A.; Roberts, T.G., Jr. Timeline: Chemotherapy and the war on cancer. *Nat. Rev. Cancer* **2005**, *5*, 65–72. [CrossRef] [PubMed]

3. Chari, R.V. Targeted cancer therapy: conferring specificity to cytotoxic drugs. *Acc. Chem. Res.* **2008**, *41*, 98–107. [CrossRef] [PubMed]
4. Perez-Herrero, E.; Fernandez-Medarde, A. Advanced targeted therapies in cancer: Drug nanocarriers, the future of chemotherapy. *Eur. J. Pharm. Biopharm.: Off. J. Arbeitsgemeinschaft fur Pharmazeutische Verfahrenstech. e.V.* **2015**, *93*, 52–79. [CrossRef] [PubMed]
5. Maeda, H.; Nakamura, H.; Fang, J. The EPR effect for macromolecular drug delivery to solid tumors: Improvement of tumor uptake, lowering of systemic toxicity, and distinct tumor imaging in vivo. *Adv. Drug Deliv. Rev.* **2013**, *65*, 71–79. [CrossRef] [PubMed]
6. Danhier, F. To exploit the tumor microenvironment: Since the EPR effect fails in the clinic, what is the future of nanomedicine? *J. Control. Release: Off. J. Controll. Release Soc.* **2016**, *244*, 108–121. [CrossRef] [PubMed]
7. Costas, D. *Pharmaceutical Nanotechnology. Fundamentals and Practical Applications*; Springer Nature: Berlin, Germany, 2016; ISBN 978-981-10-0791-0.
8. Wicki, A.; Witzigmann, D.; Balasubramanian, V.; Huwyler, J. Nanomedicine in cancer therapy: challenges, opportunities, and clinical applications. *J. Control. Release: Off. J. Control. Release Soc.* **2015**, *200*, 138–157. [CrossRef] [PubMed]
9. Hadjichristidis, N.; Pispas, S.; Floudas, G. *Block Copolymers: Synthetic Strategies, Physical Properties, and Applications*; John Wiley & Sons, Inc.: Hoboken, NJ, USA, 2003; ISBN 978-0-471-39436-5.
10. Egli, S.; Nussbaumer, M.G.; Balasubramanian, V.; Chami, M.; Bruns, N.; Palivan, C.; Meier, W. Biocompatible functionalization of polymersome surfaces: a new approach to surface immobilization and cell targeting using polymersomes. *J. Am. Chem. Soc.* **2011**, *133*, 4476–4483. [CrossRef] [PubMed]
11. Camblin, M.; Detampel, P.; Kettiger, H.; Wu, D.; Balasubramanian, V.; Huwyler, J. Polymersomes containing quantum dots for cellular imaging. *Inter. J. Nanomed.* **2014**, *9*, 2287–2298. [CrossRef]
12. Broz, P.; Benito, S.M.; Saw, C.; Burger, P.; Heider, H.; Pfisterer, M.; Marsch, S.; Meier, W.; Hunziker, P. Cell targeting by a generic receptor-targeted polymer nanocontainer platform. *J. Control. Release: Off. J. Control. Release Soc.* **2005**, *102*, 475–488. [CrossRef] [PubMed]
13. Goddard, P.; Lusie, E.; Brown, J.; Brookman, L.J. Soluble polymeric carriers for drug delivery. Part 2. Preparation and in vivo behaviour of N-acylethylenimine copolymers. *J. Control. Release* **1989**, *10*, 5–16. [CrossRef]
14. Zhang, X.Y.; Zhang, P.Y. Polymersomes in Nanomedicine—A Review. *Curr. Med. Chem.* **2017**, *13*, 124–129. [CrossRef]
15. Bobo, D.; Robinson, K.J.; Islam, J.; Thurecht, K.J.; Corrie, S.R. Nanoparticle-based medicines: a review of FDA-approved materials and clinical trials to date. *Pharm. Res.* **2016**, *33*, 2373–2387. [CrossRef] [PubMed]
16. Andresen, T.L.; Thompson, D.H.; Kaasgaard, T. Enzyme-triggered nanomedicine: drug release strategies in cancer therapy. *Mol. Membr. Biol.* **2010**, *27*, 353–363. [CrossRef] [PubMed]
17. Wolfram, J.; Zhu, M.; Yang, Y.; Shen, J.; Gentile, E.; Paolino, D.; Fresta, M.; Nie, G.; Chen, C.; Shen, H.; et al. Safety of Nanoparticles in Medicine. *Curr. Drug Targets* **2015**, *16*, 1671–1681. [CrossRef]
18. Loomis, K.; McNeeley, K.; Ravi, V. Nanoparticles with targeting, triggered release, and imaging functionality for cancer applications. *Soft Matter* **2010**, *7*, 839–856. [CrossRef]
19. Nishikawa, H.; Ozaki, Y.; Nakanishi, T.; Blomgren, K.; Tada, T.; Arakawa, A.; Suzumori, K. The role of cathepsin B and cystatin C in the mechanisms of invasion by ovarian cancer. *Gynecol. Oncol.* **2004**, *92*, 881–886. [CrossRef]
20. Guicciardi, M.E.; Miyoshi, H.; Bronk, S.F.; Gores, G.J. Cathepsin B knockout mice are resistant to tumor necrosis factor-alpha-mediated hepatocyte apoptosis and liver injury: implications for therapeutic applications. *Am. J. Pathol.* **2001**, *159*, 2045–2054. [CrossRef]
21. Fonovic, M.; Turk, B. Cysteine cathepsins and extracellular matrix degradation. *Biochim. et Biophys. Acta* **2014**, *1840*, 2560–2570. [CrossRef]
22. Gocheva, V.; Joyce, J.A. Cysteine cathepsins and the cutting edge of cancer invasion. *Cell Cycle* **2007**, *6*, 60–64. [CrossRef]
23. Sinha, A.A.; Gleason, D.F.; Deleon, O.F.; Wilson, M.J.; Sloane, B.F. Localization of a biotinylated cathepsin B oligonucleotide probe in human prostate including invasive cells and invasive edges by in situ hybridization. *Anat. Rec.* **1993**, *235*, 233–240. [CrossRef] [PubMed]

24. Adenis, A.; Huet, G.; Zerimech, F.; Hecquet, B.; Balduyck, M.; Peyrat, J.P. Cathepsin B, L, and D activities in colorectal carcinomas: relationship with clinico-pathological parameters. *Cancer Lett.* **1995**, *96*, 267–275. [CrossRef]
25. Sloane, B.F.; Dunn, J.R.; Honn, K.V. Lysosomal cathepsin B: Correlation with metastatic potential. *Science* **1981**, *212*, 1151–1153. [CrossRef] [PubMed]
26. Jedeszko, C.; Sloane, B.F. Cysteine cathepsins in human cancer. *Biol. Chem.* **2004**, *385*, 1017–1027. [CrossRef] [PubMed]
27. Barrett, A.J.; Kirschke, H. [41] Cathepsin B, cathepsin H, and cathepsin L. *Methods Enzymol.* **1981**, *80 Pt C*, 535–561. [CrossRef] [PubMed]
28. Grossen, P.; Québatte, G.; Witzigmann, D.; Prescianotto-Baschong, C.; Dieu, L.H.; Huwyler, J. Functionalized solid-sphere peg-b-pcl nanoparticles to target brain capillary endothelial cells in vitro. *J. Nanomater.* **2016**, *2016*, 13. [CrossRef]
29. Goddard, E.D.; Turro, N.J.; Kuo, P.L.; Ananthapadmanabhan, K.P. Fluorescence probes for critical micelle concentration determination. *Langmuir ACS J. Surf. Colloids* **1985**, *1*, 352–355. [CrossRef] [PubMed]
30. Porta, F.; Ehrsam, D.; Lengerke, C.; Meyer Zu Schwabedissen, H.E. Synthesis and Characterization of PDMS-PMOXA-Based Polymersomes Sensitive to MMP-9 for Application in Breast Cancer. *Mol. Pharm.* **2018**, *15*, 4884–4897. [CrossRef] [PubMed]
31. Wu, D. Amphiphilic block copolymers: Synthesis, self-assembly and applications. Doctoral Thesis, University of Basel, Basel, Switzerland, 2015.
32. Berquin, I.M.; Sloane, B.F. Cathepsin B expression in human tumors. *Adv. Exp. Med. Biol.* **1996**, *389*, 281–294. [PubMed]
33. Krepela, E.; Vicar, J.; Cernoch, M. Cathepsin B in human breast tumor tissue and cancer cells. *Neoplasma* **1989**, *36*, 41–52.
34. Downs, L.S.J.; Lima, P.H.; Bliss, R.L.; Blomquist, C.H. Cathepsins B and D activity and activity ratios in normal ovaries, benign ovarian neoplasms, and epithelial ovarian cancer. *J. Soc. Gynecol. Investig.* **2005**, *12*, 539–544. [CrossRef] [PubMed]
35. Warwas, M.; Haczynska, H.; Gerber, J.; Nowak, M. Cathepsin B-like activity as a serum tumour marker in ovarian carcinoma. *Eur. J. Clin. Chem. Clin. Biochem. J. Forum of Eur. Clin. Chem. Soc.* **1997**, *35*, 301–304. [CrossRef]
36. Podgorski, I.; Sloane, B.F. Cathepsin B and its role(s) in cancer progression. *Biochem. Soc. Symp.* **2003**, 263–276. [CrossRef]
37. Gong, Q.; Chan, S.J.; Bajkowski, A.S.; Steiner, D.F.; Frankfater, A. Characterization of the cathepsin B gene and multiple mRNAs in human tissues: evidence for alternative splicing of cathepsin B pre-mRNA. *DNA Cell Biol.* **1993**, *12*, 299–309. [CrossRef] [PubMed]
38. Berquin, I.M.; Cao, L.; Fong, D.; Sloane, B.F. Identification of two new exons and multiple transcription start points in the 5′-untranslated region of the human cathepsin-B-encoding gene. *Gene* **1995**, *159*, 143–149. [CrossRef]
39. Berardi, S.; Lang, A.; Kostoulas, G.; Horler, D.; Vilei, E.M.; Baici, A. Alternative messenger RNA splicing and enzyme forms of cathepsin B in human osteoarthritic cartilage and cultured chondrocytes. *Arthritis Rheum.* **2001**, *44*, 1819–1831. [CrossRef]
40. Zwicky, R.; Muntener, K.; Goldring, M.B.; Baici, A. Cathepsin B expression and down-regulation by gene silencing and antisense DNA in human chondrocytes. *Biochem. J.* **2002**, *367*, 209–217. [CrossRef]
41. Muntener, K.; Zwicky, R.; Csucs, G.; Baici, A. The alternative use of exons 2 and 3 in cathepsin B mRNA controls enzyme trafficking and triggers nuclear fragmentation in human cells. *Histochem. Cell Biol.* **2003**, *119*, 93–101. [CrossRef]
42. Baici, A.; Muntener, K.; Willimann, A.; Zwicky, R. Regulation of human cathepsin B by alternative mRNA splicing: Homeostasis, fatal errors and cell death. *Biol. Chem.* **2006**, *387*, 1017–1021. [CrossRef]
43. Marusyk, A.; Polyak, K. Tumor heterogeneity: causes and consequences. *Biochim. et Biophys. Acta* **2010**, *1805*, 105–117. [CrossRef]
44. Scorilas, A.; Fotiou, S.; Tsiambas, E.; Yotis, J.; Kotsiandri, F.; Sameni, M.; Sloane, B.F.; Talieri, M. Determination of cathepsin B expression may offer additional prognostic information for ovarian cancer patients. *Biol. Chem.* **2002**, *383*, 1297–1303. [CrossRef] [PubMed]

45. Pfister, T.D.; Reinhold, W.C.; Agama, K.; Gupta, S.; Khin, S.A.; Kinders, R.J.; Parchment, R.E.; Tomaszewski, J.E.; Doroshow, J.H.; Pommier, Y. Topoisomerase I levels in the NCI-60 cancer cell line panel determined by validated ELISA and microarray analysis and correlation with indenoisoquinoline sensitivity. *Mol. Cancer Ther.* **2009**, *8*, 1878–1884. [CrossRef] [PubMed]
46. Melancon, M.P.; Li, C. Multifunctional synthetic poly(L-glutamic acid)-based cancer therapeutic and imaging agents. *Mol. Imaging* **2011**, *10*, 28–42. [CrossRef] [PubMed]
47. Dai, Y.; Ma, X.; Zhang, Y.; Chen, K.; Tang, J.Z.; Gong, Q.; Luo, K. A biocompatible and cathepsin B sensitive nanoscale system of dendritic polyHPMA-gemcitabine prodrug enhances antitumor activity markedly. *Biomater. Sci.* **2018**, *6*, 2976–2986. [CrossRef] [PubMed]
48. Soler, M.; Gonzalez-Bartulos, M.; Figueras, E.; Ribas, X.; Costas, M.; Massaguer, A.; Planas, M.; Feliu, L. Enzyme-triggered delivery of chlorambucil from conjugates based on the cell-penetrating peptide BP16. *Org. Biomol. Chem.* **2015**, *13*, 1470–1480. [CrossRef] [PubMed]
49. Yang, Y.; Pan, D.; Luo, K.; Li, L.; Gu, Z. Biodegradable and amphiphilic block copolymer-doxorubicin conjugate as polymeric nanoscale drug delivery vehicle for breast cancer therapy. *Biomaterials* **2013**, *34*, 8430–8443. [CrossRef] [PubMed]
50. Zhong, Y.J.; Shao, L.H.; Li, Y. Cathepsin B-cleavable doxorubicin prodrugs for targeted cancer therapy (Review). *Int. J. Oncol.* **2013**, *42*, 373–383. [CrossRef] [PubMed]
51. Lee, G.Y.; Qian, W.P.; Wang, L.; Wang, Y.A.; Staley, C.A.; Satpathy, M.; Nie, S.; Mao, H.; Yang, L. Theranostic nanoparticles with controlled release of gemcitabine for targeted therapy and MRI of pancreatic cancer. *ACS Nano* **2013**, *7*, 2078–2089. [CrossRef]

Results III

"Design, Synthesis, and Characterization of a Paclitaxel Formulation Activated by Extracellular MMP9"

Daniel Ehrsam [1], Sandro Sieber [2], Mouhssin Oufir [3], Fabiola Porta [1], Matthias Hamburger [3], Jörg Huwyler [2], Henriette E Meyer Zu Schwabedissen [1]

Affiliations:

[1] Biopharmacy, Department Pharmaceutical Sciences, University of Basel, Klingelbergstrasse 50, 4056 Basel, Switzerland.

[2] Pharmaceutical Technology, Department Pharmaceutical Sciences, University of Basel, Klingelbergstrasse 50, 4056 Basel, Switzerland.

[3] Pharmaceutical Biology, Department Pharmaceutical Sciences, University of Basel, Klingelbergstrasse 50, 4056 Basel, Switzerland.

Contribution Daniel Ehrsam: Study design, acquisition, analysis and interpretation of data, drafting of manuscript.

PMID: 31894970 DOI: 10.1021/acs.bioconjchem.9b00865

Bioconjugate Chemistry

pubs.acs.org/bc Article

Design, Synthesis, and Characterization of a Paclitaxel Formulation Activated by Extracellular MMP9

Daniel Ehrsam, Sandro Sieber, Mouhssin Oufir, Fabiola Porta, Matthias Hamburger, Jörg Huwyler, and Henriette E. Meyer zu Schwabedissen*

Cite This: https://dx.doi.org/10.1021/acs.bioconjchem.9b00865 Read Online

ACCESS | Metrics & More | Article Recommendations | Supporting Information

ABSTRACT: The concept of triggered drug release offers a possibility to overcome the toxic side effects of chemotherapeutics in cancer treatment by reducing systemic exposure to the active drug. In the present work, the concept foresees the use of the extracellular enzyme MMP9 as an enzymatic trigger for drug release in the proximity of tumor cells. Methods: A paclitaxel-hemisuccinate-peptide conjugate as a building block for self-assembling nanoparticles was synthesized using standard conjugation approaches. The building block was purified via preparative HPLC and analyzed by LC−MS. Nanoparticles were formed using the nanoprecipitation method and characterized. For selection of a suitable in vitro model system, common bioanalytical methods were used to determine mRNA expression, enzyme amount, and activity of MMP9. Results: The MMP9-labile prodrug was synthesized and characterized. Nanoparticles were formed out of MMP9-labile conjugate-building blocks. The nanoparticle's diameter averaged at around 120 nm and presented a spherical shape. LN-18 cells, a glioblastoma multiforme derived cell line, were chosen as an in vitro model based on findings in cancer tissue and cell line characterization. The prodrug showed cytotoxicity in LN-18 cells, which was reduced by addition of an MMP9 inhibitor. Conclusion: taken together, we confirmed increased MMP9 in several cancer tissues (cervical, esophageal, lung, and brain) compared to healthy tissue and showed the effectiveness of MMP9-labile prodrug in in vitro tests.

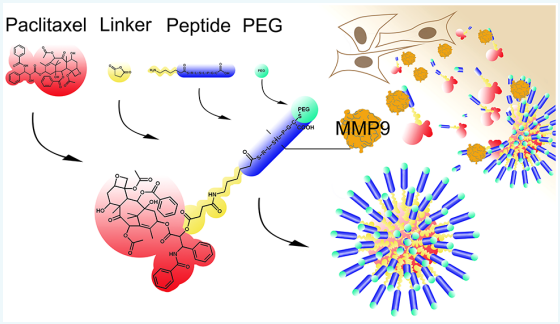

INTRODUCTION

Cancer, the abnormal growth of malignant transformed cells, is a disease as old as humankind. Documented cases have been found in ancient Egyptian manuscripts and the Greek physician Hippocrates described mass producing diseases (onkos) and ulcerating nonhealing lumps (karkinos).[1] Accordingly, discovery of treatments and a cure for cancer has long been a medical goal, with approaches ranging from surgical removal to radiotherapy and intravenous delivery of antiproliferative drugs (i.e., chemotherapy).[1] While surgical removal and radiotherapy are locally applied to the diseased area (i.e., tumor tissue), chemotherapy[2] also affects proliferation of healthy cells throughout the organism. Systemic exposure leads to adverse side effects and dosing limitations.[3,4] Therefore, current development in cancer therapy focuses on increasing the selectivity for malignant cells. By this approach, systemic exposure to the active drug can be reduced, e.g., by targeted therapy using nanoparticulate drug delivery systems (i.e., nanomedicines).[5]

Drug targeting can be reached by different mechanisms which can be divided into passive and active approaches. One mechanism considered as passive targeting is the enhanced permeability and retention effect (EPR), where macromolecules or nanoformulations are assumed to accumulate in the tumor tissue mediated by neoangiogenesis and poor lymphatic drainage. The EPR-effect seems to be useful for tumor-targeting but is also a heterogeneous phenomenon.[6] In contrast, active targeted drug delivery strategies are employing specific targeting ligands which drive an enrichment in a certain tissue or cell but are still suffering from a poor clinical translation.[7] An addition to the above-mentioned mechanism would be the use of stimuli responsive prodrugs or nanomedicines, which release the active compound upon tumor specific stimuli whereby increasing local drug effects. Elicitor stimuli for drug release include changes in pH,[8] in redox potential,[9] or enhanced enzyme activity.[10] The latter concept is based on enzymes identified as being upregulated in the extracellular environment of malignant transformed cells,[11,12]

Received: December 24, 2019
Revised: January 1, 2020
Published: January 2, 2020

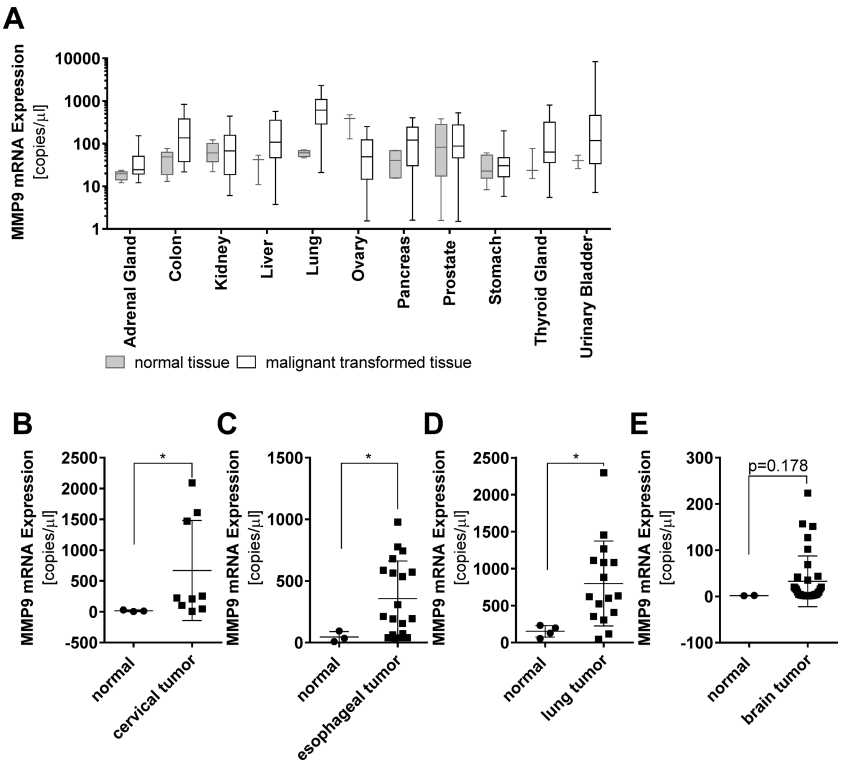

Figure 1. Comparison of MMP9 mRNA expression in normal and malignant transformed tissue. The number of mRNA copies were assessed by multiplex RT-qPCR in a variety of organs (A). In cervix (B), esophagus (C), lung (D), and brain (E), MMP9 mRNA appeared to be higher in tumor than in healthy tissue. Data were obtained in $n \geq 2$ healthy tissue samples and $n \geq 9$ tumor samples summarized in a commercial mRNA-panel. Data are presented as mean ± SD showing each data point in B to E. *$p < 0.05$ Mann−Whitney test.

which can be used for the design of targeted drug delivery or triggered release formulations.[13,14] By modifying drug molecules or the nanoparticles' surfaces with a substrate for a specific enzyme (trigger moiety), drug targeting can be achieved.[15]

An example of such enzymes qualifying as an elicitor for triggered release is the family of matrix-metalloproteinases (MMPs).[16,17] The family of MMPs contains several zinc-dependent endopeptidases, which play an important role in physiological and pathological processes.[18] MMPs are involved in the regulation of pathways important for cell growth and cancer growth including differentiation, apoptosis, migration, invasion, angiogenesis, and immune response. Notably, it has been reported that expression levels and activity of certain MMPs correlate with cancer stage, invasiveness, rate of metastasis, and poor survival.[19−21]

The MMP enzyme family is subdivided into collagenases, stromelysins, matrilysins, and gelatinases depending on their substrate specificity.[22] Especially the gelatinases MMP2 and MMP9 have attracted the attention of cancer research.[23] Both enzymes exhibit nearly identical physiological substrate specificity[24] and degrade collagen type IV. Both are actively engaged in the degradation of the extracellular matrix (ECM) and the basement membrane. This activity enables angiogenesis and tumor cell invasion,[20,25] which are key parameters of tumor progression. In contrast to MMP2 which is expressed in most cells, MMP9 is only expressed in certain cell types including malignant cells and neutrophils.[18]

Utilizing MMPs for tumor targeting has previously been described applying either a nanoformulation or a prodrug approach.[11,15,26−28] The latter approach mainly focuses on drug-substrate conjugates, which release the active moiety after degradation by MMPs.[15] For the nanoformulation approach, two strategies have been pursued. On the one hand, the peptide-substrate of the enzyme has been incorporated into the liposomal membrane. Here, enzymatic degradation of the peptide is assumed to destabilize the membrane leading to the collapse of the liposome and release of its payload.[26] On the other hand, MMP-labile peptides have been used as linkers for polyethylene glycol (PEG) coating of liposomes, where MMP-mediated cleavage results in PEG-shedding and finally cellular uptake.[11] For example, Zhu et al. studied nanoparticles that possessed an MMP2-cleavable PEG coating. After cleavage, cell-penetrating peptides are exposed, facilitating particle uptake.[27]

In our study we designed, synthesized, and characterized particles consisting of a paclitaxel-hemisuccinate-peptide (PH8) conjugate. We modified the chemotherapeutic paclitaxel to generate an amphiphilic prodrug with the tendency to self-assemble. The amphiphilic paclitaxel prodrug-molecules, namely PH8, consisted of the hydrophobic chemotherapeutic (paclitaxel) covalently bound to a MMP9-labile peptide (NH_2-SRLSLPGC-COOH) which served as the hydrophilic moiety. After formulation of nanoparticles, the surface was further modified with polyethylenglycol (PEG_{2000}) in order to increase the in vitro particle size stability.

https://dx.doi.org/10.1021/acs.bioconjchem.9b00865
Bioconjugate Chem. XXXX, XXX, XXX−XXX

Comparison of MMP9 expression revealed tumors originating from the cervix, esophagus, lung, and brain as potential indication for the designed nanoparticles. According to publicly available gene expression data sets, MMP9 expression was enhanced in brain tumors of higher grade (astrocytoma grade II and glioblastoma grade IV), suggesting that cell lines originating from these tumor entities may be a good in vitro testing system. To assess the functionality of the herein synthesized molecules and formulated particles, in vitro cell model systems were characterized for MMP9 expression, distribution, and activity. On the basis of the high activity found in the glioblastoma cell line LN-18, we investigated the triggered release mechanism as well as the efficacy in this particular cell model.

RESULTS

MMP9 mRNA Expression and Protein in Normal and Malignant Transformed Tissue. To identify a tumor entity as a model target for our MMP9 labile nanoformulation, we analyzed the expression of MMP9 by quantitative RT-qPCR comparing normal and malignant transformed tissue of various tumor entities. Even though the samples showed high interindividual variability (Figure 1A), some tumor entities exhibited a statistically significant increase in the number of MMP9 copies compared to the originating tissue. An increased amount of MMP9-mRNA copies was observed comparing normal and malignant transformed tissue originating from the cervix (Figure 1B; mean of copies ± SD; normal vs tumor; n = 3 vs n = 9; 15.35 ± 13.56 vs 668.6 ± 812.9; Mann−Whitney test; $p < 0.05$), the esophagus (Figure 1C; n = 3 vs n = 19; 45.88 ± 43.64 vs 357.4 ± 305.4; Mann−Whitney test; $p < 0.05$), and the lung (Figure 1D; n = 4 vs n = 16; 152.9 ± 77.93 vs 798 ± 575.3; Mann−Whitney test; $p < 0.05$). A similar trend for enhanced expression was detected in samples deriving from the brain (Figure 1E; n = 2 vs n = 34; 1.82 ± 0.58 versus 32.66 ± 54.92; Mann−Whitney test; $p = 0.178$).

The MMP9 mRNA expression data obtained in the tumor panel were further analyzed determining the influence of the reported tumor grade and tumor stage. Moreover, those data were supplemented with an immunohistological staining of normal and malignant transformed tissues. In detail, in samples derived from the cervix, there tended to be higher amounts of MMP9 mRNA in samples originating from tumors staged higher than II (Figure S 1A) or classified as FIGO grade G3 (Figure S 1B; normal vs grade 3; n = 4 vs 3; 92.82 ± 155.3 vs 1030 ± 888.0; $p < 0.05$; one way ANOVA with Dunn's multiple comparisons test). In comparison to normal cervical tissue (Figure S 1C), where MMP9 was not detectable, the enzyme was readily detected by immunohistochemistry in grade 3 cervical squamosa cell carcinoma (Figure S 1D).

In lung cancer, there was a higher amount of MMP9 mRNA in tumors of stage II compared to normal tissue (Figure S 2A; normal vs grade 3; n = 4 vsn = 6; 152.9 ± 77.93 vs 1090 ± 1090; $p < 0.05$; one way ANOVA with Dunn's multiple comparisons test). Immunohistochemical staining of MMP9 revealed the enzyme close to the alveoli in normal tissue (Figure S 2B), while in lung adenocarcinoma (Figure S 2C) and in grade II lung squamosa cell carcinoma (Figure S 2D), the enzyme was found in abundance close to the blood vessels. There was a significant difference in MMP9 mRNA expression comparing normal to stage III esophageal carcinoma (Figure S 3A; normal vs grade > 3; n = 3 vs 9; 45.88 ± 43.64 vs 464.0 ± 317.8; $p < 0.05$: Dunn's multiple comparisons test). In esophageal tissue (Figure S 3B), little MMP9 could be localized, scattered in the lamina propria. In esophageal squamosa cell carcinoma tissue (Figure S 3C), the enzyme was localized in the tumor cell clusters. Similar to our observation in esophageal cancer tissue, MMP9 mRNA expression in brain cancer tissue (Figure S 4A) divided into several subgroups for the increased tumor stage. Normal brain tissue (Figure S 4B) showed only little MMP-9. In grade II astrocytoma (Figure S 4C), isolated spots of MMP9 were observed. In meningioma (Figure S 4D), a strong staining for MMP9 was detected. Analysis of the data set in more detail suggested an association between tumor stage or tumor grade and MMP9 mRNA expression.

To confirm the differences in MMP9 mRNA expression and to validate the assumption that there is an association between tumor progression and amount of the enzyme, we searched for publicly available GEO data sets (GDS). However, for tumors derived from the cervix, esophagus and lung, no information on tumor grade was available in the selection-criteria matching GDS. Nevertheless, for cervical tissue we used the GDS3233 (Figure S 5A; mean ± SD; normal vs tumor; 200 ± 88.03 vs 860.3 ± 1022, $p < 0.05$; unpaired t test) and observed a statistically significant elevation of MMP9 expression comparing normal (n = 24) and malignant transformed tissue (n = 28) samples. Similar results were obtained for esophageal tissue analyzing the GDS5364 (Figure S 5B; mean ± SD; normal vs tumor; n = 21 vs 28; 381 ± 428.4 vs 1238 ± 1100, $p < 0.05$; unpaired t test) and the GDS72874 (Figure S 5C; mean ± SD; normal vs tumor; n = 10 vs 35; 6.543 ± 0.326 vs 8.283 ± 0.8822, $p < 0.05$; unpaired t test). In the GDS available for lung tumor tissue, statistically significant higher expression of MMP9 in lung cancer tissue was evident (mean ± SD; normal vs tumor; GDS1650: n = 19 vs 35; 269 ± 99.42 vs 756.9 ± 947.2, $p < 0.05$; unpaired t test; and GDS3857: n = 60 vs 60; 8.388 ± 1.383 vs 9.831 ± 1.601, $p < 0.05$; unpaired t test; Figure S 5D,E). GDS reporting on MMP9 expression and tumor grade were available only for brain. Analysis of the GDS1962 revealed a statistically significant higher expression of MMP9 in astrocytoma and glioblastoma compared to normal tissue (Figure S 6A), testing the influence of the tumor grade revealed high expression in GBM grade IV and atsrozytoma grade II (Figure S 6B; mean ± SD; brain vs astrocytoma grade II vs glioblastoma grade IV; n = 23 vs 7 vs 81; 253.8 ± 125.3 vs 1425 ± 2306 vs 1230 ± 1362, $p < 0.05$; one way ANOVA with Dunnett's multiple comparison test). A similar trend was observed in GDS4467 (healthy n = 3, tumor n = 32; Figure S 6C,D). Taken together, in brain samples, there was not only an association between tumor type but also between tumor grade and MMP9 mRNA expression, respectively.

Quantification of MMP9 Amount and Activity in Cultured Cell Lines Derived from Lung and Brain. In order to have an in vitro test system for the herein investigated nanoformulation with enzyme-triggered release, we characterized cell models commonly used for studies on glioblastoma (LN-18), astrocytoma (U87 MG), and lung cancer (A549). At first, we quantified and compared the amount of the gelatinases MMP2 and MMP9 mRNA in these cell lines. The gelatinase MMP2 was included in the characterization due to its similarity to MMP9 in terms of substrate recognition. Our analysis revealed a very high amount of MMP-2 mRNA in the U87 MG astrocytoma cell line, while MMP-9 mRNA expression was highest in LN-18 compared to the other cell

https://dx.doi.org/10.1021/acs.bioconjchem.9b00865
Bioconjugate Chem. XXXX, XXX, XXX−XXX

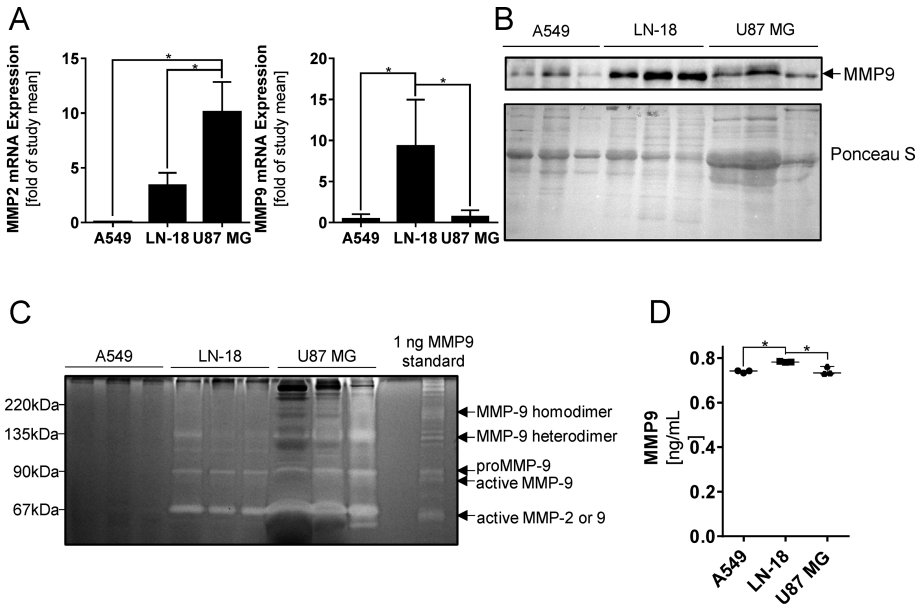

Figure 2. MMP9 expression and activity in cell lines deriving from lung and brain. MMP2 and MMP9 mRNA expression in lung (A549; $n = 3$) and brain cancer (LN-18 and U87 MG; $n = 3$) cell lines (A). Western blot analysis of extracellular MMP9 in the secretome of the cells. Ponceau staining served as loading control (B). Gelatin-zymography showing gelatinase activity in the secretome. Recombinant MMP9 was used as control (C). Quantification of MMP9 activity in the secretome of different cell lines measured by ELISA (D). Data are presented as mean ± SD showing each data point. *$p < 0.05$ one-way ANOVA with Tukey's multiple comparison test.

lines (Figure 2A; MMP2 mRNA expression mean ± SD; $n = 3$; A549 vs U87 MG vs LN-18; 0.040 ± 0.037 vs 10.08 ± 2.759 vs 3.411 ± 1.135; MMP9 mRNA expression mean ± SD; $n = 3$; A549 vs U87 MG vs LN-18; 0.045 ± 0.580 vs 0.731 ± 0.7612 vs 9.347 ± 5.632; $p < 0.05$; one way ANOVA with Tukey's multiple comparison test). However, transcription does not necessarily mean extracellular activity of the enzyme. Detection of MMP9 in the secretome of cultured cells by Western Blot analysis supported the notion that LN-18 cells secrete more MMP9 than A549 or U87 MG cells, respectively. To verify these findings, MMP9 activity was determined by zymography (Figure 2C) and quantified by ELISA (Figure 2D; mean MMP9 amount ± SD; $n = 3$; A549 vs LN-18 vs U87 MG; 0.7393 ± 0.0056 vs 0.782 ± 0.0024 vs 0.741 ± 0.0172, 10 μg/mL supernatant protein; $p < 0.05$; one way ANOVA with Tukey's multiple comparison test). Taken together, the high amount of MMP9 mRNA expression in tissue samples obtained from glioblastoma multiforme and the high activity and amount of the gelatinase in the cell model of grade IV glioblastoma multiforme qualified LN-18 as our in vitro system in this study. The LN-18 glioblastoma cell line was selected to assess the enzyme-triggered release mechanism and the biological activity of the herein designed and synthesized nanoformulation.

Synthesis of Paclitaxel-Hemisuccinate-Peptide (PH8) and Its Product Validation. As shown in Figure S 7, paclitaxel (Figure S 7A) was initially reacted with succinic anhydride yielding in paclitaxel-hemisuccinate (PH; Figure S 7B). Paclitaxel-hemisuccinate-NHS (PH-NHS; Figure S 7C) was then synthesized by a Steglich esterification of paclitaxel-hemisuccinate (PH, Figure S 7B) with NHS. Carboxyl-to-amine linking was achieved by using the NHS-ester of paclitaxel-hemisuccinate (PH-NHS; Figure S 7C) and the deprotected Ahx-SRL-peptide (Ahx = aminocaproic acid, peptide sequence = NH_2-Ahx-SRLSLPGC-COOH, Figure S 7D). This resulted in the paclitaxel-hemisuccinate-peptide conjugate (PH8; Figure S 7E).

The purified PH8 was analyzed by UHPLC-MS/MS. The calculated mass of PH8 of 1879.85 Da was confirmed by a m/z of 1881 $[M + H]^+$ at low fragmentor-voltage (80 V) in the positive mode (Figure S 8A-C). At higher fragmentor voltage (170 V), the parent mass of PH8 (m/z 1881) is mainly fragmented in a daughter mass of S-series + linker + SRL (m/z 1312) (Figure S 8B-D). The MS-spectrum for PH8 (Figure S 8C) revealed two major fragmentation peaks. The peak at 1596.61 m/z at 80 V belonged to the T-series of paclitaxel with the linker and peptide (Figure S 8C) and the peak at 1312.34 m/z at 170 V belonged to the S-series of paclitaxel with the linker and peptide (Figure S 8D).

Molecular Properties of Paclitaxel-Hemisuccinate-Peptide (PH8). PH8 exhibits a computed log P value of −0.21 as determined applying the Molinspiration software. The in silico assessment by Molinspiration Galaxy 3D for hydrophobic and hydrophilic areas supported the assumption of an amphiphilic character (Figure S 9A). This supports the idea that PH8 itself may be used to formulate nanoparticles. The pyrene fluorescent method was applied to determine the concentration at which nanoparticles are formed, that is the critical aggregating concentration (CAC). As shown in Figure S 9B, the CAC of PH8 was 38.53 μg/mL (20.48 μM).

Size and Shape of the PH8-Nanoparticles. PH8 was used to formulate nanoparticles applying the nanoprecipitation method. The resulting particles were then pegylated using PEG_{2000}-maleimide. Unreacted PEG_{2000}-maleimide was removed by size exclusion chromatography. The diameter of both, nonpeglyated and pegylated, nanoparticles was assessed

https://dx.doi.org/10.1021/acs.bioconjchem.9b00865
Bioconjugate Chem. XXXX, XXX, XXX−XXX

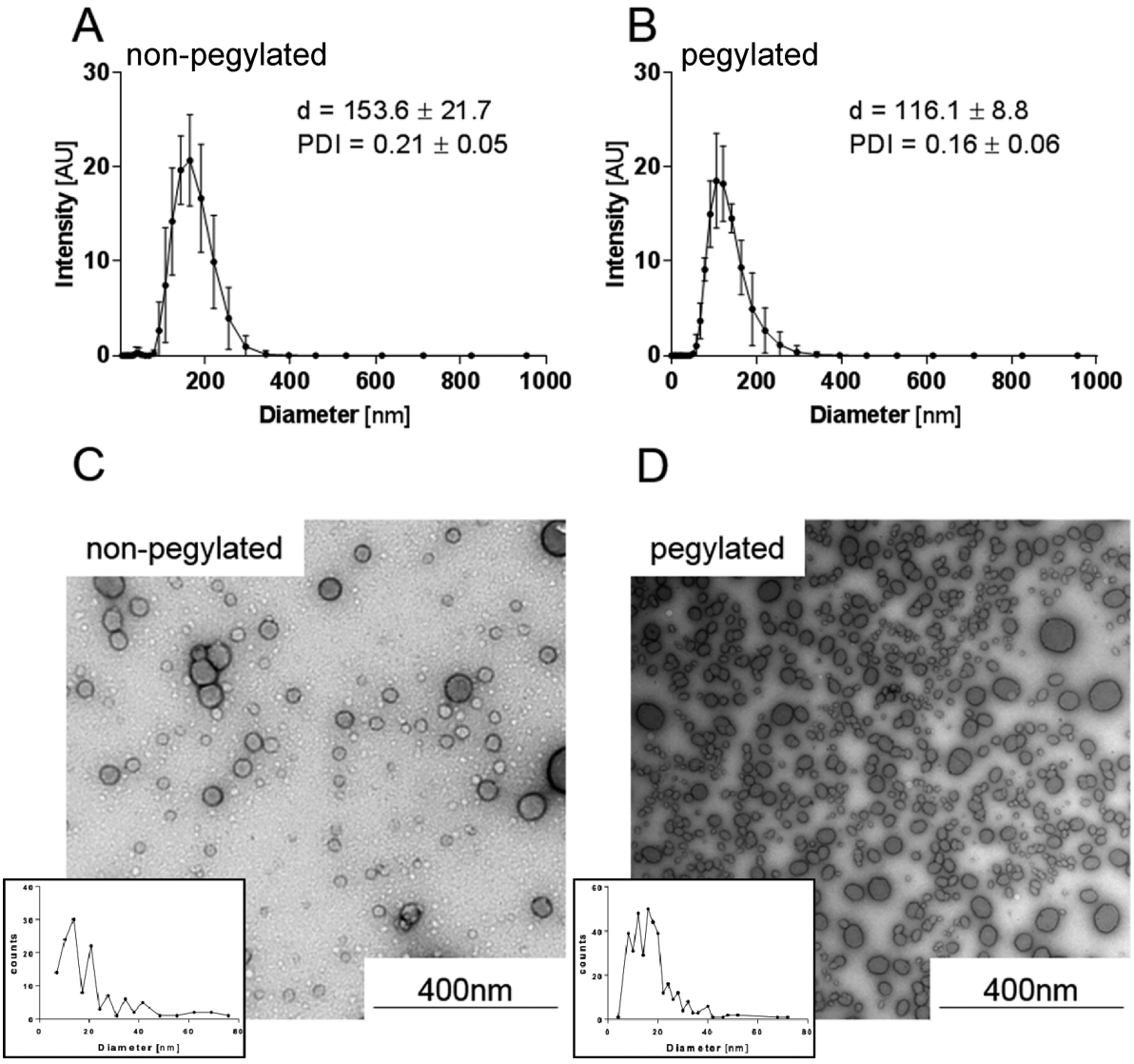

Figure 3. Assessment of PH8-nanoparticle's size and shape applying dynamic light scattering (DLS) analysis and transmission microscopy (TEM). DLS was deployed to determine the diameter (Z-average; d) and polydispersity index (PDI) of nonpegylated (A) and pegylated nanoparticles (B). Data are presented as mean ± SD showing of $n = 3$ independent measurements. Representative TEM images of nanoparticles prior to pegylation (C) and after pegylation and extrusion (D). In the bottom left corner of C and D, the diameter distribution diagram is depicted.

by dynamic light scattering (Figure 3A,B). The nonpegylated nanoparticles had a mean diameter ± SD of 153.6 ± 21.7 nm (Z-average) and a mean polydispersity index (PDI) ± SD of 0.21 ± 0.05 (Figure 3A). In comparison, the pegylated nanoparticles exhibited a mean diameter ± SD of 116.1 ± 8.8 nm and a PDI of 0.16 ± 0.06 (Figure 3B). The measured mean zeta-potential ± SD was comparable for both nonpegylated (−7.46 ± 5.21 mV) and pegylated (−7.23 ± 15.56 mV) nanoparticles. Observing the mean diameter (Z-average) over a period of 7 days of storage at 4 °C, showed an about 7.8% increase in diameter of the nonpegylated nanoparticles with a 46% increase in PDI (day 1 vs day 7, mean diameter ± SD; 125.93 ± 1.07 nm vs 135.70 ± 0.17 nm, PDI: 0.13 vs 0.19; Figure S 10A). For pegylated PH8-nanoparticles, the diameter stayed the same with an about 24% increase in PDI (145.82 ± 4.73 nm vs 148.17 ± 6.33 nm, PDI: 0.26 vs 0.35; Figure S 10B). Inspection of the formulations by transmission electron microscopy indicated that both the pegylated and the nonpegylated PH8-formulation had a round spherical shape in a dry state (Figure 3C,D).

Valdiation of the MMP9 Mediated Cleavage of the SRL-Peptide. In order to verify that MMP9 in the supernatant of cells is capable of cleaving the linker-peptide, we tested the release of fluorescein attached to a plate's surface using the SRL-peptide. By adding the cell supernatant protein of A549, LN-18, or U87 MG cells, the release of fluorescein by enzymes was quantified. The obtained results are in accordance with our findings on the expression and activity of MMP9 in the supernatant of the cell lines. Indeed, the fluorescein-release in the presence of supertnatant of cultured A549 cells was only

https://dx.doi.org/10.1021/acs.bioconjchem.9b00865
Bioconjugate Chem. XXXX, XXX, XXX−XXX

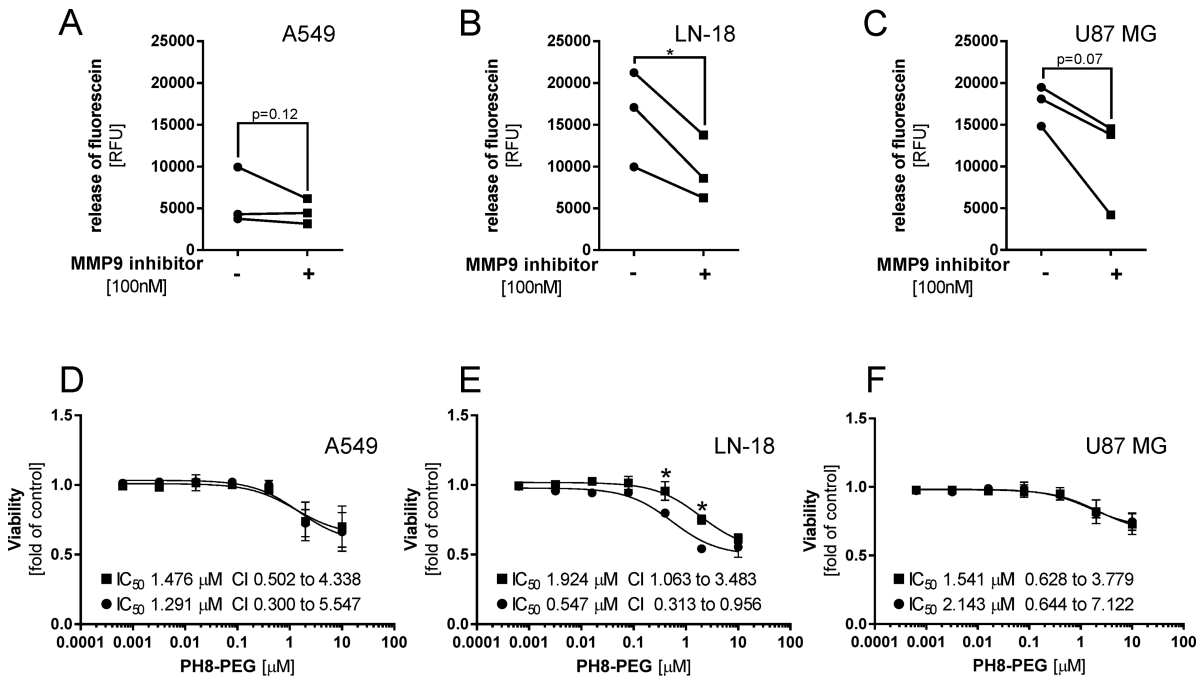

Figure 4. Influence of MMP9 on the SRL-peptide used as linker. The degradation of the SRL-peptide by MMP-9 was measured using immobilized SRL-peptide fluorescein. The release of fluorescein was measured after 24 h exposure to 20 μg cell supernatant of (A) A549, (B) LN-18, and (C) U87 MG. The impact of MMP-9 on the release of fluorescein was shown by addition of a 100 nM MMP-9 inhibitor. Data are presented as mean ± SD showing each data point. *p < 0.05 student's t test paired. The viability of different cell lines A-549(D), LN-18(E), and U87 MG(E) was determined after 24 h exposure to PH8-PEG. The prodrug was either given alone (●) or in combination with 40 nM of the MMP-9 inhibitor (■). Depicted is the viability in fold of control where the cells were only in the culture medium. Viability data are shown as mean ± SD; *p < 0.05 column statistics with one-sample student's t test.

minimal (Figure 4A). In contrast, the supernatant of cultured LN-18 or U87 MG cells (Figure 4B,C) showed higher enzyme activity compared to A549 supernatant and therefore enhanced fluorescein-release. MMP9 inhibitor was used to assess the contribution of the cell-derived MMP9 activity to the cleavage. For A549, the MMP9 inhibitor had only a limited and not statistically significant impact on the release of fluorescein (Figure 4A). For the supernant of cultured U87 MG cells, the addition of MMP9 inhibitor showed a trend (p = 0.07) for reduced fluorescein release (Figure 4C). Only using the supernant of cultured LN-18 cells, we observed a statistical significant reduction in fluorescein-release in the presence of the MMP9 inhibitor (Figure 4B; mean fluorescein released from the plate ± SD; without inhibitor vs MMP9 inhibitor; 16 092 ± 5706 vs 9538 ± 3842, p < 0.05; paired t test).

MMP9 Mediated Release of Fluorescent Dye from Fluorescein-Loaded Ph8-Nanoparticles. To investigate whether the nanoparticles' integrity is influenced by MMP9 activity, fluorescently labeled nanoparticles were immobilized at a plate's surface and then exposed to the enzyme. After 24 h exposure to MMP9 or solvent control, the fluorescent signal in the supernantant or remaining on the plate's surface was determined. The presence of 10 μg/mL MMP9 significantly increased the fluorescent signal in the supernantant (Figure S 11A; control vs MMP9; mean fluorescence ± SD; 25 605 ± 419.6 vs 36 229 ± 1823; n = 3, p < 0.05; student's t test), while significantly reducing the fluorescent signal remaining at the plate, where the fluorescein-loaded PH8-nanoparticles had been attached (Figure S 11B; 40 273 ± 2541 vs 27 396 ± 1803; n = 3, p < 0.05; student's t test).

Influence of PH8, PH8-PEG, and Paclitaxel on the Viability of LN18-Cells. LN18-cells were exposed to PH8 or paclitaxel to test cellular toxicity of the prodrug molecule in comparison to the parent compound (paclitaxel). As shown in Figure S 12A,B, the modification of paclitaxel significantly reduced its toxic potency as determined by estimating the half maximal inhibitory concentration (IC_{50}; CI_{bottom} − CI_{top}) of paclitaxel (7.482 nM; 1.566−35.750 nM) and of PH8 (494.3 nM; 382.8−638.2 nM). In a next step, we tested the influence of the MMP9, deriving from supernatant of cultured cells, on the degradation of PH8-PEG. Here, the PH8 was directly pegylated after synthesis and then used for the treatment of the cancer cell lines A549, LN-18, and U87 MG. As shown in Figure 4D−F, the cells were exposed to increasing concentrations of PH8-PEG either alone or in the presence of a 40 nM MMP9 inhibitor. In LN-18 cells, the MMP9 inhibitor significantly reduced the cytotoxicity of the pegylated prodrug (PH8-PEG) as it significantly increased the IC50 value (1.92 μM) compared to PH8-PEG alone (0.55 μM) (Figure 4E). No statistically significant difference was observed for MMP9 inhibition in A549 (Figure 4D) or U87 MG (Figure 4E) cells.

Finally, we investigated the influence of MMP9 inhibition on the cytotoxic effect of pegylated PH8-nanoparticles in LN-18 cells. The nanoparticles were formulated with PH8 and then pegylated. As shown in Figure 5, exposure to 7.5 μM pegylated nanoparticles significantly reduced the viability of the cells compared to the solvent control (mean viability fold of solvent

https://dx.doi.org/10.1021/acs.bioconjchem.9b00865
Bioconjugate Chem. XXXX, XXX, XXX−XXX

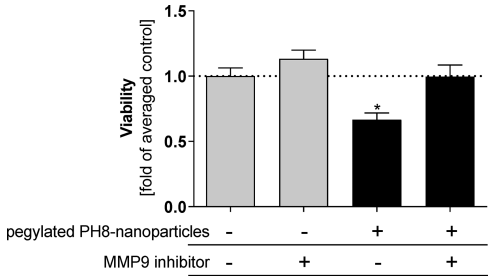

Figure 5. Influence of MMP9 inhibition on LN18 viability during treatment with pegylated PH8-nanoparticles. The viability of LN-18 brain cancer cells was measured after 24 h exposure to 7.5 μM pegylated PH8-nanoparticles and LN18 supernatant. Data are shown as mean fold control ± SD, which were cells cultured with medium control. Data are shown as mean; *p < 0.05 one-way ANOVA Dunnett's multiple comparison.

control ± SD; 0.66 ± 0.03). Importantly, addition of the MMP9 inhibitor significantly enhanced the viability of the cells (0.99 ± 0.05; n = 3, p < 0.05; column statistics, one-sample t test), showing that inhibition of the gelatinase reduced the cytotoxic effect of the pegylated PH8-nanoparticles.

DISCUSSION

In this study, we describe the synthesis and assessment of the physical and pharmacological properties of a paclitaxel-hemisuccinate-peptide (PH8) conjugate-based drug delivery system. The peptide used for modification of paclitaxel is a substrate of the gelatinase MMP9.[29] This design aims at increasing the amount of chemotherpeutic in the area of enhanced enzyme activity. Moreover, due to the amphiphilic character of PH8, the prodrug was expected to exhibit the ability to self-assemble into nanoparticles.

As the gelatinase MMP9 is a key factor of the herein tested concept, it was of utmost interest to investigate different patient-derived tumor samples with regard to MMP9 expression levels. The array included 14 tumor entities of which 3 showed significantly higher MMP9 mRNA expression in malignant tissue compared to their healthy controls. In addition to statistically significant differences in cervix, esophagus, and lung carcinoma, a trend was observed in brain carcinoma. Interestingly, in each entity mentioned, MMP9 mRNA expression showed at least a trend for increased values with increasing tumor stage or tumor grade. We used data sets sourced from the GEO database to confirm the relationship between MMP9 mRNA expression and tumor progression. The GEO data sets for cervical, esophageal, and lung tumors did not include information about the tumor stage or grade. However, the differences of MMP9 mRNA expression comparing healthy and malignant transformed tissues could be confirmed. Rao et al. reported on increased MMP9 expression in cerebrospinal fluid of brain cancer patients[30] and showed that MMP9 expression levels correlate with the aggressiveness of gliomas.[31] The correlation between MMP9 expression and aggressiveness of gliomas reflects our findings analyzing GEO data sets. Similar results have previously been reported for tumor progression of cervical carcinoma[32] and invasiveness of esophageal carcinoma.[33] In lung cancer samples, increased MMP9 mRNA expression has been detected and related to their pathologic type and clinical stage.[34,35] On the basis of the results of the tissue arrays and the GEO data set evaluation, cell models were selected. Cells and cell supernatant originating from brain (LN-18, U-87 MG) and lung (A549) carcinoma were characterized for their MMP9 mRNA expression, MMP9 content, and extracellular activity. The high MMP9 expression and activity observed in the LN-18 glioblastoma cell line led to its selection as the in vitro model system for further testing.

We synthesized a drug conjugate containing paclitaxel linked to a peptide (namely PH8) as a prodrug and building block for nanoparticles. Although effective, paclitaxel is not part of the current standard of care for glioblastoma multiforme likely because of the active removal from the brain by ABCB1 (P-gp).[36] However, we chose this molecule due to its high lipophilicity and the possibility to form an amphiphilic prodrug, when linking to a hydrophilic moiety. The particular peptide (NH_2-Ahx-SRLSLPGC-COOH) used in the synthesis of PH8 was previously investigated for MMP9 triggered release of paclitaxel from stent surfaces by Gliesche et al.[37] and from polymersomes by Porta et al.[38] The cleavage of this peptide by MMP9 was verified in a cell-free assay and reflected the herein measured MMP9 content in the supernatant of cultured LN-18, U87 MG, and A549 cells. Inhibition of the enzymatic activity by addition of the MMP9 inhibitor revealed the contribution of MMP9 to the release.

PH8 was synthesized in a 3-step reaction. First, succinic anhydride was used in a ring-opening reaction to react with paclitaxel. In a second step, the carboxylic acid was activated with *N*-hydoxysuccinimide, and last the activated paclitaxel-hemisuccinate was coupled to the deprotected peptide. When testing the purified product by mass spectrometry, the expected mass (1879.85 Da) was present. Structural analysis by MS-fragmentation revealed that paclitaxel was modified mainly at the C2′-position. In previous publications, paclitaxel derivates were created by modifying various positions of the side chain (C2′ and C3′) and of the main structure (C2, C4, C7, C10, C13, and the D-ring).[39] The C2′-OH plays an important role in the interaction with tubulin and is therefore assumed to be essential for the microtubule-stabilizing effect of paclitaxel.[40] Accordingly, the C2′-OH appears to be of major interest for a prodrug design as its modification would result in a reduced cytostatic activity. Moreover, it has been reported that C2′- compared to C7-modified paclitaxel behaves more like a prodrug, as upon exposure to human plasma, paclitaxel is released.[41] However, the cleavage of the ester-bond and release of paclitaxel might be hindered by sterically demanding groups.[42,43] When assessing PH8 in viability tests, a decreased toxicity was observed in LN-18 cells compared to paclitaxel. Interestingly, paclitaxel and PH8 reached their maximal effect at similar concentrations. Furthermore, a change in Hill slope was observed comparing paclitaxel and PH8. This suggests a change in the pharmacodynamic profile. Similar changes in Hill slope were found by Thapa et al. while researching a far-red light activated pseudoprodrug of paclitaxel with a noncleavable hemisuccinate linker.[42] The similarities as observed suggest that the hemisuccinate linker of PH8 is not cleaved. Due to experimental limitations with LC−MS/MS, we were unable to verify the cleavage product after exposing PH8 or PH8 nanoparticles to MMP9. Comparing PH8 and directly pegylated PH8-PEG showed similar inhibitory potency (IC_{50} values) and response curves in LN-18. Testing PH8-PEG in LN-18, U87 MG, and A549 cells revealed cytotoxic effects in accordance to the herein determined MMP9 expression and content in the cells. Importantly, in LN-18 cells coadministra-

https://dx.doi.org/10.1021/acs.bioconjchem.9b00865
Bioconjugate Chem. XXXX, XXX, XXX−XXX

tion of the MMP9 inhibitor reduced the inhibitory potency as shown by an increase of the observed IC_{50} value by about 2.8 fold. This suggests that MMP9 is contributing to the activation of the prodrug (PH8-PEG). No such effect was observed for U87 MG or A549 cells. The increase in IC_{50} observed in LN-18 cells matches the results obtained by Thapa et al. for a prodrug using a similar linker between paclitaxel and the targeting moiety.[42] When measuring the cell viability after exposure to the PH8-PEG nanoparticles in the presence of MMP9, a cytotoxic effect was apparent. The addition of the MMP9 inhibitor diminished the cytotoxic effect. Having said that, MMP9 concentrations range from 11 to 600 ng/mL in patients with cancer.[44] However, when testing MMP9 content in cultured cells we found 0.74−0.78 ng active MMP9/10ug secreted proteins. Accordingly, we expect that about 15 ng/mL active MMP9 were present in the in vitro viability studies, which lies at the lower end of the reported physiological range.

Since PH8 is predicted to be an amphiphilic molecule, we speculated it may be suitable as a building block for nanoparticles. In these nanoparticles, the peptide would be part of the packaging, paclitaxel would form the hydrophobic core of the structure, while the peptide points toward the hydrophilic environment. We assume that the particles form by self-assembly, driven by paclitaxel developing stacks via intermolecular hydrogen bonds as previously reported by Tian et al.[45] When generating nanoparticles, the size is of importance as it influences the behavior in the organism. In general, a particle's hydrodynamic diameter between 10 and 200 nm is considered best to keep renal filtration, liver and spleen accumulation, and complement system activation at a minimum.[46] The mean hydrodynamic diameter of the herein generated PH8 nanoparticles ranged from 150 nm for nonpegylated nanoparticles to 120 nm for pegylated nanoparticles. The observed size is comparable to the mean diameter of similar particles generated by Tian et al. (130 nm).[45] The CAC of PH8 was 20.48 μM and lies between a typical CMC of surfactants (CMC between 10^{-3}−10^{-4} M) and polymeric micelles with enhanced stability (CMC between 10^{-6}−10^{-7} M).[47]

In conclusion, we report on MMP9 levels in tumor tissue and identification of a cell line suitable for in vitro testing of a MMP9-labile formulation. We synthesized a paclitaxel-hemisuccinate-peptide (PH8) conjugate, which is able to self-assemble into nanoparticles. The PH8-nanoparticles exhibit a spherical shape with an average diameter between 120 nm and150 nm (Z-average). The MMP9-triggered drug release and cytotoxcity was shown in in vitro assays. In comparison to paclitaxel, the PH8 showed a different pharmacodynamic profile and a reduced cytotoxic effect. The herein reported results, obtained by testing PH8-nanoparticles, have to be considered as a proof of concept.

EXPERIMENTAL PROCEDURES

Quantification of mRNA Amounts in Cancer Tissue by MultiPlex RT-qPCR. To determine transcripts in different tumor entities, commercially obtained cDNA collections were used (CSRT103 and HBRT102, Origene, Rockville, USA). The number of transcripts was assessed by multiplex quantitative real-time polymerase chain reaction (RT-qPCR) using the following TaqMan assays Hs01548727_m1-ABY, Hs00234579_m1-FAM to quantify matrix metalloproteinase 2 (MMP2), and matrix metalloproteinase 9 (MMP9). The reaction was carried out at a volume of 15 μL containing 0.75 μL of each TaqMan assay, 4.5 μL H_2O, and 7.5 μL TaqMan multiplex Mastermix (Applied Biosystems, LubioSciences, Lucerne, Switzerland). The ViiA 7 RT-qPCR System was set up as recommended by the manufacturer (Applied Biosystems). For copy number determination, PCR standards were generated by ligating the respective PCR-amplicon into pDrive (Qiagen, Hilden, Germany). After transformation and amplification in *E. coli*, the sequence of the plasmids was verified (Microsynth, Balgach, Switzerland). The number of transcripts in each sample was calculated by linear regression. The Ct value obtained in serial dilutions of the standard-plasmids served as the basis. For determination of expression in cell lines, the data were analyzed using the $2^{-\Delta\Delta CT}$ method described by Livak et al.[48] and are reported as fold of study mean.

In Silico Analysis of GEO Data Sets. The gene expression omnibus (GEO) database (https://www.ncbi.nlm.nih.gov/geo/) was searched for data sets using "human", "gene expression array", and the selected "organ of origin" (brain, cervix, endometrium, lung, or urinary bladder). For most organs (tumor entities), only a few (<5) gene expression data sets (GDS) met the search criteria, and we analyzed the data sets that contained at least 20 samples. For tumor entities where multiple data sets were obtained in the primary search, only studies including data on normal or healthy tissue samples were included. The information on expression of MMP9 was extracted and analyzed.

Immunohistochemical Staining of Human Tissue. Immunohistochemical detection of MMP9 was performed using a commercially obtained array of paraffin-embedded tissue sections containing malignant transformed and normal tissue samples (MTU951, Pantomics, Richmond, USA). After deparaffinization in two changes of xylol, the tissue slides were rehydrated in a decreasing ethanol series ranging from 96% to 50%. A heat-induced epitope retrieval was performed in 0.1 M citrate buffer (pH = 6.0) and in a pressurized atmosphere for 20 min. The endogenous peroxidase was subsequently quenched in 3%-H_2O_2-methanol for 20 min followed by several washing steps in phosphate-buffered saline (PBS; 13.7 mM NaCl, 2.7 mM KCl, 8.1 mM Na_2HPO_4, 1.8 mM KH_2PO_4, pH 7.4). Then, the slides were exposed for 1 h to a blocking solution (5% FCS - 1% BSA in PBS). Overnight incubation at 4 °C with the primary anti-MMP9-antibody (ab76003, abcam, Cambridge, UK), diluted 1:100 in a blocking solution, was followed by several washes in PBS. The tissue slides were then incubated for 2 h with the secondary antibody (horseradish peroxidase-coupled goat anti-rabbit, 1:100, Bio-Rad, Cressier, Switzerland) at room temperature (RT) followed by several washes with PBS. For visualization, the horseradish peroxidase substrate diaminobenzidine (DAB) 1 mg/mL in 0.05 M PBS containing 0.02% H_2O_2 was added. Hematoxylin solution (Roth AG, Arlesheim, Switzerland) was used to stain the nuclei. Light microscopic images were taken using a Leica DMi8 microscope (Leica, Heerbrugg, Switzerland). Image analysis was performed using LAS software version 4.6 (Leica).

Cell Culture. The cell lines A549 (ATCC number CCL-185), LN-18 (CRL-2610), and U-87 MG (ATCC HTB-14) were obtained from the American Type Culture Collection (Manassas, USA). All cells were cultured in a humidified atmosphere supplemented with 5% CO_2 in Dulbecco's modified Eagle medium (DMEM; Sigma-Aldrich, Buchs, Switzerland) supplemented with 10% fetal calf serum (FCS)

https://dx.doi.org/10.1021/acs.bioconjchem.9b00865
Bioconjugate Chem. XXXX, XXX, XXX−XXX

(BioConcept AG, Allschwil, Switzerland) and 1% GlutaMAX (BioConcept AG).

Enrichment of Secreted Proteins. For collection of cellular and extracellular secreted proteins (secretome), cells were seeded at a density of 1×10^6 cells/10 cm-dish. After reaching 80% confluence, cells were carefully washed with PBS and cultured in basal medium (DMEM) to avoid contamination with serum proteins. After 24 h, the supernatant was collected and supplemented with 10% trichloric acid (TCA) for protein precipitation. After 15 min of equilibration on ice, precipitated proteins were enriched by centrifugation for 20 min at 17 000*g* and 4 °C, and then washed twice with ice-cold acetone. Finally, the protein was air-dried for 30 min at RT. After solubilizing in 6 M urea, protein content was determined by the Bradford assay (Thermo Fisher, Reinach, Switzerland).

Determination of MMP9 Activity by Zymography. Activity of the gelatinases MMP9 and MMP2 was determined by zymography. Briefly, secreted proteins were supplemented with nonreducing 4× Laemmli-buffer (8% SDS, 40% glycerol in 1 M Tris-HCl, pH 6.8, supplemented with a small amount of bromophenol blue) and then separated by 10% SDS−PAGE containing 0.7 mg/mL gelatin at 4 °C. After separation, gels were washed three times under constant shaking for 10 min at RT with wash buffer I (2.5% Triton-X-100, 10 mM $CaCl_2$, 1 μM $ZnCl_2$, 30.5 mM sodium azide in 50 mM Tris-HCl, pH 7.5). This was followed by incubation with wash buffer II (1% Triton-X-100, 10 mM $CaCl_2$, 1 μM $ZnCl_2$, 30.5 mM sodium azide in 50 mM Tris-HCl, pH 7.5) for 24 h at 37 °C. Proteins were stained with 0.5 vol % Coomassie Brilliant Blue R-250 (Sigma-Aldrich) in 10% acetic acid-30% ethanol for 14 h at RT. After destaining with 10% acetic acid-30% ethanol under constant shaking, staining was digitalized with the ChemiDoc MP (Bio-Rad).

Western Blot Analysis. For Western blot analysis, protein samples were supplemented with 2× Laemmli-buffer (Sigma-Aldrich, Buchs, Switzerland) and incubated at 95 °C for 5 min. They were then separated by SDS−PAGE using the Mini Trans-Blot Cell (Bio-Rad) and blotted onto a nitrocellulose membrane (GE Healthcare, Glattbrugg, Switzerland). After visualization of the protein transfer with Ponceau S solution (Sigma-Aldrich), the membrane was first incubated for 1 h with 5% FCS-0.1% BSA-TBS-T, followed by incubation with the respective primary antibody overnight at 4 °C. The primary antibodies used were the antiactin antibody sc1616 (Santa-Cruz, LabForce AG, Muttenz, Switzerland; diluted 1:1 000) and the anti-MMP9 antibody ab76003 (diluted 1:5 000). After vigorous washing with TBS-T, the membranes were probed with the respective secondary horseradish-peroxidase-coupled antibody (rabbit anti-goat or goat anti-rabbit HRP conjugate, Bio-Rad; diluted 1:3000). To visualize and digitalize immobilization of the secondary HRP-coupled antibody, the chemiluminescence of the Pierce ECL Plus Western blotting substrate (Thermo Scientific) was imaged using the ChemiDoc MP and was analyzed using the Image Lab Software (Bio-Rad, version 4.1)

Determination of MMP9 Activity by ELISA. Briefly, for each measurement, 10 μg of the secretome (proteins in the supernatant) were used. In the cell supernatant, MMPs are present as inactive preform (zymogen) and as active MMPs. MMP9's proteolytic activity in the cell supernatant was quantified using the Anaspec Sensolyte Plus 520 assay kit (ANAWA, Wangen, Switzerland). The assay was performed according to the manufacturer's instructions. The MMP9 activity in the samples was quantified assessing the turnover of a MMP9-specific FRET peptide (provided as a part of the commercial kit) using the microplate reader Infinite M200 PRO (ex λ = 490 nm, em λ = 520 nm, Tecan, Maennedorf, Switzerland).

Fluorescein-SRL-Peptide-Release by MMP9. Five milligrams SRL-peptide (NH_2-Ahx-SRLSLPGC-COOH) were solved in 300 μL dimethylformamide (DMF 99.8% extra dry over molecular sieve, ACROS Organics, Thermo Fisher), and then 38 mg Fluorescein-NHS (Sigma-Aldrich) and 2700 μL sodium bicarbonate buffer (50 mM sodium bicarbonate, pH 8.5) were added. The resulting fluorescein-peptide conjugate was then bound to the Pierce maleimide-activated black 96-well-plate (Thermo Fisher) according to the manufacturer's instructions using a peptide solution containing 50 μg/mL. The binding was carried out overnight. The fluorescein-SRL-peptide plates were used to quantify the release after 24 h of exposure to 10 μg of the secretome of A549, LN-18, or U-87 MG cells at 37°C. A MMP9 inhibitor (Calbiochem MMP-9 Inhibitor I, Sigma-Aldrich) was used to determine the contribution of the MMP9. For quantification, the supernatant was transferred to a new plate and measured using the microplate reader (ex λ = 490 nm, em λ = 525 nm). For statistical analysis using a paired *t* test, the cell supernatant without inhibitor was compared to the same cell supernatant supplemented with the inhibitor in a paired *t* test.

Synthesis, Purification, and Product Validation of Paclitaxel-Hemisuccinate-Peptide (PH8). Paclitaxel-hemisuccinate (PH; Figure S 7B) was synthesized combining 115.8 mg (0.13 mmol) paclitaxel (Figure S 7A; MedChemtronica AB, Stockholm, Sweden), 23.2 mg (0.23 mmol) succinic anhydride (CAS: 108-30-5, Sigma-Aldrich), and a catalytic amount of 4-(dimethylamino)-pyridine (DMAP, CAS: 1122-58-3, Sigma-Aldrich) in 6.9 mL dichloromethane (DCM, CAS: 75-09-2, J.T. Baker, Phillipsburg, USA). After adding 115 μL pyridine (CAS: 110-89-4, Sigma-Aldrich), the solution was stirred at RT for 3 days. Subsequently, the solvent was fully evaporated, and for crude purification, the product was solved in 10 mL ice-cold diethyl ether, sonicated, then stirred at RT for 20 min followed by centrifugation at 17 000*g* for 5 min. To 102.7 mg (0.11 mmol) of collected and vacuum-dried paclitaxel-hemisuccinate (Figure S 7B), 37.07 mg (0.32 mmol) *N*-hydroxysuccinimide (NHS, CAS: 6066-82-6, Sigma-Aldrich), 28.06 mg (0.14 mmol) *N*,*N*′-dicyclohexylcarbodiimid (DCC, CAS: 538-75-0, Sigma-Aldrich), and a catalytic amount of DMAP were added and dissolved in 17.4 mL DCM, and then stirred at RT for 3 days. Subsequently a silica plug was performed to separate precipitated dicyclohexylurea from the product paclitaxel-hemisuccinate-*N*-hydroxysuccinimide-ester (Figure S 7C). Thirty milligrams (0.03 mmol) of the product were combined with 7 mg (0.007 mmol) of the deprotected peptide (Figure S 7D, NH_2-Ahx-SRLSLPGC-COOH, Biomatik, Wilmington, USA), each solved in 0.75 mL DMF. Under constant stirring, 0.18 mmol DMAP dissolved in 2 mL DMF were added dropwise and left to react overnight. Then, the DMF was evaporated under vacuum followed by an additional diethyl ether precipitation. Finally, PH8 (Figure S 7E) was purified by semipreparative HPLC (Agilent 1100 series with UV-detector coupled to the MS spectrometer, Agilent Technologies, Basel, Switzerland). The mobile phase consisted of water (A) and acetonitrile (B) both containing 0.1% formic acid. Semipreparative purification of the product was achieved using a SunFire C18 OBD prep

https://dx.doi.org/10.1021/acs.bioconjchem.9b00865
Bioconjugate Chem. XXXX, XXX, XXX−XXX

column (100A, 10 × 150 mm, 5 μm, Waters, Baden, Switzerland) and a SunFire C18 Prep Guard precolumn (10 × 10 mm, 5 μm, Waters) with a gradient of 40% to 100% B in 23 min. The gradient started after 1 min at a flow rate of 3 mL/min. PH8 was eluted at around 9.0 min.

PH8 was analyzed on a 1290 Infinity UHPLC system coupled to a 6460 Triple Quadrupole mass spectrometer (all Agilent, Waldbronn, Germany). The mobile phase consisted of water (A) and acetonitrile (B) both containing 0.1% formic acid (FA). Separation for fragmentation pattern analysis of the conjugate was achieved using a SunFire C18 column (100A, 3.0 × 150 mm, 3.5 μm, Waters, Baden, Switzerland) and a SunFire C18 VanGuard precolumn (2.1 × 5 mm 3.5 μm, Waters) with a gradient of 40% to 100% B in 8 min, starting after 1 min at a flow rate of 0.6 mL/min. The fragmentor voltage was varied between 80 and 170 V. Measurements were performed in electrospray ionization positive ion mode (ESI+) and MSScan2 mode.

In Silico Analysis of Paclitaxel-Hemisuccinate-Peptide (PH8). PH8 was analyzed for its molecular lipophilicity potential. To assess, visualize, and compute the molecular lipophilicity potential and log *P* value, the open access Molinspiration software (www.molinspiration.com, version 2018.10) was applied.

Generation of Nanoparticles. Nanoparticles were generated by nanoprecipitation. 0.7 mg purified PH8 were dissolved in 1 mL acetone supplemented with 5 μL DMSO (solvent) and added drop-by-drop to 1 mL ddH_2O (non-solvent) under constant stirring. To evaporate the solvent, the emulsion was stirred overnight at RT. Subsequently, maleimide-polyethylene $glycol_{2000}$ (Mal-PEG_{2000}, Laysan Bio Inc., Arab, AL, USA) was linked to the nanoparticle's surface via the maleimide reaction. 1.0 mg Mal-PEG_{2000} was dissolved in 1 mL 2 × PBS (27.4 mM NaCl, 5.4 mM KCl, 16.2 mM Na_2HPO_4, 3.6 mM KH_2PO_4, pH 7.4) and then added dropwise to the PH8-nanoparticles in 1 mL ddH_2O. The solution was stirred at RT for 8 h under light protection. Thereafter, the nanoparticles were purified from unreacted Mal-PEG_{2000} by dialysis (MWCO = 12−14 kDa) in ddH_2O for 24 h. The pegylated PH8-nanoparticles were extruded with nucleopore membranes (Whatman, Maidstone, UK) holding 400, 200, and 100 nm wide pores to get a uniform shape (21 strokes per membrane). Size exclusion chromatography (SEC) was used to separate free PEG_{2000} or fluorescent dye after fluorescein loading (see below) from the pegylated PH8-nanoparticle. An Äkta pure 25 fast protein liquid chromatography (FPLC, GE Healthcare, Glattbrugg, Switzerland) equipped with a monochannel 280 nm UV-detector and a HiTrap Desalting Column (GE Healthcare) was applied for nanoparticle purification. Separation was achieved under isocratic conditions and a flow rate of 1 mL/min. The peaks were collected by a fraction collector. The nanoparticles eluted after 2 min.

Determination of Particle Size of the Formulated Nanoparticles. Dynamic light scattering (DLS) analysis was performed using degassed samples and the Malvern Zetasizer Nano (Malvern Instruments GmbH, Herrenberg, Germany) to determine the diameter (Z-average) and the size distribution (PDI = polydispersity index) of the generated nanoparticles

Measuring the Critical Aggregation Concentration of the Paclitaxel-Hemisuccinate-Peptide (PH8). The critical aggregation concentration (CAC) of PH8 was determined utilizing pyrene as previously described.[49,50] Pyrene, as a fluorescent dye exhibits different fluorescent characteristics depending on its hydrophobic or hydrophilic surrounding. In brief, 500 μL 2.4 μM pyrene acetone solution containing different amounts of PH8 (500, 50, 5, 0.5, 0.05, 0.005, 0.0005, and 0.0005 μg) were added to a glass vial. The solvent was completely evaporated (1.5 h at 40°C) under a constant flow of nitrogen. Thereafter, 1 mL of ultrapure water was added, and the sample was ultrasonicated. The fluorescent signal of pyrene was measured with an excitation at 332 nm and emission at I_1 = 373 nm and at I_3 = 384 nm, respectivly. The measurements were conducted on a Infinite M200 Pro microplate reader (Tecan). To determine the CAC, I_3/I_1 was plotted against the logarithm of the conjugate concentration. The intersection of the linear slopes is the CAC.

Transmission Electron Microscopy of the Nanoparticle. For size and shape inspection of the formulated nanoparticles, transmission electron microscopy (TEM; Phillips, CM200) was performed at the Center for Cellular Imaging and Nanoanalytics (C−CINA, University of Basel) after drying the samples. Before adding 5 μL of the sample onto a 400 mesh copper grid (in house preparation), an ion etching was performed. The samples were washed four times with water and stained twice with 1% uranyl-acetate solution.

MMP9 Mediated Release of Fluorescent Dye from Nanoparticle. 250 μg PH8 and 10 μg of fluorecein was used to make nanoparticles in the above-described manner. Briefly, the nanoparticles were formed in the presence of fluorescein, pegylated, and then extruded. Finally, the fluorescein-loaded PH8-nanoparticles were separated by size exclusion using the Äkta pure 25 FPLC (GE Healthcare) as described above. 75 μL (125 μg/mL) of nanoparticle solution per well was used to bind to the Pierce maleimide activated black 96-well-plate (Thermo Fisher) according to the manufacturer's manual (the only exception: wash buffer was prepared without Tween to avoid interruption of the nanoparticles). The binding was carried out overnight. The fluorescent nanoparticle bound to the maleimide plate were used to quantify the release of fluorescent dye after a 24 h exposure to 10 μg/mL MMP9 at 37 °C. The supernatant was transferred and measured for fluorescein content. Moreover, the fluorescence remaining at the plates was measured using the microplate reader (Tecan, ex λ = 490 nm, em λ = 525 nm). Release was calculated, and the student's *t* test was applied for statistical analysis.

Assessment of Cellular Viability in Cells. A549 (lung cancer), LN-18 (glioblastoma multiforme), and U87 MG (astrocytoma) cells were seeded at a density of 7 500 cells/well in 96-well plates. Twenty-four hours after seeding, the cells were exposed to pegylated PH8-nanoparticles, paclitaxel, or solvent control. By adding 40 nM MMP-9-inhibitor (Calbiochem MMP-9 Inhibitor I, Sigma-Aldrich), the contribution of these gelatinase to the release of paclitaxel was tested. The media was supplemented with 10 μg/mL supernatant proteins to study the triggered release. After 24 h of exposure, cell viability was determined using the Resazurin Fluorometric Cell Viability Kit (PromoCell GmbH, Heidelberg, Germany) according to the manufacturers' instructions. The Infinite M200Pro plate reader (Tecan; ex λ = 530 nm, em λ = 590 nm) was used to detect the fluorescence. Viability of cells exposed to pegylated-PH8-nanoparticles or paclitaxel was normalized against cells treated with the solvent control. Data are reported as fold of control. For statistical analysis, column statistics using a one-sample student's *t* test was applied. The

https://dx.doi.org/10.1021/acs.bioconjchem.9b00865
Bioconjugate Chem. XXXX, XXX, XXX−XXX

inhibitory potency was estimated applying a variable slope (four parameters).

Statistical Analysis. Statistical analysis was performed using the GraphPad prims software (version 6, GraphPad Software Inc. La Jolla, CA, USA). For the statistical analysis of RT-qPCR- and GEO-data, a one-way ANOVA with multi-comparison, or a Mann−Whitney U test (if only two groups were available in the study) was applied. The fluorescein-SRL peptide release by MMP9 was statistically analyzed by a paired student's *t* test. Cell viability studies were statistically analyzed with the column statistics with one-sample student's *t* test. The in vitro data reported in this study represent data from at least 3 independent experiments, each performed in triplicates. A *p*-value below 0.05 was considered statistically significant.

■ ASSOCIATED CONTENT

Supporting Information

The Supporting Information is available free of charge at https://pubs.acs.org/doi/10.1021/acs.bioconjchem.9b00865.

Figure S1: MMP9 expression in normal and malignant transformed cervix tissue, Figure S2: MMP9 expression in normal and malignant transformed lung tissue, Figure S3: MMP9 expression in normal and malignant transformed esophageal tissue, Figure S4: MMP9 expression in normal and malignant transformed brain tissue, Figure S5: analysis of public available GEO data sets comparing mRNA expression in samples originating from cervical, esophageal, and lung tumors, Figure S6: analysis of publicly available GEO data sets comparing mRNA expression in samples originating from brain tumors, Figure S7: synthetic scheme for the paclitaxel-hemisuccinate-peptide (PH8) prodrug molecule as a building block for nanoparticles, Figure S8: LC/MS and fragmentation pattern analysis of PH8, Figure S9: assessment of the amphiphilic character and critical aggregation concentration (CAC) of PH8, Figure S10: stability of the PH8-nanoparticles, Figure S11: fluorescein release from fluorescein loaded PH8-nanoparticles after exposure to MMP9, and Figure S12: cell viability after administration of the PH8 prodrug or paclitaxel to the glioblastima cell line LN-18 (PDF)

■ AUTHOR INFORMATION

Corresponding Author

Henriette E. Meyer zu Schwabedissen − *University of Basel, Basel, Switzerland;* orcid.org/0000-0003-0458-4579; Phone: +41 61 207 14 95; Email: h.meyerzuschwabedissen@unibas.ch

Other Authors

Daniel Ehrsam − *University of Basel, Basel, Switzerland;* orcid.org/0000-0001-7444-3806

Sandro Sieber − *University of Basel, Basel, Switzerland*

Mouhssin Oufir − *University of Basel, Basel, Switzerland*

Fabiola Porta − *University of Basel, Basel, Switzerland*

Matthias Hamburger − *University of Basel, Basel, Switzerland;* orcid.org/0000-0001-9331-273X

Jörg Huwyler − *University of Basel, Basel, Switzerland;* orcid.org/0000-0003-1748-5676

Complete contact information is available at: https://pubs.acs.org/10.1021/acs.bioconjchem.9b00865

Author Contributions

Conceptualization, D.E., H.E.M.z.S., and J.H.; methodology, D.E., S.S., M.O., F.P. and H.E.M.z.S; formal analysis, D.E.; investigation, D.E., M.O., and H.E.M.z.S.; resources, H.E.M.z.S., M.H., and J.H..; writing—original draft preparation, D.E.; writing—review and editing, D.E., S.S., J.H., and H.E.M.z.S.; visualization, D.E., and H.E.M.z.S; supervision, H.E.M.z.S.; project administration, D.E., M.H., J.H., and H.E.M.z.S.

Notes

The authors declare no competing financial interest.

■ ACKNOWLEDGMENTS

We want to thank Davy Poupin-Daubian for helpful input concerning the synthesis and Orlando Fertig for his support. This research received no external funding.

■ ABBREVIATIONS

BSA, bovine serum albumin; DCC, *N,N′*-dicyclohexylcarbodiimid; DCM, dichloromethane; DLS, dynamic light scattering; DMAP, 4-(dimethylamino)-pyridine; DMEM, Dulbecco's modified Eagle medium; DMF, dimethylformamide; ECM, extracellular matrix; EPR, enhanced permeability and retention effect; FCS, fetal calf serum; FPLC, fast protein liquid chromatography; FRET, Förster resonance energy transfer; GEO, Gene Expression Omnibus; HPLC, highpressure liquid chromatography; HRP, horseradish peroxidase; LC−MS, liquid chromatography mass spectrometry; MMP, matrix metalloproteinase; MS, mass spectrometry; NHS, *N*-hydroxysuccinimide; PBS, phosphate buffered system; PCR, polymerase chain reaction; PDI, polydispersity index; PEG, polyethylene glycol; PH8, paclitaxel-hemisuccinate-peptide, (6-(4-((1-benzamido-3-((6,12b-diacetoxy-12-(benzoyloxy)-4,11-dihydroxy-4a,8,13,13-tetramethyl-5-oxo-2a,3,4,4a,5,6,9,10,11,12,12a,12b-dodecahydro-1H-7,11-methanocyclodeca[3,4]benzo[1,2-*b*]oxet-9-yl)oxy)-3-oxo-1-phenylpropan-2-yl)oxy)-4-oxobutanamido)hexanoyl)-serylarginylleucylserylleucylprolylglycylcysteine; RT, room temperature; RT-qPCR, quantitative real-time polymerase chain reaction; SDS−PAGE, sodium dodecyl sulfate polyacrylamide gel electrophoresis; TCA, trichloric acid; TEM, transmission electron microscopy; UV, ultraviolet

■ REFERENCES

(1) Faguet, G. *The War on Cancer: An Anatomy of Failure, A Blueprint for the Future*; Springer, 2005.

(2) Chabner, B. A., and Roberts, T. G., Jr. (2005) Timeline: Chemotherapy and the war on cancer. *Nat. Rev. Cancer 5*, 65−72.

(3) Chari, R. V. (2008) Targeted cancer therapy: conferring specificity to cytotoxic drugs. *Acc. Chem. Res. 41*, 98−107.

(4) Perez-Herrero, E., and Fernandez-Medarde, A. (2015) Advanced targeted therapies in cancer: Drug nanocarriers, the future of chemotherapy. *Eur. J. Pharm. Biopharm. 93*, 52−79.

(5) Wicki, A., Witzigmann, D., Balasubramanian, V., and Huwyler, J. (2015) Nanomedicine in cancer therapy: challenges, opportunities, and clinical applications. *J. Controlled Release 200*, 138−57.

(6) Danhier, F. (2016) To exploit the tumor microenvironment: Since the EPR effect fails in the clinic, what is the future of nanomedicine? *J. Controlled Release 244*, 108−121.

(7) Wilhelm, S., Tavares, A. J., Dai, Q., Ohta, S., Audet, J., Dvorak, H. F., and Chan, W. C. W. (2016) Analysis of nanoparticle delivery to tumours. *Nature Reviews Materials 1*, 16014.

(8) Zhang, X., Zhang, H., Yin, L., Hu, R., Qiu, T., Yin, Y., Xiong, X., Zheng, H., and Wang, Q. (2016) A pH-Sensitive Nanosystem Based

on Carboxymethyl Chitosan for Tumor-Targeted Delivery of Daunorubicin. *J. Biomed. Nanotechnol. 12*, 1688−98.
(9) Zheng, H., Yin, L., Zhang, X., Zhang, H., Hu, R., Yin, Y., Qiu, T., Xiong, X., and Wang, Q. (2016) Redox Sensitive Shell and Core Crosslinked Hyaluronic Acid Nanocarriers for Tumor-Targeted Drug Delivery. *J. Biomed. Nanotechnol. 12*, 1641−53.
(10) Mura, S., Nicolas, J., and Couvreur, P. (2013) Stimuli-responsive nanocarriers for drug delivery. *Nat. Mater. 12*, 991.
(11) Andresen, T. L., Thompson, D. H., and Kaasgaard, T. (2010) Enzyme-triggered nanomedicine: drug release strategies in cancer therapy. *Mol. Membr. Biol. 27*, 353−63.
(12) Hanahan, D., and Weinberg, R. A. (2011) Hallmarks of cancer: the next generation. *Cell 144*, 646−74.
(13) Lammers, T., Kiessling, F., Hennink, W. E., and Storm, G. (2012) Drug targeting to tumors: principles, pitfalls and (pre-) clinical progress. *J. Controlled Release 161*, 175−87.
(14) Rautio, J., Meanwell, N. A., Di, L., and Hageman, M. J. (2018) The expanding role of prodrugs in contemporary drug design and development. *Nat. Rev. Drug Discovery 17*, 559−587.
(15) Giang, I., Boland, E. L., and Poon, G. M. (2014) Prodrug applications for targeted cancer therapy. *AAPS J. 16*, 899−913.
(16) Forsyth, P. A., Wong, H., Laing, T. D., Rewcastle, N. B., Morris, D. G., Muzik, H., Leco, K. J., Johnston, R. N., Brasher, P. M., Sutherland, G., et al. (1999) Gelatinase-A (MMP-2), gelatinase-B (MMP-9) and membrane type matrix metalloproteinase-1 (MT1-MMP) are involved in different aspects of the pathophysiology of malignant gliomas. *Br. J. Cancer 79*, 1828−35.
(17) Bauvois, B. (2012) New facets of matrix metalloproteinases MMP-2 and MMP-9 as cell surface transducers: outside-in signaling and relationship to tumor progression. *Biochim. Biophys. Acta, Rev. Cancer 1825*, 29−36.
(18) Van den Steen, P. E., Dubois, B., Nelissen, I., Rudd, P. M., Dwek, R. A., and Opdenakker, G. (2002) Biochemistry and molecular biology of gelatinase B or matrix metalloproteinase-9 (MMP-9). *Crit. Rev. Biochem. Mol. Biol. 37*, 375−536.
(19) Egeblad, M., and Werb, Z. (2002) New functions for the matrix metalloproteinases in cancer progression. *Nat. Rev. Cancer 2*, 161−74.
(20) Vandooren, J., Van den Steen, P. E., and Opdenakker, G. (2013) Biochemistry and molecular biology of gelatinase B or matrix metalloproteinase-9 (MMP-9): the next decade. *Crit. Rev. Biochem. Mol. Biol. 48*, 222−72.
(21) Ugalde, A. P., Ordonez, G. R., Quiros, P. M., Puente, X. S., and Lopez-Otin, C. (2010) Metalloproteases and the degradome. *Methods Mol. Biol. 622*, 3−29.
(22) Bourboulia, D., and Stetler-Stevenson, W. G. (2010) Matrix metalloproteinases (MMPs) and tissue inhibitors of metalloproteinases (TIMPs): Positive and negative regulators in tumor cell adhesion. *Semin. Cancer Biol. 20*, 161−8.
(23) Vandooren, J., Van den Steen, P. E., and Opdenakker, G. (2013) Biochemistry and molecular biology of gelatinase B or matrix metalloproteinase-9 (MMP-9): the next decade. *Crit. Rev. Biochem. Mol. Biol. 48*, 222−72.
(24) Eisen, Z. A., Sarkar, S. K., Neuman, K. C., and Goldberg, G. I. *Handbook of Proteolytic Enzymes. Vol. 3: Matrix Metallopeptidase 9 /Gelatinase B* (Rawlings, N. D., and Salvesen, G. Y., Eds.; Academic Press: London, 2013; Chapter 157, pp 754−762.
(25) Mook, O. R., Frederiks, W. M., and Van Noorden, C. J. (2004) The role of gelatinases in colorectal cancer progression and metastasis. *Biochim. Biophys. Acta, Rev. Cancer 1705*, 69−89.
(26) Sarkar, N., Banerjee, J., Hanson, A. J., Elegbede, A. I., Rosendahl, T., Krueger, A. B., Banerjee, A. L., Tobwala, S., Wang, R., Lu, X., et al. (2008) Matrix metalloproteinase-assisted triggered release of liposomal contents. *Bioconjugate Chem. 19*, 57−64.
(27) Zhu, L., Wang, T., Perche, F., Taigind, A., and Torchilin, V. P. (2013) Enhanced anticancer activity of nanopreparation containing an MMP2-sensitive PEG-drug conjugate and cell-penetrating moiety. *Proc. Natl. Acad. Sci. U. S. A. 110*, 17047−52.
(28) Nultsch, K., and Germershaus, O. (2018) Matrix metalloprotease triggered bioresponsive drug delivery systems - Design, synthesis and application. *Eur. J. Pharm. Biopharm. 131*, 189−202.
(29) Steinhagen, M., Hoffmeister, P. G., Nordsieck, K., Hotzel, R., Baumann, L., Hacker, M. C., Schulz-Siegmund, M., and Beck-Sickinger, A. G. (2014) Matrix metalloproteinase 9 (MMP-9) mediated release of MMP-9 resistant stromal cell-derived factor 1alpha (SDF-1alpha) from surface modified polymer films. *ACS Appl. Mater. Interfaces 6*, 5891−9.
(30) Rao, J. S., Steck, P. A., Mohanam, S., Stetler-Stevenson, W. G., Liotta, L. A., and Sawaya, R. (1993) Elevated levels of M(r) 92,000 type IV collagenase in human brain tumors. *Cancer research 53*, 2208−11.
(31) Rao, J. S., Yamamoto, M., Mohaman, S., Gokaslan, Z. L., Fuller, G. N., Stetler-Stevenson, W. G., Rao, V. H., Liotta, L. A., Nicolson, G. L., and Sawaya, R. E. (1996) Expression and localization of 92 kDa type IV collagenase/gelatinase B (MMP-9) in human gliomas. *Clin. Exp. Metastasis 14*, 12−8.
(32) Li, Y., Wu, T., Zhang, B., Yao, Y., and Yin, G. (2012) Matrix metalloproteinase-9 is a prognostic marker for patients with cervical cancer. *Med. Oncol. 29*, 3394−9.
(33) Li, Y., Ma, J., Guo, Q., Duan, F., Tang, F., Zheng, P., Zhao, Z., and Lu, G. (2009) Overexpression of MMP-2 and MMP-9 in esophageal squamous cell carcinoma. *Diseases of the esophagus: official journal of the International Society for Diseases of the Esophagus 22*, 664−7.
(34) El-Badrawy, M. K., Yousef, A. M., Shaalan, D., and Elsamanoudy, A. Z. (2014) Matrix metalloproteinase-9 expression in lung cancer patients and its relation to serum mmp-9 activity, pathologic type, and prognosis. *Journal of bronchology & interventional pulmonology 21*, 327−34.
(35) Canete-Soler, R., Litzky, L., Lubensky, I., and Muschel, R. J. (1994) Localization of the 92 kd gelatinase mRNA in squamous cell and adenocarcinomas of the lung using in situ hybridization. *American journal of pathology 144*, 518−27.
(36) Kemper, E. M., van Zandbergen, A. E., Cleypool, C., Mos, H. A., Boogerd, W., Beijnen, J. H., and van Tellingen, O. (2003) Increased penetration of paclitaxel into the brain by inhibition of P-Glycoprotein. *Clin. Cancer Res. 9*, 2849−55.
(37) Gliesche, D. G., Hussner, J., Witzigmann, D., Porta, F., Glatter, T., Schmidt, A., Huwyler, J., and Meyer zu Schwabedissen, H. E. (2016) Secreted Matrix Metalloproteinase-9 of Proliferating Smooth Muscle Cells as a Trigger for Drug Release from Stent Surface Polymers in Coronary Arteries. *Mol. Pharmaceutics 13*, 2290−300.
(38) Porta, F., Ehrsam, D., Lengerke, C., and Meyer zu Schwabedissen, H. E. (2018) Synthesis and Characterization of PDMS-PMOXA-Based Polymersomes Sensitive to MMP-9 for Application in Breast Cancer. *Mol. Pharmaceutics 15*, 4884−4897.
(39) Meng, Z., Lv, Q., Lu, J., Yao, H., Lv, X., Jiang, F., Lu, A., and Zhang, G. (2016) Prodrug Strategies for Paclitaxel. *Int. J. Mol. Sci. 17*, 796.
(40) Moyna, G., Williams, H. J., Scott, A. I., Ringel, I., Gorodetsky, R., and Swindell, C. S. (1997) Conformational studies of paclitaxel analogs modified at the C-2′ position in hydrophobic and hydrophilic solvent systems. *J. Med. Chem. 40*, 3305−11.
(41) Damen, E. W., Wiegerinck, P. H., Braamer, L., Sperling, D., de Vos, D., and Scheeren, H. W. (2000) Paclitaxel esters of malic acid as prodrugs with improved water solubility. *Bioorg. Med. Chem. 8*, 427−32.
(42) Thapa, P., Li, M., Bio, M., Rajaputra, P., Nkepang, G., Sun, Y., Woo, S., and You, Y. (2016) Far-Red Light-Activatable Prodrug of Paclitaxel for the Combined Effects of Photodynamic Therapy and Site-Specific Paclitaxel Chemotherapy. *J. Med. Chem. 59*, 3204−14.
(43) Fu, Q., Wang, Y., Ma, Y., Zhang, D., Fallon, J. K., Yang, X., Liu, D., He, Z., and Liu, F. (2015) Programmed Hydrolysis in Designing Paclitaxel Prodrug for Nanocarrier Assembly. *Sci. Rep. 5*, 12023.
(44) Iizasa, T., Fujisawa, T., Suzuki, M., Motohashi, S., Yasufuku, K., Yasukawa, T., Baba, M., and Shiba, M. (1999) Elevated levels of

https://dx.doi.org/10.1021/acs.bioconjchem.9b00865
Bioconjugate Chem. XXXX, XXX, XXX−XXX

circulating plasma matrix metalloproteinase 9 in non-small cell lung cancer patients. *Clin. Cancer Res. 5*, 149−53.
(45) Tian, R., Wang, H., Niu, R., and Ding, D. (2015) Drug delivery with nanospherical supramolecular cell penetrating peptide-taxol conjugates containing a high drug loading. *J. Colloid Interface Sci. 453*, 15−20.
(46) Hoshyar, N., Gray, S., Han, H., and Bao, G. (2016) The effect of nanoparticle size on in vivo pharmacokinetics and cellular interaction. *Nanomedicine 11*, 673−92.
(47) Kulthe, S. S., Choudhari, Y. M., Inamdar, N. N., and Mourya, V. (2012) Polymeric micelles: authoritative aspects for drug delivery. *Des. Monomers Polym. 15*, 465−521.
(48) Livak, K. J., and Schmittgen, T. D. (2001) Analysis of relative gene expression data using real-time quantitative PCR and the 2(-Delta Delta C(T)) Method. *Methods 25*, 402−8.
(49) Goddard, E. D., Turro, N. J., Kuo, P. L., and Ananthapadmanabhan, K. P. (1985) Fluorescence probes for critical micelle concentration determination. *Langmuir 1*, 352−5.
(50) Grossen, P., Quebatte, G., Witzigmann, D., Prescianotto-Baschong, C., Dieu, L.-H., and Huwyler, J. (2016) Functionalized Solid-Sphere PEG-b-PCL Nanoparticles to Target Brain Capillary Endothelial Cells In Vitro. *J. Nanomater. 2016*, 1.

https://dx.doi.org/10.1021/acs.bioconjchem.9b00865
Bioconjugate Chem. XXXX, XXX, XXX−XXX

Conclusion

In this PhD thesis, we explored design possibilities of stimuli-responsive drug delivery systems for use in cancer treatment. A corner stone of the designs was the interaction with enzymes which play a role in angiogenesis. We could build on previous work done in our lab on angiogenesis and stimuli-responsive drug release from polymer-surfaces. In the introduction, we discussed the crucial role of angiogenesis for tumor growth and expansion. Specifically, the enzymes MMP9 and cathepsin B were used as stimuli for drug release.

The MMP9 and cathepsin B expression was extensively researched in patient samples, cancer cell lines and gene expression databases. This allowed us to select the most suitable cell models for in vitro examination of the stimuli-responsive drug delivery systems.

At the core of all mentioned concepts were enzyme-degradable peptides. Two fundamentally different stimuli-responsive drug delivery systems were explored: polymeric nanoparticles with a peptide-modified surface and self-assembling bioconjugate-molecules composed of a chemotherapeutic and a peptide. In all approaches we combined chemotherapeutics with nanotechnology. The stimuli-responsive release is based on enzymes which are targets for targeted therapy. In the case of the bioconjugate-based nanoparticles, also the idea of prodrug was implemented in the design.

We started with the development of stimuli-responsive polymeric nanoparticles due to the relative ease of formulation. Compared to a bioconjugate drug delivery system, the formulation of polymeric nanoparticles is less complex, less time consuming and research into polymeric nanoparticle is better established.

The diblock copolymer PDMS-PMOXA was used to form polymeric nanoparticles. The polymeric nanoparticles were synthesized to be responsive to MMP9- or cathepsin B activation for drug release (result I & II). The drug delivery systems contained the chemotherapeutic paclitaxel. In all cases, we tracked the modification of the nanoparticles' surface with FT-IR. All formed nanoparticles were assessed for their appearance and physico-chemical properties. The polymeric nanoparticle had a spherical shape and the diameter in range of what is considered best for prolonged circulation (*37, 42*). The critical aggregation concentration was comparable to the critical micelle concentration measured for similar polymers (Doctoral Thesis: Amphiphilic block copolymers: Synthesis, self-

assembly and applications; Wu,D, unibas, Basel, Switzerland 2015) (*43*). The concepts were tested in vitro on cancer cells. In both cases, a cytotoxic effect was observed when polymersomes were exposed to enzymes. The cytotoxic effect was reduced by enzyme inhibitor. In addition, MMP9-responsive polymersomes were tested in zebrafish using a novel in vivo approach. The zebrafish were xenografted with red fluorescent cancer cells and the tumor size was determined after treatment by RT-qPCR. The results reflected the in vitro results. The Cathepsin B-responsive polymeric nanoparticles were fluorescently labeled, immobilized and the release of fluorescent dye was measured after exposure to enzyme.

For the conjugate design approach (result III), we synthesized an amphiphilic molecule including paclitaxel and a MMP9-substrate. The synthesis steps were surveyed by HPLC. The final compound was purified via semi-preparative HPLC and MS and analyzed by MS and fragmentation patterns. The resulting amphiphilic molecules self-assembled into nanoparticles with a critical aggregation concentration between the critical micelle concentration of surfactants and for polymeric micelles with enhanced stability (47). The nanoparticles had a diameter considered in range. Viability tests showed a decreased toxicity of the bioconjugate molecule compared to paclitaxel. However, the maximal toxic effect was reached at similar concentrations suggesting a change in pharmacodynamic profile. The stimuli-responsiveness was most evident in cancer cells with proven high MMP9 activity.

In comparison to the bioconjugate nanoparticles (result III), the polymeric nanoparticles (result I & II) were easier to synthesize. Polymeric nanoparticles are better established and the polymers are commercially available. The chemotherapeutic is enclosed by the polymers, assuring a similar drug effect as the molecule alone when released. In contrast, the bioconjugate nanoparticles consist of a single molecule, wherein the chemotherapeutic is covalently bound to the enzyme substrate. The bioconjugate showed a different pharmacodynamic profile due to the modifications. Since the bioconjugate nanoparticles were formed from a single pure molecule, the concentration of chemotherapeutic was known at all time.

Going on from a specific to a more general point of view. For the last three decades, there have been impressive advances in nanotechnology - and its use in healthcare. Progress

was made in understanding how matter interacts on a nanoscale level and within biological systems. Vast arrays of drug delivery systems with innovative release systems and targeting abilities were researched, including enzyme-triggered release as described in this thesis. However, medicinal nanotechnology suffers from low translation from bench to bedside. Today's low success rate of nanomedicine can be explained by several factors: inflated expectations, difficulties translating in vitro results into in vivo, concerns of unknown toxicity, regulatory hurdles, high production costs and skeptical public perception.

Although nanomedicine-based treatments often show improvements compared to the standard treatment (e.g. small molecules), these benefits are frequently overshadowed by unmet high expectations of the overall outcome. While the use of nanotechnology leads to an increased circulation time and a safer toxicologic profile, it fails to deliver increased overall patient survival (*44, 45*).

Frequently, preclinical trials do not translate well into clinical trials and treatment success depends on many factors. For example, anti-cancer nanomedicines rely heavily on the EPR-effect for tumor targeting. Although the EPR effect can be used for tumor targeting, it seems to be a heterogenous effect leading to inconsistent clinical outcomes and provokes skeptical opinions (*46, 47*). This complicates the development of novel nanomedicines.

At nanoscale, quantum effects impact the physical properties of fluorescence, conductivity, melting point and reactivity (*48*). In addition, nanosized materials behave differently in vitro compared to in vivo. This dictates extensive in vivo testing including research on the protein corona, cellular interactions, tissue transportation, diffusion and biocompatibility (*44, 45*). Validated models for these phenomena are expensive or not yet in place. Fortunately, more affordable early stage in vivo systems like the zebrafish (Danio rerio) are being extensively investigated and may serve as model systems in the future (*49*).

Another area of concern related to the unique properties on a nanoscale material is toxicity including unintended crossing of the blood-brain barrier or long-term toxicity (*48*). Reservations about the safety and immune response against polymers have been expressed (*50-52*) leading to an increased interest in alternatives, e.g. amphiphilic peptides (*53*).

The nanomedicine`s size is a key characteristic, but not the only one and it is difficult to generalize findings. This means that each nanomedicine must be assessed individually, which poses a challenge for the developers as well as the regulatory agencies. Furthermore, the term nanotechnology is broadly used in media coverage and the public perception influences the benevolence towards nanomedicine. The reservation of the public against nanotechnology includes safety concerns and possible risks (*54*). Equal hesitation of consumers towards novel technologies can be observed in gene modification (*55*).

Despite the need to address the aforementioned issues, targeted nanomedicine is a valuable option for the development of small molecule formulations, immune and gene therapies.

Compared to surgery and radiotherapy, chemotherapeutics are able to reach early stage tumors or metastases. For the benefit of the patient, the toxic and pharmacologic profile of such compounds can be altered by using targeted nanomedicine approaches. This is accomplished by delivering the drug more specifically to the diseased area and cope with unfavorable properties. Recently, nanomedicine research is focusing on exploiting formulation-specific accumulation patterns to treat organ-specific diseases i.e. lung or liver accumulation (*56*) and the combination of different targeting abilities (e.g. stimuli-responsive and active targeting).

Especially, the emerging trend of CRISPR-Cas9, immunotherapy and gene therapy seem to open up a new era of nanomedicine. Compared to previous methods, the CRISPR-Cas9 system allows gene editing of mammalian cells at desired locations. First treatment methods using CRISPR-Cas9 reached clinical stages using ex vivo gene editing of cells. Viral vectors are most commonly used to introduce CRISPR-Cas9 into cells. The ultimate goal would be to edit genes in vivo. Unfortunately, immunogenicity of viral vectors and off-target editing effects are posing potential problems (*57, 58*). Targeted nanoparticle vectors are a useful option to cope with these adverse events.

Furthermore, advances in artificial intelligence, machine learning and deep learning are promising faster and less expensive development of nanomedicine and better understanding of their behavior. As a result, nanomedicine will hopefully live up to the expectations and become common in pharmaceutical formulation development.

All in all, targeted or stimuli-responsive nanomedicine is a mainstay of pharmaceutical research with a bright future in cancer, immune and gene therapy.

Acknowledgement

To begin with, I am grateful to Prof. Dr. H.E. Meyer zu Schwabedissen for giving me the opportunity to do this multi-disciplinary PhD project in her lab, for her guidance, support and many fruitful discussions.

I would like to thank Prof. Dr. O. Germershaus for accepting to be my coreferee.

Furthermore, I would like to thank Prof. Dr. J. Huwyler, Prof. Dr. M. Hamburger, Prof. Dr. A. Odermatt, Prof. Dr. B. Ernst and their group members for having an open door and sharing their experience and thoughts.

I would also like to thank the current and former members of the Biopharmacy group, namely Vanessa Malagnino, Celio Ferreira, Anima Schäfer, Janine Hussner, Fabiola Porta, Katharina Prestin, Isabel Seibert, Petra Rohrwild, Karin Brecht Brüngger, and Daniel Gliesche, for being there during this important period of my life, supporting me in times of doubt as well as celebrating the successes with me.

A warm thank you goes to my fellow students from the Pharmaceutical Sciences master graduation class of 2014 for staying in contact after our studies.

I would like to express many thanks to everybody whom I met during my PhD studies and I look forward to our paths crossing again in the future.

Finally, my special thanks go to my family and friends, who supported me and gave me fresh heart when I needed it most.

References

(1) WHO. (2018), World Health Organisation.
(2) Pellettieri, J., and Sanchez Alvarado, A. (2007) Cell turnover and adult tissue homeostasis: from humans to planarians. *Annu Rev Genet 41*, 83-105.
(3) Hochwald, S. N. (2010) Molecular-targeted therapy for cancer and nanotechnology. *Methods Mol Biol 624*, 11-23.
(4) Lodish, H. B., A.; Zipursky, S. L.; Matsudaira, P.; Baltimore, D.; Darnell, J. (2000) *Molecular Cell Biology*, 4th ed., Garland Science.
(5) Knudson, A. G., Jr. (1971) Mutation and cancer: statistical study of retinoblastoma. *Proc Natl Acad Sci U S A 68*, 820-3.
(6) Hanahan, D., and Weinberg, R. A. (2011) Hallmarks of cancer: the next generation. *Cell 144*, 646-74.
(7) Almendro, V., Marusyk, A., and Polyak, K. (2013) Cellular heterogeneity and molecular evolution in cancer. *Annu Rev Pathol 8*, 277-302.
(8) Shackleton, M., Quintana, E., Fearon, E. R., and Morrison, S. J. (2009) Heterogeneity in cancer: cancer stem cells versus clonal evolution. *Cell 138*, 822-9.
(9) Burrell, R. A., McGranahan, N., Bartek, J., and Swanton, C. (2013) The causes and consequences of genetic heterogeneity in cancer evolution. *Nature 501*, 338-45.
(10) Rak, J., Yu, J. L., Kerbel, R. S., and Coomber, B. L. (2002) What do oncogenic mutations have to do with angiogenesis/vascular dependence of tumors? *Cancer Res 62*, 1931-4.
(11) Tonini, T., Rossi, F., and Claudio, P. P. (2003) Molecular basis of angiogenesis and cancer. *Oncogene 22*, 6549-56.
(12) Almog, N. (2010) Molecular mechanisms underlying tumor dormancy. *Cancer Lett 294*, 139-46.
(13) Kumar, R., and Yarmand-Bagheri, R. (2001) The role of HER2 in angiogenesis. *Semin Oncol 28*, 27-32.
(14) Rak, J., Yu, J. L., Klement, G., and Kerbel, R. S. (2000) Oncogenes and angiogenesis: signaling three-dimensional tumor growth. *J Investig Dermatol Symp Proc 5*, 24-33.
(15) Semenza, G. L. (2000) Hypoxia, clonal selection, and the role of HIF-1 in tumor progression. *Crit Rev Biochem Mol Biol 35*, 71-103.
(16) Rundhaug, J. E. (2005) Matrix metalloproteinases and angiogenesis. *J Cell Mol Med 9*, 267-85.
(17) Mason, S. D., and Joyce, J. A. (2011) Proteolytic networks in cancer. *Trends Cell Biol 21*, 228-37.
(18) Rak, J., Filmus, J., Finkenzeller, G., Grugel, S., Marme, D., and Kerbel, R. S. (1995) Oncogenes as inducers of tumor angiogenesis. *Cancer Metastasis Rev 14*, 263-77.
(19) Milkiewicz, M., Ispanovic, E., Doyle, J. L., and Haas, T. L. (2006) Regulators of angiogenesis and strategies for their therapeutic manipulation. *Int J Biochem Cell Biol 38*, 333-57.
(20) Arpino, V., Brock, M., and Gill, S. E. (2015) The role of TIMPs in regulation of extracellular matrix proteolysis. *Matrix Biol 44-46*, 247-54.

(21) Kim, Y. S., Kim, S. H., Kang, J. G., and Ko, J. H. (2012) Expression level and glycan dynamics determine the net effects of TIMP-1 on cancer progression. *BMB Rep 45*, 623-8.
(22) Rao, J. S. (2003) Molecular mechanisms of glioma invasiveness: the role of proteases. *Nat Rev Cancer 3*, 489-501.
(23) Ramos-DeSimone, N., Hahn-Dantona, E., Sipley, J., Nagase, H., French, D. L., and Quigley, J. P. (1999) Activation of matrix metalloproteinase-9 (MMP-9) via a converging plasmin/stromelysin-1 cascade enhances tumor cell invasion. *J Biol Chem 274*, 13066-76.
(24) Kostoulas, G., Lang, A., Nagase, H., and Baici, A. (1999) Stimulation of angiogenesis through cathepsin B inactivation of the tissue inhibitors of matrix metalloproteinases. *FEBS Lett 455*, 286-90.
(25) Chabner, B. A., and Roberts, T. G., Jr. (2005) Timeline: Chemotherapy and the war on cancer. *Nat Rev Cancer 5*, 65-72.
(26) Zawilska, J. B., Wojcieszak, J., and Olejniczak, A. B. (2013) Prodrugs: a challenge for the drug development. *Pharmacol Rep 65*, 1-14.
(27) Walther, R., Rautio, J., and Zelikin, A. N. (2017) Prodrugs in medicinal chemistry and enzyme prodrug therapies. *Adv Drug Deliv Rev 118*, 65-77.
(28) Onoue, S., Yamada, S., and Chan, H. K. (2014) Nanodrugs: pharmacokinetics and safety. *Int J Nanomedicine 9*, 1025-37.
(29) Ventola, C. L. (2012) The nanomedicine revolution: part 1: emerging concepts. *P T 37*, 512-25.
(30) Senapati, S., Mahanta, A. K., Kumar, S., and Maiti, P. (2018) Controlled drug delivery vehicles for cancer treatment and their performance. *Signal Transduct Target Ther 3*, 7.
(31) Rizvi, S. A. A., and Saleh, A. M. (2018) Applications of nanoparticle systems in drug delivery technology. *Saudi Pharm J 26*, 64-70.
(32) Matsumura, Y., and Maeda, H. (1986) A new concept for macromolecular therapeutics in cancer chemotherapy: mechanism of tumoritropic accumulation of proteins and the antitumor agent smancs. *Cancer Res 46*, 6387-92.
(33) Maeda, H. (2015) Toward a full understanding of the EPR effect in primary and metastatic tumors as well as issues related to its heterogeneity. *Adv Drug Deliv Rev 91*, 3-6.
(34) Hare, J. I., Lammers, T., Ashford, M. B., Puri, S., Storm, G., and Barry, S. T. (2017) Challenges and strategies in anti-cancer nanomedicine development: An industry perspective. *Adv Drug Deliv Rev 108*, 25-38.
(35) Rosenblum, D., Joshi, N., Tao, W., Karp, J. M., and Peer, D. (2018) Progress and challenges towards targeted delivery of cancer therapeutics. *Nat Commun 9*, 1410.
(36) Seymour, L. W., Miyamoto, Y., Maeda, H., Brereton, M., Strohalm, J., Ulbrich, K., and Duncan, R. (1995) Influence of molecular weight on passive tumour accumulation of a soluble macromolecular drug carrier. *Eur J Cancer 31A*, 766-70.
(37) Hoshyar, N., Gray, S., Han, H., and Bao, G. (2016) The effect of nanoparticle size on in vivo pharmacokinetics and cellular interaction. *Nanomedicine (Lond) 11*, 673-92.
(38) Devarajan, P. V. J., S. (2015) *Targeted Drug Delivery: Concepts and Design*, Springer International Publishing.

(39) Raza, A., Rasheed, T., Nabeel, F., Hayat, U., Bilal, M., and Iqbal, H. M. N. (2019) Endogenous and Exogenous Stimuli-Responsive Drug Delivery Systems for Programmed Site-Specific Release. *Molecules 24*.
(40) Alonso, M. J. G.-F., M. (2014) *Nano-Oncologicals: New Targeting and Delivery Approaches*, Springer International Publishing.
(41) Demetzos, C. (2016) Pharmaceutical Nanotechnology. Fundamentals and Practical Applications. *Anticancer Res 36*, 4373.
(42) Moghimi, S. M., Hunter, A. C., and Murray, J. C. (2001) Long-circulating and target-specific nanoparticles: theory to practice. *Pharmacol Rev 53*, 283-318.
(43) Wu, D. (2015) in *Chemistry*, University of Basel.
(44) Salvioni, L., Rizzuto, M. A., Bertolini, J. A., Pandolfi, L., Colombo, M., and Prosperi, D. (2019) Thirty Years of Cancer Nanomedicine: Success, Frustration, and Hope. *Cancers (Basel) 11*.
(45) Farjadian, F., Ghasemi, A., Gohari, O., Roointan, A., Karimi, M., and Hamblin, M. R. (2019) Nanopharmaceuticals and nanomedicines currently on the market: challenges and opportunities. *Nanomedicine (Lond) 14*, 93-126.
(46) Maeda, H., and Khatami, M. (2018) Analyses of repeated failures in cancer therapy for solid tumors: poor tumor-selective drug delivery, low therapeutic efficacy and unsustainable costs. *Clin Transl Med 7*, 11.
(47) Golombek, S. K., May, J. N., Theek, B., Appold, L., Drude, N., Kiessling, F., and Lammers, T. (2018) Tumor targeting via EPR: Strategies to enhance patient responses. *Adv Drug Deliv Rev 130*, 17-38.
(48) Paradise, J. (2019) Regulating Nanomedicine at the Food and Drug Administration. *AMA J Ethics 21*, E347-355.
(49) Sieber, S., Grossen, P., Bussmann, J., Campbell, F., Kros, A., Witzigmann, D., and Huwyler, J. (2019) Zebrafish as a preclinical in vivo screening model for nanomedicines. *Adv Drug Deliv Rev 151-152*, 152-168.
(50) Nel, A., Xia, T., Madler, L., and Li, N. (2006) Toxic potential of materials at the nanolevel. *Science 311*, 622-7.
(51) Turecek, P. L., Bossard, M. J., Schoetens, F., and Ivens, I. A. (2016) PEGylation of Biopharmaceuticals: A Review of Chemistry and Nonclinical Safety Information of Approved Drugs. *J Pharm Sci 105*, 460-475.
(52) Shiraishi, K., and Yokoyama, M. (2019) Toxicity and immunogenicity concerns related to PEGylated-micelle carrier systems: a review. *Sci Technol Adv Mater 20*, 324-336.
(53) Qiu, F., Chen, Y., Tang, C., and Zhao, X. (2018) Amphiphilic peptides as novel nanomaterials: design, self-assembly and application. *Int J Nanomedicine 13*, 5003-5022.
(54) Jouberta, I. A. G., M.; , and Essa, S. N., R.; Gadermaiera, G.; Duschla, A.; Bathkec, A. C.; Himly, M. (2019) Public perception and knowledge on nanotechnology: A study based on a citizen science approach. *NanoImpact 17*.
(55) Kato-Nitta, N., Maeda, T., Inagaki, Y., and Tachikawa, M. (2019) Expert and public perceptions of gene-edited crops: attitude changes in relation to scientific knowledge. *Palgrave Communications 5*, 137.
(56) Givens, B. E., Naguib, Y. W., Geary, S. M., Devor, E. J., and Salem, A. K. (2018) Nanoparticle-Based Delivery of CRISPR/Cas9 Genome-Editing Therapeutics. *AAPS J 20*, 108.

(57) Dai, W. J., Zhu, L. Y., Yan, Z. Y., Xu, Y., Wang, Q. L., and Lu, X. J. (2016) CRISPR-Cas9 for in vivo Gene Therapy: Promise and Hurdles. *Mol Ther Nucleic Acids 5*, e349.
(58) Wilbie, D., Walther, J., and Mastrobattista, E. (2019) Delivery Aspects of CRISPR/Cas for in Vivo Genome Editing. *Acc Chem Res 52*, 1555-1564.

Curriculum Vitae

Daniel S. Ehrsam

Private address
Ochsengasse 19
CH-4058 Basel
mobile +41 79 291 10 63
daniel.ehrsam@unibas.ch

Date of birth
January 23, 1985

Nationality
Swiss (born in Basel)

Experience

2015/08 – 2020/09 PhD in Pharmaceutical Sciences, Biopharmacy, University of Base

2015/01 – 2015/05 Civilian service in the Helminth Drug Development unit at the Swiss Tropical and Public Health Institute

2014/08 – 2014/12 Internship in Solids Manufacturing at Hoffmann-La Roche in Basel

2009/08 – 2014/04 Studies in Pharmaceutical Sciences at the University of Basel
Graduated with a MSc in Pharmaceutical Sciences
Investigating the influence of Triacsin C on the sphingolipid ratio in brain cells using isotope-labeled tracer (master thesis at Texas Tech in Amarillo, TX, USA)

Publications

Ehrsam D, Sieber S, Oufir M, Porta F, Hamburger M, Huwyler J, Meyer Zu Schwabedissen HE. Design, synthesis and characterization of a paclitaxel formulation activated by extracellular MMP9. Bioconjug Chem. 2020 Jan 2; PubMed PMID: 31894970

Ehrsam D, Porta F, Hussner J, Seibert I, Meyer Zu Schwabedissen HE. PDMS-PMOXA-Nanoparticles Featuring a Cathepsin B-Triggered Release Mechanism. Materials 2019 Sep 3;12(17). PubMed PMID: 31484396

Ehrsam D, Porta F, Mori M, Schwabedissen H, Dalla Via L, Garcia-Argaez AN, et al. Unravelling the Antiproliferative Activity of 1,2,5-oxadiazole Derivatives. Anticancer research. 2019 Jul;39(7):3453-61. PubMed PMID: 31262869.

Porta F, Ehrsam D, Lengerke C, Meyer Zu Schwabedissen HE. Synthesis and Characterization of PDMS-PMOXA-Based Polymersomes Sensitive to MMP-9 for Application in Breast Cancer. Molecular pharmaceutics. 2018 Nov 5;15(11):4884-97. PubMed PMID: 30274515.

The Role of the Long Chain Fatty Acyl CoA Synthetase during Brain Ischemia; Master thesis project at Texas Tech University, Institute for Biomedical Sciences in Amarillo TX, USA

Oral Presentation

Strategy for the development of an enzymatically triggered nanoformulation
19th Barrier- and Transporter Meeting Bad Herrenalb, Bad Herrenalb, Germany, 2017/05/15-2017/05/17

Poster Presentations

Annual Research Meeting of the Pharmacenter 2019, Basel, Switzerland, 2019/02/08

10th Swiss Pharma Science Day 2017, Bern, Switzerland, 2017/08/22

6th World Congress on Medicinal Chemistry and Drug Design, best poster award, Milano, Italy, 2017/06/07-2017/06/08

Annual Research Meeting of the Pharmacenter 2017, Basel, Switzerland, 2017/02/10

Annual Research Meeting of the Pharmacenter 2016, Basel, Switzerland, 2016/02/10